STANFORD UNIVERSITY
ENGINEERING IN MEDICINE AND BIOLOGY

DYNAMIC BEHAVIOR OF EYE GLOBES

ROBERT H. TUFFIAS
MAX ANLIKER

BIOMECHANICS LABORATORY

FEBRUARY 1967

This research was sponsored by the Office of Naval Research under Contract NAVY 0007 and in part by a NASA Training Grant and by the National Institutes of Health under Grant NBO 6328-01

SUDAAR NO. 302

Department of Aeronautics and Astronautics
Stanford University
Stanford, California

3 DYNAMIC BEHAVIOR OF EYE GLOBES 6

by

6 Robert H. Tuffias

and

Max Anliker 9

SUDAAR 302

9 February 1967 10 CY

The research was sponsored by the Office of Naval Research
under Contract Navy 0007 and in part by a NASA Training
Grant and by the National Institutes of Health
under Grant NBO-6328-01

PRECEDING PAGE BLANK NOT FILMED.

ACKNOWLEDGMENT

The authors are indebted to Dr. Donald T. Hayashi for his medical counsel and stimulating discussions. They also wish to thank the Ames Research Center of the NASA for providing the dog eyes, the vibrator and the Fotonic Sensor.

TABLE OF CONTENTS

Table of Contents (Continued)

LIST OF ILLUSTRATIONS

List of Illustrations (Continued)

List of Illustrations (Continued)

NOTATION

A	area
$A_{mn}, B_{mn}, C_{mn}, \phi_{mn}, D_{mn}, E_{mn}$	expansion coefficients
$C_1, C_2, C_3, C_4, C_5, C_6$	constants
D	extensional rigidity
E, E_1	Young's modulus
E_D	dissipated energy (Chapter X)
E_0	pressure dependent term in Young's modulus
F	body force per unit area
J	see chapter IX
K	flexural rigidity
$\mathcal{K}$	function of φ
L	see chapter IX
L_{ik}	linear differential operator
M_n	apparent mass (sec. 4.3)
M	mass of piston (sec. 7.2)
N	stress resultant
P	non-dimensional intraocular pressure
P_n^m	associated Legendre polynomial of 1st kind
Q_n^m	associated Legendre polynomial of 2nd kind
R	radius of curvature
$\mathcal{R}$	function of r
S	described surface of eye

T	surface tension; kinetic energy
U,V,W	functions of θ and φ
V	potential energy
V_o	volume of eye
f	frequency (cps)
h	wall (scleral) thickness
i	imaginary number $\sqrt{-1}$
k	see (4.1.4); spring constant
ℓ	arc length
ℓ,n	axisymmetric mode number
m	asymmetric mode number; apparent mass
p	pressure
Δp	intraocular pressure (dynes/cm^2)
$\vec{q}$	velocity vector
r	radius
r_o	external radius
t	time
u,v,w	displacements in the φ,θ,r directions
Θ	function of θ
Λ	see (3.2.3)
$\sum$	summation
Φ	velocity potential
γ	solid angle

ϵ	strain
ϵ_1, ϵ_2	functions of pressure (see (7.1.2))
ζ	radial displacement
η	cos θ; physiologic constant
θ	colatitude measured from the pole
μ	apparent density; viscosity coefficient
ν	Poisson's ratio
ρ	density
σ	eigenfrequency squared
τ	time constant
φ	longitude
ψ	function of r, θ, φ

Subscripts:

1,2	internal and external; principal directions
10,20	internal and external initial conditions
e	eye
ℓ, m, n	function of ℓ, m, n
Δp	component due to Δp
s	shell
t, r, θ, φ	differentiation with respect to t, r, θ, φ
v	vibrator
ζ	component due to radial displacement

I. INTRODUCTION

1.1 General Remarks

The eye, long recognized as being interdisciplinary in nature, has traditionally been examined only with regard to its biological, physiological, and optical behavior. Recently it has been realized that many of its functions and disorders (e.g., retinal detachment) are mechanical and should be analyzed as such. Nickerson and his collaborators[1] studied the damaging effects on ocular structures by rectilinear sinusoidal forces applied to the whole body of normal dogs. They determined the fundamental frequency of the eyes of these dogs to be 32-35 cycles per second, depending on the direction of the oscillatory force, and also found that these vibrations temporarily reduced the intraocular pressure. No quantitative results were reported but qualitatively they observed that larger stresses were accompanied by greater tissue damage. Anliker, Hayashi[2], and Silvis[3] investigated the feasibility of using dynamic loading (e.g., vibrational, rotatory, and centrifugal) to resettle detached retinas. Their experimental results indicated that certain rotatory and centrifugal force fields considerably improved the normal resettling times.

Space flight has placed man in a hazardous dynamic environment which is pushing the limits of his tolerance level. It has been found that the low frequency, high-g vibration level that is associated with large boosters may be a major constraint in the exploration of the solar system. Short-time tests[4] of human tolerance to sinusoidal vibrations from one to fifteen cps indicated that the lower levels of tolerance was found to be between one and two -g at three to four cps and seven to eight cps. The highest tolerance level of seven to eight -g was found at fifteen cps.

The intraocular pressure is a significant diagnostic parameter in clinical ophthalmology. It is the primary parameter used in diagnosing glaucoma, a major cause of irreversible adult blindness, presently afflicting about two per cent of all people over 40 years of age. Glaucoma is an ocular condition in which the intraocular pressure is so elevated as to jeopardize the cellular integrity of the retina upon which vision depends. The pressure level that may be tolerated without damage to the eye varies widely among individuals but it is agreed that a nominal value of 20 mm Hg is normal for a healthy eye. Instrumental measurement[5] of the intraocular pressure began about one hundred years ago with the impression tonometer of von Graefe. Since then, many tonometers have been devised using mainly the principles of indentation or applanation.

Maklakov, in 1885, invented the first applanation tonometer. This device is still in use today. It consists of a cylindrical weight with a flat base of opal glass. If the footplate is coated with a thin film of dye and the tonometer is made to rest on the cornea, a white ring is produced which corresponds to the area of the flattened corneal surface. In clinical use, the Maklakov tonometer gives readings which are as valid and of the same order of accuracy as those given by most other tonometers. The most commonly used contemporary applanation tonometer was invented by Goldmann[6]. It is used in conjunction with a biomicroscope to measure the force required to flatten a segment of the cornea that is 3.06 mm in diameter. (This 3.06 mm diameter corresponds to an area over which 1 gram applied load is equivalent to an average pressure of 10 mm Hg.)

The Schiotz[7] tonometer (Fig. 1.1) is the most popular indentation tonometer which is used today. Here, the intraocular pressure is estimated by the depth of corneal indentation which a plunger of known weight produces. Because of the complicated geometric shape of the indentation, a reasonable analytical description of this device is not in evidence, and since its inception the conversion curves (from tonometer reading to pressure) have been changed several times.

The Mackay-Marg[8] applanation tonometer is one of the most recently developed instruments. With this device, the cornea is flattened by a guard ring and a sensitive, centrally located transducer measures the radial force produced by the intraocular pressure.

With all of these instruments, except the Mackay-Marg tonometer, it is necessary to anesthetize the cornea so that the patient can tolerate the apparatus which is placed in contact with the eye. This anesthesia may affect the measurement. Also, these instruments are inherently inaccurate.

If it is assumed that the natural frequencies of the eye are a function of the intraocular pressure, then it should be possible to make use of the vibrational modes to infer the intraocular pressure. In addition, it should be possible to excite the eye without contacting it by making use of pressure or sound waves, and detect the oscillatious optically. A device of this sort should eliminate many of the disadvantages of the eye-contact instruments previously described. It would also have the advantage that ocular contact and anesthesia will be unnecessary.

The former is extremely important since an instrument that requires ocular contact necessitates operation by an ophthalmologist. If the ocular contact constraint is removed the intraocular pressure could be measured by any moderately trained individual. This makes it extremely attractive for space use, that is, measuring the effects of space flight on the ocular system. It should also be noted that by making use of the eigenvibrations of the eye it should be possible to study the effects of the surroundings of the eye (e.g., muscles, optic nerve, etc.).

The object of this dissertation is to study the dynamic behavior of the eye both analytically and experimentally. The analytical investigation consists of developing a simple dynamic model of the eye from which the eigenfrequency dependence on intraocular pressure can be obtained. In addition, experiments were performed to validate this model and to give insight into possible modifications to the model.

1.2 Anatomy of the Eye[9,10,11]

There are four basic coats on the eyeball (Fig. 1.2):

a. The fibrous tunic consists of the sclera or "white tunic" posteriorly and the cornea anteriorly. The sclera occupies about 5/6 and the transparent cornea about 1/6 of the horizontal circumference of the eyeball.

b. The vascular tunic or uvea consists of the choroid, the ciliary body, and the iris.

c. The pigment epithelium of the retina.

d. The retina.

The sclera is a dense, fibrous, relatively avascular structure. Anteriorly it comprises the "white" of the eye. Its thickness (Fig. 1.3) varies from approximately 1.0 mm at the posterior pole to about 0.4 to 0.5 mm at the equator. It is only 0.3 mm thick below the tendons of the rectus muscles. The sclera is made up of three ill-defined layers called (1) the episclera, (2) the sclera proper, and (3) the lamina fusca.

The episclera is the outermost superficial layer. It is composed of loosely intertwined fibrous tissue strands connected to Tenon's capsule.

The sclera proper is composed of bundles of connective tissue and elastic fibers. The bundles are randomly arranged except around the optic nerve where they are more circular.

The lamina fusca is the innermost layer of the sclera and is very rich in elastic fibers. It is this layer which might well control (elastically) the dynamic behavior of a vibrating eye.

The eyeball is not exactly a sphere but is a very good approximation (see Fig. 1.4). It is slightly asymmetrical and this asymmetry is called "temporal bulge."

The vitreous body is a transparent, avascular, gelatinous material which fills the vitreous cavity between the lens and the optic nerve. The vitreous body is 99.8% water.

The bony orbits are the sockets which contain the eyeballs, the extraocular muscles, connective tissue fascia and ligaments, fat, blood vessels, and nerves (Fig. 1.5). The eyeball occupies only 20% of the orbital volume. It is situated anteriorly in the orbit just within the fascial attachements, and Tenon's capsule, with an extramuscular fat pad.

The intraocular pressure of the normal eye is about 20 mm Hg, a higher pressure than is found in any other organ of the body. This pressure depends upon the volume of the contents of the eye and the elasticity of its coats. The maintenance of the normal intraocular pressure depends mostly on the amount of aqueous humor present at any one moment in the eye. The aqueous humor is constantly being formed, and constantly being eliminated so that a quasi-equilibrium maintains a constant intraocular pressure in a healthy eye.

From the aforementioned description of the eyeball and its surroundings, a simple mathematical model can be conceived in the form of a spherical shell (corneo-scleral membrane) containing an incompressible liquid (vitreous body) and surrounded by an incompressible liquid (fat, muscle, etc.). The viscosity of the vitreous body will be neglected (see Appendix C). The variation in the diameter and the variation in the thickness of the cornea and sclera will also be neglected.

With this description in mind the eye was first treated as a spherical droplet held together by surface tension. This was refined slightly by adding an external medium to simulate the surrounding tissue. Elastic properties were then added to the sclera and, still in the one-degree-of-freedom realm, the effects of bending were examined. Continuing along this vein two-degree-of-freedom membrane (elastic) and later shell (bending) models were examined. And finally the complete shell model with internal and external media was constructed. At every step the newest effect was examined, evaluated, and compared to the less refined models. Thus the three-degree-of-freedom shell model of the eye has, in effect, evolved from a water droplet.

II. BASIC EQUATIONS

2.1 Fluid Mechanics

For any fluid (assuming that fluid is neither created nor destroyed) the equation of continuity is

$$\frac{\partial \rho}{\partial t} + \nabla \cdot (\rho \vec{q}) = 0, \tag{2.1.1}$$

where ρ is the fluid density, t is time, and $\vec{q}$ is the fluid velocity. If it is assumed that the fluid density is constant then from (2.1.1)

$$\nabla \cdot \vec{q} = 0 . \tag{2.1.2}$$

If it is assumed that the flow is irrotational, this implies that

$$\nabla \times \vec{q} = 0, \tag{2.1.3}$$

and therefore $\vec{q}$ may be expressed with the aid of a potential as

$$\vec{q} \equiv - \nabla\Phi \tag{2.1.4}$$

In addition the incompressible equation of continuity reduces to

$$\nabla \cdot \vec{q} = - \nabla \cdot \nabla\Phi = - \nabla^2\Phi = 0, \tag{2.1.5}$$

that is, the velocity potential satisfies Laplace's equation.

For an invicid fluid Euler's equation can be written as (neglecting body forces)

$$\frac{\partial \vec{q}}{\partial t} + (\vec{q} \cdot \nabla)\vec{q} = - \frac{1}{\rho} \nabla p , \tag{2.1.6}$$

where p is the pressure.

By making use of the identity

$$(\vec{q} \cdot \nabla)\vec{q} = \frac{1}{2} \nabla(\vec{q} \cdot \vec{q}) - \vec{q} \times(\nabla \times \vec{q}), \tag{2.1.7}$$

and the assumption of irrotationality $(\nabla \times \vec{q} = 0)$, Euler's equation becomes

$$\frac{\partial \vec{q}}{\partial t} + \frac{1}{2} \nabla(\vec{q} \cdot \vec{q}) = -\frac{1}{\rho} \nabla p \ . \tag{2.1.8}$$

If it is assumed that the flow velocities are small $(q^2 \approx 0)$ and when making use of the velocity potential, (2.1.8) becomes

$$\nabla \left[\frac{\partial \Phi}{\partial t} - \frac{p}{\rho} \right] = 0 \ . \tag{2.1.9}$$

Integration of (2.1.9) produces

$$p = \rho \frac{\partial \Phi}{\partial t} \ , \tag{2.1.10}$$

where the integration constant is absorbed in Φ.

The kinematic boundary condition of a fluid may be expressed in general by

$$\frac{DS}{Dt} (\theta, \varphi, t) = 0 \ , \tag{2.1.11}$$

where $S = 0$ is the equation of the bounding surface and

$$\frac{D}{Dt} = \frac{\partial}{\partial t} + \vec{q} \cdot \nabla \ . \tag{2.1.12}$$

θ is the colatitude measured from the pole, and φ is the longitude.

2.2 Equation of Motion/Dynamic Boundary Condition

Consider an element of the surface of the eyeball acted upon by an internal pressure p_1, an external pressure p_2, and a radial body force F (per unit area). Let the stress resultants in the principal directions be N_1 and N_2 and the associated radii of curvature R_1

and R_2. Then the radial D'Alembert equilibrium equation can be written as

$$p_1 - p_2 = \frac{N_1}{R_1} + \frac{N_2}{R_2} - F \, . \qquad (2.2.1)$$

In all cases treated F will be an inertia force.

2.3 Geometry

When considering only infinitesimal radial disturbances ζ from the equilibrium position at $r = R$, the equation of the surface of the eyeball can be written as

$$S(r,\theta,\varphi,t) = r - [R + \zeta(\theta,\varphi,t)] = 0 \, . \qquad (2.3.1)$$

By applying the kinematic boundary condition (2.1.11) to (2.3.1) we get

$$\frac{\partial r}{\partial t} - \frac{\partial \zeta}{\partial t} + \vec{q} \cdot \nabla S = 0 \, . \qquad (2.3.2)$$

On linearizing and making use of (2.1.4), the kinematic boundary condition becomes

$$\frac{\partial \zeta}{\partial t} = - \frac{\partial \Phi}{\partial r} \, . \qquad (2.3.3)$$

Consider[12] a surface whose principal radii of curvature, at a point on the surface, are R_1 and R_2. R_1 and R_2 are positive, if the surface is concave. When the surface undergoes an infinitesimal normal displacement $\delta\zeta$, the elements of length $d\ell_1$ and $d\ell_2$ on the surface in its principal directions change in length by the amounts $(\delta\zeta/R_1)d\ell_1$ and $(\delta\zeta/R_2)d\ell_2$ respectively. It should be noted that $d\ell_1$ and $d\ell_2$ are elements of the circumference of circles with radii R_1 and R_2 respectively. The area of the surface element before displacement may be written as

$$dA = d\ell_1 d\ell_2 \ , \tag{2.3.4}$$

and after displacement as

$$dA = d\ell_1 \left(1 + \frac{\delta\zeta}{R_1}\right) d\ell_2 \left(1 + \frac{\delta\zeta}{R_2}\right) \ . \tag{2.3.5}$$

If (2.3.5) is expanded and linearized it yields

$$dA = \left(1 + \frac{\delta\zeta}{R_1} + \frac{\delta\zeta}{R_2}\right) d\ell_1 d\ell_2 \ , \tag{2.3.6}$$

and therefore the change in surface area due to the displacement is

$$\delta A = \int \delta\zeta \left(\frac{1}{R_1} + \frac{1}{R_2}\right) dA \ . \tag{2.3.7}$$

In spherical coordinates the area of a surface can be written as

$$A = \int_0^{2\pi}\int_0^{\pi} \left[r^2 + \left(\frac{\partial r}{\partial \theta}\right)^2 + \frac{1}{\sin^2\theta}\left(\frac{\partial r}{\partial \varphi}\right)^2\right]^{1/2} r \sin\theta \, d\theta d\varphi \ . \tag{2.3.8}$$

When making use of the equation for the displaced surface of the eyeball (2.3.1) the area becomes

$$A = \int_0^{2\pi}\int_0^{\pi} \left[(R + \zeta)^2 + \left(\frac{\partial \zeta}{\partial \theta}\right)^2 + \frac{1}{\sin^2\theta}\left(\frac{\partial \zeta}{\partial \varphi}\right)^2\right]^{1/2} (R + \zeta) \sin\theta d\theta d\varphi \ . \tag{2.3.9}$$

On expanding the square root term in a Taylor series about the equilibrium position $(\zeta = 0)$ and linearizing, (2.3.9) becomes

$$A = \int_0^{2\pi}\int_0^{\pi}\left\{(R+\zeta)^2 + \frac{1}{2}\left[\left(\frac{\partial\zeta}{\partial\theta}\right)^2 + \frac{1}{\sin^2\theta}\left(\frac{\partial\zeta}{\partial\varphi}\right)^2\right]\right\}\sin\theta\, d\varphi d\theta \ . \qquad (2.3.10)$$

The variation of the area δA when ζ changes is

$$\delta A = \int_0^{2\pi}\int_0^{\pi}\left[2(R+\zeta)\delta\zeta + \frac{\partial\zeta}{\partial\theta}\frac{\partial\delta\zeta}{\partial\theta} + \frac{1}{\sin^2\theta}\frac{\partial\zeta}{\partial\varphi}\frac{\partial}{\partial\varphi}\delta\zeta\right]\sin\theta\, d\theta d\varphi \ . \qquad (2.3.11)$$

If the second term is integrated by parts with respect to θ, and the third term by parts with respect to φ, (2.3.11) yields

$$\delta A = \int_0^{2\pi}\int_0^{\pi}\left[2(R+\zeta) - \frac{1}{\sin\theta}\frac{\partial}{\partial\theta}\left(\sin\theta\frac{\partial\zeta}{\partial\theta}\right) - \frac{1}{\sin^2\theta}\frac{\partial^2\zeta}{\partial\varphi^2}\right]\delta\zeta \sin\theta\ d\theta d\varphi \ . \qquad (2.3.12)$$

In addition, when we divide (2.3.12) by $R(R+2\zeta)$, expand in a Taylor series, and linearize, it can be shown that

$$\delta A = \int_0^{2\pi}\int_0^{\pi}\left\{\frac{2}{R} - \frac{2\zeta}{R^2} - \frac{1}{R^2}\left[\frac{1}{\sin\theta}\frac{\partial}{\partial\theta}\left(\sin\theta\frac{\partial\zeta}{\partial\theta}\right) + \frac{1}{\sin^2\theta}\frac{\partial^2\zeta}{\partial\varphi^2}\right]\right\}$$

$$\left\{R(R+2\zeta)\sin\theta\ d\theta d\varphi\right\}\delta\zeta \ . \qquad (2.3.13)$$

From (2.3.10) a linearized element of surface area can be written as

$$dA = R(R+2\zeta)\sin\theta\ d\theta d\varphi \ . \qquad (2.3.14)$$

By comparing (2.3.7) and (2.3.13), while we make use of (2.3.14), we find that

$$\frac{1}{R_1} + \frac{1}{R_2} = \frac{2}{R} - \frac{2\zeta}{R^2} - \frac{1}{R^2}\left[\frac{1}{\sin\theta}\frac{\partial}{\partial\theta}\left(\sin\theta\frac{\partial\zeta}{\partial\theta}\right) + \frac{1}{\sin^2\theta}\frac{\partial^2\zeta}{\partial\varphi^2}\right] \qquad (2.3.15)$$

or

$$\frac{1}{R_1} + \frac{1}{R_2} = \frac{1}{R}\left[2 - \frac{1}{R}\left\{2\zeta + \cot\theta\,\frac{\partial\zeta}{\partial\theta} + \frac{\partial^2\zeta}{\partial\theta^2} + \csc^2\theta\,\frac{\partial^2\zeta}{\partial\varphi^2}\right\}\right] . \qquad (2.3.16)$$

2.4 Laplace's Equation in Spherical Coordinates

Laplace's equation in spherical coordinates is

$$\nabla^2\Psi = \frac{1}{r^2}\frac{\partial}{\partial r}\left(r^2\frac{\partial\Psi}{\partial r}\right) + \frac{1}{r^2\sin\theta}\frac{\partial}{\partial\theta}\left(\sin\theta\,\frac{\partial\Psi}{\partial\theta}\right) + \frac{1}{r^2\sin^2\theta}\frac{\partial^2\Psi}{\partial\varphi^2} = 0 . \qquad (2.4.1)$$

A solution to this equation can be obtained by a separation of variables of the form

$$\Psi(r,\theta,\varphi) = \mathcal{R}(r)\Theta(\theta)\mathcal{K}(\varphi) . \qquad (2.4.2)$$

On making use of (2.4.2), Laplace's equation reduces to three ordinary differential equations of the form

$$r^2\frac{d^2\mathcal{R}}{dr^2} + 2r\frac{d\mathcal{R}}{dr} - n(n+1)\mathcal{R} = 0 , \qquad (2.4.3)$$

$$\frac{d^2\mathcal{K}}{d\varphi^2} + m^2\mathcal{K} = 0 , \qquad (2.4.4)$$

and

$$\frac{d^2\Theta}{d\theta^2} + \cot\theta\,\frac{d\Theta}{d\theta} + \left[n(n+1) - \frac{m^2}{\sin^2\theta}\right]\Theta = 0 , \qquad (2.4.5)$$

where $n(n+1)$ and $-m^2$ are separation constants.

Equation (2.4.3) has as solution

$$\mathcal{R}(r) = c_1 r^n + c_2 r^{-(n+1)} . \qquad (2.4.6)$$

Equation (2.4.4) is a linear homogeneous equation with constant coefficients and its solution is

$$\Phi(\varphi) = C_3 e^{im\varphi} + C_4 e^{-im\varphi} . \tag{2.4.7}$$

Equation (2.4.5) is Legendre's equation and has solutions of the form (see Appendix A)

$$\Theta(\theta) = C_5 P_n^m(\cos\theta) + C_6 Q_n^m(\cos\theta) , \tag{2.4.8}$$

where $P_n^m(\cos\theta)$ and $Q_n^m(\cos\theta)$ are associated Legendre polynomials of the first and second kind respectively.

An examination of these solutions permits some of the constants to be determined by the physical nature of the problem:

(a) $C_6 = 0$ since $Q_n^m(\cos\theta)$ is not bounded at $\theta = 0, \pi$.

(b) n must be zero or a positive integer to maintain $P_n^m(\cos\theta)$ finite at the poles.

(c) For continuity and periodicity of the exponential function, which is necessary for the eyeball, m must be zero or an integer.

(d) By the definition of $P_n^m(\cos\theta)$, $m \le n$ (see Appendix A).

(e) For internal problems $r^{-(n+1)}$ is unbounded at $r = 0$ and therefore $C_2 = 0$.

(f) For external problems r^n is unbounded at $r = \infty$ and therefore $C_1 = 0$.

By making use of these observations, the complete solution can be written as

$$\Psi(r,\theta,\varphi) = \sum_{m=-n}^{n} \sum_{n=0}^{\infty} C_{mn} e^{im\varphi} r^n P_n^m \qquad r \le R \quad \Bigg)$$

(continued)

$$\left.\Psi(r,\theta,\varphi) = \sum_{m=-n}^{n} \sum_{n=0}^{\infty} \phi_{mn} e^{im\varphi} r^{-(n+1)} P_n^m \qquad r \geq R \right\} . \tag{2.4.9}$$

It should be noted that the notation used requires that

$$P_n^m = P_n^{-m} = P_n^{|m|} . \tag{2.4.10}$$

III. SIMPLE MODELS

3.1 Droplet Model

As the simplest model the eye will be considered to consist of a liquid core surrounded by an infinite liquid. The interface material between the core and the surroundings will be under a constant tension $T = N_1 = N_2$. The liquids will be considered as imcompressible and invicid, and the flow will be irrotational. Gravity will be neglected.

When making use of (2.2.1), (2.1.10), and (2.3.16), the equation of motion can be written as

$$p_{10} + \rho_1 \Phi_{1t} - p_{20} - \rho_2 \Phi_{2t} = \frac{T}{R}\left[2 - \frac{1}{R}\left\{2\zeta + \cot\theta\ \zeta_\theta + \zeta_{\theta\theta} + \csc^2\theta\ \zeta_{\varphi\varphi}\right\}\right] + \mu\zeta_{tt}\ , \tag{3.1.1}$$

where p_{10} and p_{20} are the internal and external equilibrium pressures, ρ_1 and ρ_2 the internal and external densities, Φ_1 and Φ_2 the internal and external velocity potentials, t is time, and μ is the surface density of the corneo-scleral membrane. Subscripts of θ, φ, and t represent differentiation with respect to these variables. (3.1.1) implies that the equilibrium $(\zeta = 0)$ pressure distribution is

$$p_{10} - p_{20} = \Delta p = \frac{2T}{R}\ . \tag{3.1.2}$$

Δp is referred to as the intraocular pressure. If we differentiate (3.1.1) with respect to time and make use of the kinematic boundary conditions (2.3.3), we find that

$$\rho_1\Phi_{1tt} - \rho_2\Phi_{2tt} = \frac{\Delta p}{2R}\left[2\Phi_{1r} + \cot\theta\ \Phi_{1r\theta} + \Phi_{1r\theta\theta} + \csc^2\theta\ \Phi_{1r\varphi\varphi}\right] - \mu\Phi_{1rtt}\ . \tag{3.1.3}$$

It should be noted that the equation of motion (3.1.3) should in fact be satisfied at $r = R + \zeta$ but since second order ζ-terms have consistently been neglected, (3.1.3) may be validly satisfied at $r = R$.

To obtain the solution of the equation of motion a space-time separation is attempted:

$$\left.\begin{aligned}\Phi_1(r,\theta,\varphi,t) &= \psi_1(r,\theta,\varphi)e^{i\sqrt{\sigma}t}\\ \Phi_2(r,\theta,\varphi,t) &= \psi_2(r,\theta,\varphi)e^{i\sqrt{\sigma}t}\end{aligned}\right\} \tag{3.1.4}$$

where σ is the eigenfrequency squared.

A substitution of (3.1.4) in (3.1.3) yields

$$-\sigma\left[\rho_1\psi_1 - \rho_2\psi_2 + \mu\psi_{1r}\right] = \frac{\Delta p}{2R}\left[2\psi_{1r} + \cot\theta\ \psi_{1r\theta} + \psi_{1r\theta\theta} + \csc^2\theta\psi_{1r\varphi\varphi}\right]. \tag{3.1.5}$$

In reference to Laplace's equation in spherical coordinates (2.4.1), if it is differentiated with respect to r and rearranged, it becomes

$$\left[r^2\Psi_r\right]_{rr} + \cot\theta\ \Psi_{r\theta} + \Psi_{r\theta\theta} + \csc^2\theta\Psi_{r\varphi\varphi} = 0\ . \tag{3.1.6}$$

Since Φ_1 and Φ_2 satisfy Laplace's equation ψ_1 and ψ_2 do also. Therefore (3.1.6) can be used in (3.1.5) to produce

$$-\sigma\left[\rho_1\psi_1 - \rho_2\psi_2 + \mu\psi_{1r}\right] = \frac{\Delta p}{2R}\left\{2\psi_{1r} - \left[r^2\psi_{1r}\right]_{rr}\right\}\ . \tag{3.1.7}$$

In addition, the solutions for Laplace's equation inside the eye (for ψ_1) and outside the eye (for ψ_2) can be written as

$$\left.\begin{aligned} \psi_1(r,\theta,\varphi) &= \sum_m \sum_n C_{1mn} e^{im\varphi} r^n P_n^m \qquad r \le R, \\ \psi_2(r,\theta,\varphi) &= \sum_m \sum_n C_{2mn} e^{im\varphi} r^{-(n+1)} P_n^m \qquad r \ge R, \end{aligned}\right\} \tag{3.1.8}$$

and also

$$\psi_{1r}(r,\theta,\varphi) = \sum_m \sum_n C_{1mn} e^{im\varphi} n r^{n-1} P_n^m , \tag{3.1.9}$$

and

$$\left[r^2 \psi_{1r}\right]_{rr} = \sum_m \sum_n C_{1mn} e^{im\varphi} n^2 (n+1) r^{n-1} P_n^m . \tag{3.1.10}$$

It should be noted that the thickness of the sclera (corneo-scleral membrane) is considered to be constant, that is each part of the sclera is assumed to move with its corresponding middle surface point. Therefore an important boundary condition across the sclera is that the normal velocity be continuous. This may be written as

$$\frac{\partial \psi_1}{\partial r} = \frac{\partial \psi_2}{\partial r} \quad \text{at} \quad r = R . \tag{3.1.11}$$

This implies, from (3.1.8), that

$$C_{1mn} n R^{n-1} = - C_{2mn} (n+1) R^{-(n+2)} \tag{3.1.12}$$

or

$$C_{2mn} = -\left(\frac{n}{n+1}\right) R^{2n+1} C_{1mn} \ . \tag{3.1.13}$$

By making use of (3.1.8), (3.1.9), (3.1.10), (3.1.12), and (3.1.13) in (3.1.7) at $r = R$ we obtain

$$\sum_m \sum_n C_{1mn} e^{im\varphi} R^{n-1} P_n^m \left[\sigma_{mn} \left\{\rho_1 R + \frac{n}{n+1}\rho_2 R + \mu n\right\} + \frac{\Delta p}{2R}\left\{2n - n^2(n+1)\right\}\right] = 0 \ . \tag{3.1.14}$$

The linear independence of the functions requires that

$$\sigma_{mn}\left[\rho_1 R + \frac{n}{n+1}\rho_2 R + \mu n\right] + \frac{\Delta p}{2R} n \left[2 - n(n+1)\right] = 0 \tag{3.1.15}$$

or

$$\sigma_{mn} = \frac{\Delta p(n+2)(n-1)n}{2R^2\left[\rho_1 + \frac{n}{n+1}\rho_2 + \frac{\mu n}{R}\right]} \ . \tag{3.1.16}$$

A similar solution has been obtained (shell inertia not included) before and may be found in the books by Lamb[13] and Rayleigh[14] among others. Although it is not new some comments about the results bear repeating:

(a) The eigenfrequencies are independent of m. This means that for a given n there corresponds $2n + 1$ different eigenfunctions. Thus each of the eigenfrequencies correspond to $2n + 1$ different oscillations.

(b) The eigenfrequency is zero for $n = 0$. This corresponds to radial oscillations. On physical grounds for an incompressible fluid, radial oscillations are impossible.

(c) As the external fluid density decreases the natural frequencies increase. This is to be expected since less mass is being moved during oscillation.

Figures 3.1, 3.2, and 3.3 show curves of eigenfrequency squared (σ_{mn}) versus intraocular pressure for this spherical droplet model with various side conditions.

These curves were plotted using the nominal values of $R = 1.3$ cm, $\rho_1 = \rho_2 = 1.0$ gm/cm^3 and $\mu = 0.1$ gm/cm^2. Figure 3.1 treats the spherical droplet problem with no side conditions. Figure 3.2 adds the inertia of the shell. And Figure 3.3 adds the external medium. In comparing the three curves, it can be seen that each additional condition lowers the eigenfrequencies. This may be explained by the fact that each addition increases the apparent mass of the system. It should be noted that since the shell depends entirely on the internal pressure to retain its shape when the pressure goes to zero so do the natural frequencies. At the nominal intraocular pressure of 20 mm Hg the lowest mode $(n = 2)$ exhibits eigenfrequencies of 40, 37, and 30 cps for the three cases mentioned.

3.2 Elastic (Membrane) Model

This model differs from the flexible model in that the tension in the sclera will no longer be considered as constant but account will be taken of its elastic properties. That is the sclera will be treated as a membrane and the membrane assumptions — only in-plane stresses, plane sections remain plane — will be used. Again only radial displacements will be allowed.

As in the case of the flexible model the stress resultants due to the intraocular pressure Δp, can be written as

$$N_{1\Delta p} = N_{2\Delta p} = \frac{R\ \Delta p}{2} \ . \tag{3.2.1}$$

In addition, the stress resultants due to a radial deformation can be obtained from Hooke's law as

$$N_{1\zeta} = N_{2\zeta} = \frac{Eh}{1-\nu}\frac{\zeta}{R} = \Lambda\frac{\zeta}{R} \ , \tag{3.2.2}$$

where

$$\Lambda = \frac{Eh}{1-\nu} \ , \tag{3.2.3}$$

E is Young's Modulus, ν is Poisson's ratio, and h is the thickness of the corneo-scleral membrane. By superposing (3.2.1) and (3.2.2), the total stress resultants are

$$N_1 = N_2 = \frac{R\ \Delta p}{2} + \Lambda\frac{\zeta}{R} \ . \tag{3.2.4}$$

When making use of (3.2.4), (2.1.10), and (2.3.16) in (2.2.1) the equation of motion becomes

$$p_{10} + \rho_1\Phi_{1t} - p_{20} - \rho_2\Phi_{2t} = \left(\frac{R\ \Delta p}{2} + \Lambda\frac{\zeta}{R}\right)\frac{1}{R}\left\{2 - \frac{1}{R}\left[2\zeta + \cot\theta\ \zeta_\theta + \zeta_{\theta\theta} + \csc^2\theta\zeta_{\varphi\varphi}\right] + \mu\zeta_{tt}\right\}. \tag{3.2.5}$$

From which equilibrium requires that

$$p_1 - p_2 = \Delta p \ . \tag{3.2.6}$$

If we differentiate (3.2.5) with respect to time and make use of the kinematic boundary condition (2.3.3), we obtain

$$\rho_1 \Phi_{1tt} - \rho_2 \Phi_{2tt} = - \mu \Phi_{1rtt} - \frac{2\Lambda}{R^2} \Phi_{1r} + \frac{\Delta p}{2R} \Big[2\Phi_{1r} + \Phi_{1r\theta} \cot\theta +$$

$$+ \Phi_{1r\theta\theta} + \Phi_{1r\varphi\varphi} \csc^2\theta \Big] . \tag{3.2.7}$$

On attempting the space-time separation as in (3.1.4), (3.2.7) transforms into

$$\sigma \Big[\rho_1 \psi_1 - \rho_2 \psi_2 + \mu \psi_{1r} \Big] - \frac{2\Lambda}{R^2} \psi_{1r} + \frac{\Delta p}{2R} \Big\{ 2\psi_{1r} + \psi_{1r} \cot\theta$$

$$+ \psi_{1r\theta\theta} + \psi_{1r\varphi\varphi} \csc^2\theta \Big\} = 0 . \tag{3.2.8}$$

By applying (3.1.6), (3.1.8), (3.1.9), (3.1.10), and the continuity of the normal velocity across the sclera (3.1.11), and (3.1.13), (3.2.8) yields

$$\sum_m \sum_n C_{1mn} e^{im\varphi} R^{n-1} P_n^m \Big[\sigma_{mn} \Big\{ \mu n + \rho_1 R + \rho_2 R \frac{n}{n+1} \Big\} - \frac{2\Lambda n}{R^2}$$

$$+ \frac{\Delta p}{2R} n \Big\{ 2 - n(n+1) \Big\} \Big] = 0 . \tag{3.2.9}$$

The linear independence of the functions requires that

$$\sigma_{mn} \Big[\mu n + \rho_1 R + \rho_2 R \frac{n}{n+1} \Big] - \frac{2\Lambda n}{R^2} + \frac{\Delta p}{2R} n \Big[2 - n(n+1) \Big] = 0 \tag{3.2.10}$$

or

$$\sigma_{mn} = \frac{4\Lambda n + R\Delta p(n+2)(n-1)n}{2R^3 \Big[\rho_1 + \rho_2 \frac{n}{n+1} + \frac{\mu n}{R} \Big]} . \tag{3.2.11}$$

Some observations about this result are now in order:

(a) from a comparison of (3.2.11) and (3.1.16) it can be seen that the elastic model is in reality a linear superposition of the droplet model and a term due to the elasticity of the sclera (corneo-scleral membrane);

(b) as in the droplet model the eigenfrequencies are independent of m, and

(c) (3.2.11) shows that radial pulsations cannot exist, since this would imply that the fluid was compressible;

(d) Figure 3.4 shows a graph of σ_{mn} versus intraocular pressure for the one degree of freedom membrane model, for $n = 0,1,\ldots,6$. This curve was plotted using the nominal values of $R = 1.3$ cm, $h = 0.1$ cm, $\rho_1 = \rho_2 = 1.0$ gm/cm^3, $\mu = 0.1$ gm/cm^2, $\nu = 0.5$, and $E = 7.0 \times 10^6$ dynes/cm^2. In comparing Fig. 3.4 with Fig. 3.3, it is seen that the eigenfrequencies of the elastic model do not vanish at $\Delta p = 0$. It should also be noted that the slopes of the corresponding modes are the same for both models. At the normal pressure of 20 mm Hg the elastic model exhibits a frequency of 193 cps for the lowest pressure dependent mode (n=2). This increase in eigenfrequency (from 30 cps for the droplet model to 193 cps for the membrane model) is due entirely to the elastic forces which are considered in the elastic model. In the tonometers now in use the difference in elastic properties from eye to eye is normally neglected, but as can be seen from the comparison of Figs. 3.3 and 3.4, elasticity has a large effect;

(e) in the elastic model the $n = 1$ mode exists and is pressure independent. If all three orthonormal displacements were considered this mode would be a linear translation which is obviously independent of the intraocular pressure. If only radial displacements are taken into account (as is presently the case) then this mode ($n = 1$) becomes a constrained translation (nodes at $\pi/2$ and $3\pi/2$). In reality this constrained translational mode cannot exist and therefore can be ignored.

IV. SHELL MODEL AND SPECIAL CASES

4.1 Equations of Motion

The shell model differs from the elastic model in that bending stresses and the θ and φ displacements are not neglected. Since bending is small in the first few modes the elastic (membrane) model is probably a good approximation but if higher modes are to be considered bending must be taken into account.

The equations of motion are obtained by making use of the Flügge equations[15] for a spherical shell and adding the D'Alembert forces due to the shell and internal and external liquids. The equations of motion can be written as

$$\begin{aligned}
&(1+k)(1+\nu)[u' + \dot{v}\sin\theta + v\cos\theta + 2w\sin\theta] - k[\ddot{u}' - \dot{u}'\cot\theta \\
&\quad + u'(3+\cot^2\theta) + u'''\csc^2\theta + \dddot{v}\sin\theta + 2\ddot{v}\cos\theta - \dot{v}\cot\theta\cos\theta \\
&\quad + v(3+\cot^2\theta)\cos\theta + \dot{v}''\csc\theta + v''\cot\theta\csc\theta] + k[\ddddot{w}\sin\theta \\
&\quad + 2\dddot{w}\cos\theta - (1+\nu+\cot^2\theta)\ddot{w}\sin\theta + \dot{w}(2-\nu+\cot^2\theta)\cos\theta \\
&\quad - 2(1+\nu)w\sin\theta + 2\ddot{w}''\csc\theta - 2\dot{w}''\cot\theta\csc\theta + w''(3-\nu+4\cot^2\theta) \\
&\quad\ \csc\theta + w''''\csc^3\theta] - P[2w + \ddot{w} + \dot{w}\cot\theta + w''\csc^2\theta]\sin\theta \\
&\quad + [m_s + m_1 + m_2]\frac{\partial^2 w}{\partial t^2}\sin\theta = 0\ , \qquad (4.1.1)
\end{aligned}$$

$$\begin{aligned}
&(1+k)\left[\left(\frac{1+\nu}{2}\right)\dot{u}' - \left(\frac{3-\nu}{2}\right)u'\cot\theta + \ddot{v}\sin\theta + \dot{v}\cos\theta\right. \\
&\quad \left. - v\left(\frac{\cos^2\theta + \nu\sin^2\theta}{\sin\theta}\right) + \left(\frac{1-\nu}{2}\right)v''\csc\theta + (1+\nu)\dot{w}\sin\theta\right]
\end{aligned}$$

(continued)

$$- k[\dddot{w} \sin\theta + \ddot{w} \cos\theta + \dot{w}(1 - \cot^2\theta) \sin\theta + \dot{w}'' \csc\theta$$

$$- 2w'' \cot\theta \csc\theta] - m_s \frac{\partial^2 v}{\partial t^2} \sin\theta = 0 \ , \tag{4.1.2}$$

and

$$(1+k) \left[\left(\frac{1-\nu}{2}\right) \ddot{u} \sin\theta + \dot{u} \cos\theta - u(\cot^2\theta - 1)\sin\theta + u'' \csc\theta \right.$$

$$\left. + \left(\frac{1+\nu}{2}\right) \dot{v}' + \left(\frac{3-\nu}{2}\right) v' \cot\theta + (1+\nu)w' \right] - k[\ddot{w}' + \dot{w}' \cot\theta$$

$$+ 2w' + w''' \csc^2\theta] - m_s \frac{\partial^2 u}{\partial t^2} \sin\theta = 0 \ , \tag{4.1.3}$$

where

$$k = \frac{K}{DR^2} = \frac{h^2}{12R^2} \ , \tag{4.1.4}$$

$$D = \frac{Eh}{1-\nu^2} \ , \qquad K = \frac{Eh^3}{12(1-\nu^2)} \tag{4.1.5}$$

$$P = \frac{R\Delta p}{2D} \ , \tag{4.1.6}$$

$$m_s = \frac{R^2}{D} \mu_s \ , \quad m_1 = \frac{R^2}{D} \mu_2 \ , \quad m_3 = \frac{R^2}{D} \mu_3 \tag{4.1.7}$$

and

$$M_n = m_s + m_1 + m_2 \ . \tag{4.1.8}$$

u, v, w are the displacements in the φ, θ, and r directions, D is the extensional rigidity, K is the flexural rigidity, μ_s is the surface density of the shell and μ_1 and μ_2 are apparent density terms of the inner and outer liquids.

$$\frac{\partial}{\partial\theta}(\ ) = (\dot{\ })$$
$$\frac{\partial}{\partial\varphi}(\ ) = (\ )' \tag{4.1.9}$$

4.2 Solution

To solve equations (4.1.1), (4.1.2), and (4.1.3) a space-time separation of the following form will be attempted:

$$w(\theta,\varphi,t) = e^{i\sqrt{\sigma}t}\, W(\theta,\varphi)$$
$$v(\theta,\varphi,t) = e^{i\sqrt{\sigma}t}\, V(\theta,\varphi) \tag{4.2.1}$$
$$u(\theta,\varphi,t) = e^{i\sqrt{\sigma}t}\, U(\theta,\varphi) \ .$$

If the space-time separation is used in (4.1.1), (4.1.2), and (4.1.3) we obtain

$$L_{11}(w) + L_{12}(v) + L_{13}(u) + M_n \sigma W \sin\theta = 0 \tag{4.2.2}$$

$$L_{21}(w) + L_{22}(v) + L_{23}(u) + m_s \sigma V \sin\theta = 0 \tag{4.2.3}$$

and

$$L_{31}(w) + L_{32}(v) + L_{33}(u) + m_s \sigma U \sin\theta = 0 \ , \tag{4.2.4}$$

where L_{ik} $(i,k = 1,2,3)$ are linear differential operators as defined from (4.1.1), (4.1.2), and (4.1.3).

The space variables $W(\theta,\varphi)$, $V(\theta,\varphi)$, and $U(\theta,\varphi)$ can be expanded as

$$W(\theta,\varphi) = \sum_m \sum_n A_{mn} \cos m\varphi \; P_n^m(\cos\theta)$$

(continued)

$$\left.\begin{aligned} V(\theta,\varphi) &= \sum_m \sum_n B_{mn} \cos m\varphi \frac{d}{d\theta} P_n^m(\cos\theta) \\ U(\theta,\varphi) &= \sum_m \sum_n C_{mn} \sin m\varphi \csc\theta\, P_n^m(\cos\theta) \ . \end{aligned}\right\} \tag{4.2.5}$$

A differentiation of $U(\theta,\varphi)$ with respect to θ produces

$$\frac{\partial}{\partial\theta} U(\theta,\varphi) = \sum_m \sum_n C_{mn} \sin m\varphi \left[- \cot\theta \csc\theta\, P_n^m + \csc\theta \frac{d}{d\theta} P_n^m \right] \tag{4.2.6}$$

and

$$\begin{aligned} \frac{\partial^2}{\partial\theta^2} U(\theta,\varphi) = \sum_m \sum_n C_{mn} \sin m\varphi \Bigg[& (\csc^3\theta + \cot^2\theta \csc\theta) P_n^m \\ & - 2 \cot\theta \csc\theta \frac{d}{d\theta} P_n^m + \csc\theta \frac{d^2}{d\theta^2} P_n^m \Bigg] . \end{aligned} \tag{4.2.7}$$

Let

$$\frac{d}{d\theta} P_n^m = \dot{P}_n^m \qquad \text{and} \qquad \frac{d}{d\eta} P_n^m = P_n^{m\prime} , \tag{4.2.8}$$

where

$$\eta = \cos\theta \ . \tag{4.2.9}$$

By making use of (4.2.5), (4.2.6), (4.2.7), and (4.2.8), in (4.2.2), (4.2.3), and (4.2.4), the equations of motion become

$$\begin{aligned} \sum_m \sum_n \Bigg\{ A_{mn} \Bigg[& 2(1+k)(1+\nu) P_n^m + k \Bigg[\dddot{P}_n^m + 2\ddot{P}_n^m \cot\theta - \dot{P}_n^m \Big\{ 1 + \nu + \cot^2\theta \\ & + 2m^2 \csc^2\theta \Big\} + \dot{P}_n^m \cot\theta (2 - \nu + \cot^2\theta + 2m^2 \csc^2\theta) \\ & + P_n^m \Big\{ - 2(1+\nu) - m^2 \csc^2\theta (3 - \nu + 4 \cot^2\theta) + m^4 \csc^4\theta \Big\} \Bigg] \end{aligned}$$

(continued)

$$- P\left(2P_n^m + \ddot{P}_n^m + \dot{P}_n^m \cot\theta - m^2 P_n^m \csc^2\theta\right) - M_n \sigma_{mn} P_n^m \Big]$$

$$+ B_{mn} \Big[(1+k)(1+\nu)\left\{P_n^m + \dot{P}_n^m \cot\theta\right\} - k\Big\{\dddot{P}_n^m + 2\ddot{P}_n^m \cot\theta$$

$$-\ddot{P}_n^m(\cot^2\theta + m^2 \csc^2\theta) + \dot{P}_n^m \cot\theta(3 + \cot^2\theta - m^2 \csc^2\theta)\Big\}\Big]$$

$$+ C_{mn} \Big[(1+k)(1+\nu)m \csc^2\theta\, P_n^m - km \csc^2\theta \Big\{\ddot{P}_n^m - 3 \cot\theta\, \dot{P}_n^m$$

$$+ \csc^2\theta(4-m^2)P_n^m\Big\}\Big]\Big\} \cos m\varphi = 0 , \qquad (4.2.10)$$

$$\sum_m \sum_n \Big\{ A_{mn}\, k \sin\theta \Big[\dddot{P}_n^m + \ddot{P}_n^m \cot\theta + \dot{P}_n^m(1 - \cot^2\theta - m^2 \csc^2\theta$$

$$- (1+k)(1+\nu)/k) + 2m^2 P_n^m \cot\theta \csc^2\theta \Big] - B_{mn}(1+k) \Big[\dddot{P}_n^m \sin\theta$$

$$+ \ddot{P}_n^m \cos\theta - \dot{P}_n^m \sin\theta \Big\{ \cot^2\theta + \frac{m^2}{2} \csc^2\theta - \frac{m_s \sigma_{mn}}{1+k}$$

$$- \nu\left(\frac{m^2}{2} \csc^2\theta - 1\right)\Big\}\Big] - C_{mn}(1+k)(1+\nu)\, \frac{m}{2} \csc\theta \Big[\ddot{P}_n^m(1+\nu)$$

$$- 4\, P_n^m \cot\theta \Big]\Big\} \cos m\varphi = 0 , \qquad (4.2.11)$$

and

$$\sum_m \sum_n \Big\{ A_{mn}\, km \Big[\ddot{P}_n^m + \dot{P}_n^m \cot\theta + (2 - m^2 \csc^2\theta)P_n^m$$

$$- (1+k)(1+\nu)P_n^m/k \Big] - B_{mn}\, \frac{m}{2} \Big[\dddot{P}_n^m + 3\ddot{P}_n^m \cot\theta + \nu(\ddot{P}_n^m$$

$$- \dot{P}_n^m \cot\theta)\Big] (1+k) + C_{mn} \left(\frac{1+k}{2}\right) \Big[\ddot{P}_n^m - \cot\theta\, \dot{P}_n^m + 2(1 - m^2 \csc^2\theta)P_n^m$$

$$+ \left(\frac{2}{1+k}\right) m_s \sigma_{mn} P_n^m - \nu\left(\ddot{P}_n^m - \dot{P}_n^m \cot\theta + 2P_n^m\right)\Big]\Big\} \sin m\varphi = 0 .$$

4.3 Apparent Mass Terms

For an incompressible fluid under irrotational flow, continuity requires that

$$\nabla^2\Phi = 0 \ . \tag{4.3.1}$$

In addition, as was previously the case, the solution to Laplace's equation for the internal and external liquids are

$$\left.\begin{aligned} \Phi_1 &= \sum_m \sum_n e^{i\sqrt{\sigma}t} D_{mn} r^n \cos m\varphi \, P_n^m \qquad r \le R \\ &\text{and} \\ \Phi_2 &= \sum_m \sum_n e^{i\sqrt{\sigma}t} E_{mn} r^{-(n+1)} \cos m\varphi \, P_n^m \qquad r \ge R \ . \end{aligned}\right\} \tag{4.3.2}$$

The kinematic boundary conditions require that

$$\frac{\partial w}{\partial t} = -\frac{\partial \Phi_1}{\partial r} = -\frac{\partial \Phi_2}{\partial r} \quad \text{at} \quad r = R \ . \tag{4.3.3}$$

By making use of (4.3.3), (4.2.1) and (4.2.5) in (4.3.2) and the orthogonality of the $\cos m\varphi$'s and P_n^m's, we find that

$$i\sqrt{\sigma}\,A_{mn} = -D_{mn} n R^{n-1} = E_{mn}(n+1)R^{-(n+2)} \ . \tag{4.3.4}$$

A rearrangement of (4.3.4) produces

$$\left.\begin{aligned} D_{mn} &= -\frac{i\sqrt{\sigma}}{nR^{n-1}} A_{mn} \\ &\text{and} \\ E_{mn} &= \frac{i\sqrt{\sigma}}{n+1} R^{n+2} A_{mn} \ . \end{aligned}\right\} \tag{4.3.5}$$

If μ_1 and μ_2 are defined by

$$\left.\begin{aligned} &\mu_1 \frac{\partial^2 w}{\partial t^2} = - \rho_1 \frac{\partial \Phi_1}{\partial t} \quad \text{at} \quad r = R \\ \text{and} \\ &\mu_2 \frac{\partial^2 w}{\partial t^2} = \rho_2 \frac{\partial \Phi_2}{\partial t} \quad \text{at} \quad r = R , \end{aligned}\right\} \tag{4.3.6}$$

when using (4.3.5) in (4.3.6) we obtain

$$\mu_1 = \frac{\rho_1 R}{n} , \qquad \mu_2 = \frac{\rho_2 R}{n+1} . \tag{4.3.7}$$

In addition M_n becomes

$$M_n = \frac{R^2}{D} \left[\mu_s + \frac{\rho_1 R}{n} + \frac{\rho_2 R}{n+1} \right] . \tag{4.3.8}$$

Rather than continue with the complete solution at this time, it is better to treat several special cases which are easily attacked from this point. The complete solution will be treated in section 4.7.

4.4 Special Case 1: One Degree of Freedom Shell Model

Consider that the shell has only one degree of freedom, that is, the displacement can only be radial e.g.

$$\left.\begin{aligned} &A_{mn} = A_{mn} \\ &B_{mn} = C_{mn} = 0 . \end{aligned}\right\} \tag{4.4.1}$$

If use is made of the orthogonality of the $\cos m\varphi$ terms and (4.4.1), equation (4.2.10) reduces, for each value of m, to

$$\sum_n A_{mn}\left\{2(1+k)(1+\nu)P_n^m + k\left[\dddot{P}_n^m + 2\ddot{P}_n^m \cot\theta - \ddot{P}_n^m(1+\nu + \cot^2\theta + 2m^2 \csc^2\theta)\right.\right.$$

$$+ \dot{P}_n^m \cot\theta(2-\nu + \cot^2\theta + 2m^2 \csc^2\theta) + P_n^m \left[-2(1+\nu) - m^2 \csc^2\theta(3\right.$$

$$\left.\left. - \nu + 4 \cot^2\theta) + m^4 \csc^4\theta\right]\right] - P(2P_n^m + \ddot{P}_n^m$$

$$\left. + \dot{P}_n^m \cot\theta - m^2 P_n^m \csc^2\theta) - M_n \sigma_{mn} P_n^m\right\} = 0 . \qquad (4.4.2)$$

By making use of (8.3.3), (8.3.4), (8.3.5), (8.3.6) in Appendix A, define I_1 as

$$I_1 = \dddot{P}_n^m + 2\ddot{P}_n^m \cot\theta - \left[1 + \cot^2\theta + 2m^2 \csc^2\theta\right] \ddot{P}_n^m$$

$$+ \cot\theta \left[2 + \cot^2\theta + 2m^2 \csc^2\theta\right] \dot{P}_n^m - \left[2 + m^2(3 + 4 \cot^2\theta)\csc^2\theta\right.$$

$$\left. - m^4 \csc^4\theta\right] P_n^m = (1-\eta^2)^2 P_n^{m''''} - 8\eta(1-\eta^2)P_n^{m'''} + \left[13\eta^2 - 5 - 2m^2\right] P_n^{m''}$$

$$+ 2\eta P_n^{m'} - \left[2 - \frac{m^2}{1-\eta^2} - \frac{m^2(m^2-4)}{(1-\eta^2)^2}\right] P_n^m . \qquad (4.4.3)$$

When using (8.3.12) and (8.3.10), (4.4.3) reduces to

$$I_1 = \left[n^2(n+1)^2 - n(n+1) - 2\right] P_n^m . \qquad (4.4.4)$$

Similarly define I_2 as

$$I_2 = - \ddot{P}_n^m - \dot{P}_n^m \cot\theta - P_n^m(2 - m^2 \csc^2\theta)$$

$$= - (1-\eta^2)P_n^{m''} + 2\eta P_n^{m'} - \left(2 - \frac{m^2}{1-\eta^2}\right) P_n^m . \qquad (4.4.5)$$

Legendre's equation, reduces (4.4.5) to

$$I_2 = (n+2)(n-1)P_n^m . \qquad (4.4.6)$$

The use of (4.4.4) and (4.4.6), permits (4.4.2) to be rewritten

$$\sum_n A_{mn}\left\{2(1+k)(1+\nu) + k\left[n^2(n+1)^2 - n(n+1) - 2 + \nu(n+2)(n-1)\right]\right.$$

$$\left. + P(n+2)(n-1) - M_n\sigma_{mn}\right\} P_n^m = 0 \ . \qquad (4.4.7)$$

By making use of the orthogonality of the P_n^m's, this reduces to the requirement that

$$2(1+k)(1+\nu) + k\left[n^2(n+1)^2 - n(n+1) - 2 + \nu(n+2)(n-1)\right]$$

$$+ P(n+2)(n-1) + M_n\sigma_{mn} = 0 \ , \qquad (4.4.8)$$

from which σ_{mn} is found to be

$$\sigma_{mn} = \left\{2(1+k)(1+\nu) + k(n+2)(n-1)\left[n(n+1)+(1+\nu) + P/K\right]\right\}\Big/ M_n \qquad (4.4.9)$$

Or, from the previously defined symbols of (3.2.3), (4.1.6) and (4.3.8), σ_{mn} becomes

$$\sigma_{mn} = \frac{n\left\{4\Lambda(1+k) + R\Delta p(n+2)(n-1) + \frac{2K}{R^2}(n+2)(n-1)\left[n(n+1)+(1+\nu)\right]\right\}}{2R^3\left[\rho_1 + \rho_2\frac{n}{n+1} + \frac{\mu_s n}{R}\right]} \ . \qquad (4.4.10)$$

When comparing this result to that for the droplet and membrane models it is seen that

(a) the one degree of freedom shell solution is a linear superposition of the droplet model and terms due to the membrane and bending stresses;

(b) even for this shell model the eigenfrequencies are independent of m (in the one degree of freedom case);

(c) the radial (n=0) mode vanishes due to the nature of the apparent mass term. This is an obvious consequence of the assumption that the fluid contained in the shell is imcompressible.

Fig. 4.1 shows a graph of σ_{mn} versus intraocular pressure for the one degree of freedom shell model for $n = 0,1,\ldots,6$. The physical constants used are the same as for the previous models.

At a nominal pressure of 20 mm Hg the lowest pressure dependent eigenfrequency is 193 cps.

Fig. 4.2 shows a comparison between the one degree of freedom droplet, membrane, and shell models. From this figure it can be seen that

(a) only for $n \geq 4$ do the membrane and shell models differ appreciably. For $n = 3$ the frequency difference is approximately 1%. Even for the $n = 4$ mode the frequency difference is only about 3%. This is as one would expect since bending terms are only important for the higher modes;

(b) the marked difference between the elastic models and the droplet model indicates that the elastic properties play an important part in the dynamic behavior of the eye.

4.5 Special Case 2: Axisymmetric Modes

If m is set equal to zero, (v, u no longer neglected) in (4.2.10), (4.2.11), and (4.2.12) it is found that the equations of motion separate into two groups:

(a) equation (4.2.12) becomes independent of A_{mn} and B_{mn} and therefore describes a completely torsional oscillation. Since this oscillation is independent of pressure (no pressure terms appear in the equation) it is uninteresting with regard to the originally stated objectives and so will not be discussed further;

(b) equations (4.2.10) and (4.2.11) interconnect A_{mn} and B_{mn} (and are independent of C_{mn}) and therefore describe a motion which is partly radial and partly tangential.

A similar condition was discovered by Lamb[16] in which he considered the problem of a vibrating spherical membrane. He referred to these separate vibrations as vibrations of the First and Second Classes. His problem will be discussed in section 4.6.

If $m = 0$ and use is made of the orthogonality of the $\cos m\varphi$ terms, equations (4.2.10) and (4.2.11) reduce to

$$\sum_n \Bigg[\Bigg[A_n \Bigg[2(1+k)(1+\nu)P_n + k\Big(\ddddot{P}_n + 2\dddot{P}_n \cot\theta - \ddot{P}_n(1+\nu + \cot^2\theta) + \dot{P}_n \cot\theta(2-\nu + \cot^2\theta) - 2P_n(1+\nu)\Big) - P(2P_n + \ddot{P}_n + \dot{P}_n \cot\theta) - M_n \sigma_n P_n \Bigg] + B_n \Bigg[(1+k)(1+\nu)(\ddot{P}_n + \dot{P}_n \cot\theta) - k\Big\{ \ddddot{P}_n + 2\dddot{P}_n \cot\theta - \ddot{P}_n \cot^2\theta + \dot{P}_n \cot\theta(3 + \cot^2\theta)\Big\}\Bigg]\Bigg]\Bigg] = 0 \tag{4.5.1}$$

and

$$\sum_n \left\{ A_n k \left[\dddot{P}_n + \ddot{P}_n \cot\theta + \dot{P}_n\left(1 - \cot^2\theta - \frac{(1+\nu)(1+k)}{k}\right)\right] - B_n(1+k)\left[\dddot{P}_n + \ddot{P}_n \cot\theta - \dot{P}_n\left(\cot^2\theta + \nu - \frac{m_s \sigma_n}{1+k}\right)\right]\right\} = 0 . \tag{4.5.2}$$

If use is made of (4.4.4), (4.4.6), (4.5.4), (4.5.6), (4.5.8), and (4.5.10) in (4.5.1) and (4.5.2), this produces

$$\sum_n \Big\{ A_n \Big[2(1+k)(1+\nu) + k(n+2)(n-1) \Big[\!\Big[n(n+1) + 1 + \nu + P/k \Big]\!\Big] - M_n \sigma_n \Big]$$

$$- B_n \Big[+(1+k)(1+\nu)n(n+1) + kn(n+1)(n+2)(n-1) \Big] \Big\} P_n = 0 \qquad (4.5.11)$$

and

$$\sum_n \Big\{ A_n k \Big[(n-1)(n+2) + \frac{(1+\nu)(1+k)}{k} \Big] - B_n(1+k) \Big[(n-1)(n+2) + (1+\nu)$$

$$- \frac{m_s \sigma_n}{1+k} \Big] \Big\} (n+1) \Big[\eta P_n - P_{n+1} \Big] = 0 \ . \qquad (4.5.12)$$

By using (8.2.7), $\eta P_n - P_{n+1}$ becomes

$$\eta P_n - P_{n+1} = \frac{n}{2n+1} \Big[P_{n-1} - P_{n+1} \Big] \ . \qquad (4.5.13)$$

When differentiating (4.5.13) with respect ot η we obtain

$$\frac{d}{d\eta} \Big[\eta P_n - P_{n+1} \Big] = \frac{n}{2n+1} \frac{d}{d\eta} \Big[P_{n-1} - P_{n+1} \Big]$$

$$= \frac{n}{2n+1} \Big[P'_{n-1} - P'_{n+1} \Big]^* = - nP_n \ . \qquad (4.5.14)$$

If we differentiate (4.5.12) and apply (4.5.13) and (4.5.14), we find that

$$\sum_n \Big\{ A_n k \Big[(n-1)(n+2) + \frac{(1+\nu)(1+k)}{k} \Big] - B_n(1+k) \Big[(n-1)(n+2)$$

$$+ (1+\nu) - \frac{m_s \sigma_n}{1+k} \Big] \Big\} n(n+1)P_n = 0 \ . \qquad (4.5.15)$$

*Note: $P'_{n+1} - P'_{n-1} = (2n+1)P_n$, (see reference 18, p. 136).

In conjunction with (8.3.3), (8.3.4), (8.3.5), and (8.3.6), we define I_3, I_4, I_5, and I_6 in the following manner:

$$I_3 = \ddddot{P}_n + 2\dddot{P} \cot\theta - \ddot{P}_n \cot^2\theta + \dot{P}_n \cot\theta(3 + \cot^2\theta)$$

$$= (1-\eta^2)^2 P''''_n - 8\eta(1-\eta^2)P'''_n + 4(3\eta^2-1)P''_n \ . \qquad (4.5.3)$$

With (8.3.12) and (8.3.10), this becomes

$$I_3 = n(n+1)(n+2)(n-1)P_n \ . \qquad (4.5.4)$$

Also

$$I_4 = \ddot{P}_n + \dot{P}_n \cot\theta = (1-\eta^2)P''_n - 2\eta P'_n \ . \qquad (4.5.5)$$

Legendre's equation reduces this to

$$I_4 = - n(n+1)P_n \ . \qquad (4.5.6)$$

In addition

$$I_5 = \left[\dddot{P}_n + \ddot{P}_n \cot\theta - \dot{P}_n \cot^2\theta\right] \sin\theta$$

$$= - (1-\eta^2) \left[(1-\eta^2)P'''_n - 4\eta P''_n - P'_n\right]. \qquad (4.5.7)$$

When combining (4.5.7), (8.3.11), and (8.3.9) we obtain

$$I_5 = (n+1)\left[(n-1)(n+2) + 1\right]\left[\eta P_n - P_{n+1}\right]. \qquad (4.5.8)$$

Let

$$I_6 = \dot{P}_n \sin\theta = - (1-\eta^2)P'_n \ . \qquad (4.5.9)$$

With (8.3.9) this reduces to

$$I_6 = - (n+1) \left[\eta P_n - P_{n+1}\right]. \qquad (4.5.10)$$

Since the P_n's are orthogonal functions, (4.5.11) and (4.5.15) require that

$$A_n \left[2(1+k)(1+\nu) + k(n+2)(n-1) \left\{ n(n+1) + (1+\nu) + P/k \right\} - M_n \sigma_n \right]$$
$$- B_n \left[(1+k)(1+\nu) + k(n+2)(n-1) \right] n(n+1) = 0 \qquad (4.5.16)$$

and

$$A_n k \left[(n-1)(n+2) + \frac{(1+\nu)(1+k)}{k} \right] - B_n (1+k) \left[(n-1)(n+2) \right.$$
$$\left. + (1+\nu) - \frac{m_s \sigma_n}{1+k} \right] = 0 \ . \qquad (4.5.17)$$

The fact that these are linear homogeneous algebraic equations for each value of n implies that solutions for the constants, A_n and B_n, exist only if the determinant of their coefficients is zero. This requires that the frequency equation be

$$\left[2(1+k)(1+\nu) + k(n+2)(n-1) \left\{ n(n+1) + (1+\nu) + P/k \right\} - M_n \sigma_n \right]$$
$$\left[(n-1)(n+2)+(1+\nu) - \frac{m_s \sigma_n}{1+k} \right] (1+k) - k \left[(n-1)(n+2) \right.$$
$$\left. + \frac{(1+\nu)(1+k)}{k} \right] \left[(1+k)(1+\nu) + k(n+2)(n-1) \right] n(n+1) = 0 \ . \qquad (4.5.18)$$

This may be rewritten as

$$a\sigma_n^2 - b\sigma_n + c = 0 \ , \qquad (4.5.19)$$

where

$$a = m_s M_n$$
$$b = + (M_n + 2m_s)(1+\nu)(1+k) + (n+2)(n-1) \left[M_n (1+k) + m_s k \left\{ n(n+1) \right. \right.$$
$$\left. \left. + (1+\nu) + P/k \right\} \right]$$

(continued)

$$c = (1+k)\left[(n-1)(n+2)+(1+\nu)\right]\left[2(1+k)(1+\nu) + k(n+2)(n-1)\left\{n(n+1)\right.\right.$$
$$\left.\left. + (1+\nu) + P/k\right\}\right] - n(n+1)\left[(1+k)(1+\nu) + k(n-1)(n+2)\right]^2 . \qquad (4.5.20)$$

It should be noted that the frequency equation (4.5.19) is a quadratic which implies that for each value of n there are two independent eigenfrequencies. It follows therefore that there are also two independent eigenfunctions or mode shapes (see Appendix D). Since the product $4ac$ is small compared to b^2 (from (4.5.16)) these two frequencies (corresponding to each n) differ by about an order of magnitude.

Fig. 4.3 shows a plot of the eigenfrequency squared versus the intraocular pressure (calculations were based on the nominal values previously discussed). It should be noted that the high frequency modes are almost pressure independent (for the $n = 2,3,4,5,6$ modes the frequency changes less than .01% from 0 to 40 mm Hg). The low frequency $n = 0,1$ modes both have zero eigenfrequency. These correspond to radial pulsation and translation (see Appendix D) the first of which is clearly impossible, and the second having no restoring force has no oscillation. The frequency for nominal pressure of 20 mm Hg for the first observable mode ($n = 2$) is 85 cps.

Fig. 4.4 compares the one degree of freedom and two degree of freedom shell models. It should be noted that the frequencies for corresponding modes are lower for the two degree of freedom model than for the one degree of freedom model.

4.6 Special Case 3: Two Degree of Freedom Membrane Model

The results of section 4.5 permit a comparison between the two degree of freedom models to assess the effects of bending. By setting

$k = 0$ in (4.5.16) and (4.5.17), the effects of bending are eliminated and the solution is valid for the two degree of freedom membrane model. The frequency equation with $k = 0$ becomes

$$a\sigma_n^2 - b\sigma_n + c = 0 \tag{4.6.1}$$

where

$$\begin{aligned} a &= m_s M_n \\ b &= (M_n + 2m_s)(1+\nu) + (n+2)(n-1)\left[M_n + m_s P\right] \\ c &= \left[(n-1)(n+2)+(1+\nu)\right]\left[2(1+\nu)+(n+2)(n-1)P\right] - n(n+1)(1+\nu)^2 \end{aligned} \tag{4.6.2}$$

If the internal and external liquids and the pressure terms are eliminated, this reduces to Lamb's[16] solution for a vibrating membrane.

Fig. 4.5 shows a graph of σ_n versus intraocular pressure for the $n = 1,2,\ldots,6$ modes for the two degree of freedom membrane model. (All calculations based on previously mentioned nominal constants). The modes shown are the low frequency modes (Note: there are two eigenfrequencies and mode shapes for each value of n since the frequency equation is quadratic) which are the most pressure dependent and therefore the most interesting for the problem being considered. At a nominal intraocular pressure of 20 mm Hg, the lowest mode $(n = 2)$ corresponds to a frequency of 84 cps.

Fig. 4.6 compares the one and two degree of freedom membrane models. As predicted by theory the two degree of freedom model exhibits lower frequencies than the one degree of freedom model. It should also be noted that the corresponding slopes for the two degree model are the same as for the one degree model. Camparative frequencies for $n = 2$ at 20 mm Hg are 193 and 84 cps for the one and two degree of freedom models respectively.

Fig. 4.7 compares the two degree of freedom membrane and shell models for $n = 1,2,\ldots,6$. As was the case with the one degree of freedom models the curves do not differ appreciably until $n \geq 4$. This is to be expected since the modes exhibit little bending until $n = 4$ (see Appendix D for mode shapes). It should also be noted that the slopes of the corresponding curves are exactly the same. This could have been anticipated by examining equation (4.5.20) which shows that the pressure term is unaffected by bending.

4.7 The Complete Shell Model

A brief discussion describing the solution of the complete equations of motion (4.2.10), (4.2.11), and (4.2.12) will now be given. A more detailed description can be found in Appendix B.

By rewriting equations (4.2.10), (4.2.11) and (4.2.12) the orthogonality of the $\sin m\varphi$, $\cos m\varphi$, and P_n^m terms can be taken advantage of to "reduce" the equations of motion to three algebraic equations for each value of m and ℓ. These equations can be written as (ℓ has replaced n as the axisymmetric mode number)

$$\begin{aligned} &A_{m,\ell-4} J^1_{m\ell} + A_{m,\ell-2} J^2_{m\ell} + A_{m,\ell} J^3_{m\ell} + A_{m,\ell+2} J^4_{m\ell} + A_{m,\ell+4} J^5_{m\ell} \\ &+ B_{m,\ell-4} J^6_{m\ell} + B_{m,\ell-2} J^7_{m\ell} + B_{m,\ell} J^8_{m\ell} + B_{m,\ell+2} J^9_{m\ell} \\ &+ B_{m,\ell+4} J^{10}_{m\ell} + C_{m,\ell-2} J^{11}_{m\ell} + C_{m\ell} J^{12}_{m\ell} + C_{m,\ell+2} J^{13}_{m\ell} = 0 \; , \quad (4.7.1) \end{aligned}$$

$$A_{m,\ell-3} J^{14}_{m\ell} + A_{m,\ell-1} J^{15}_{m\ell} + A_{m,\ell+1} J^{16}_{m\ell} + A_{m,\ell+3} J^{17}_{m\ell}$$

$$+ B_{m,\ell-3} J^{18}_{m\ell} + B_{m,\ell-1} J^{19}_{m\ell} + B_{m,\ell+1} J^{20}_{m\ell} + B_{m,\ell+3} J^{21}_{m\ell}$$

$$+ C_{m,\ell-1} J^{22}_{m\ell} + C_{m,\ell+1} J^{23}_{m\ell} = 0 \,, \tag{4.7.2}$$

and

$$A_{m,\ell-2} J^{24}_{m\ell} + A_{m,\ell} J^{25}_{m\ell} + A_{m,\ell+2} J^{26}_{m\ell} + B_{m,\ell-2} J^{27}_{m\ell} + B_{m,\ell} J^{28}_{m\ell}$$

$$+ B_{m,\ell+2} J^{29}_{m\ell} + C_{m,\ell-2} J^{30}_{m\ell} + C_{m,\ell} J^{31}_{m\ell} + C_{m,\ell+2} J^{32}_{m\ell} = 0 \,, \tag{4.7.3}$$

where the A's, B's, and C's are the expansion coefficients defined in (4.2.5) and the J's are defined in Appendix B.

Equations (4.7.1), (4.7.2), and (4.7.3) each constitute an infinite set (one equation for each value of ℓ, with $\ell = 1,2,\ldots$) of linear homogeneous algebraic equations for each value of m ($m = 0,1,\ldots,\ell$). In order for a nontrivial solution for the A's, B's, and C's to exist, the determinant of their coefficients must vanish. This determinantal equation constitutes the frequency equation for each value of m.

A solution is not possible unless the determinant is truncated at some finite order. Although the solution obtained by truncating the determinant is not exact, a nearly exact solution can be obtained by considering enough terms. In order to solve these equations for the eigenfrequencies a digital computer program was developed that computes the $J^i_{m\ell}$'s ($i = 1,2,\ldots,32$) for specified values of m and ℓ, evaluates the truncated determinant for varied values of σ, and plots the value of the determinant as a function of σ. The curve crosses the abscissa (determinant equals zero) at the eigenfrequencies.

Truncating the determinant at $\ell = 6$, equations (4.7.1), (4.7.2), and (4.7.3) have been solved for $m = 0,1,\ldots,5$.

Figures 4.8 through 4.12 are graphs of the eigenfrequency (in cps) versus pressure (in mm Hg) of asymmetric vibrations for $\ell = 2,3,4,5,6$ respectively. Each figure shows curves for $m = 0,\ldots,\ell$, that is those asymmetric modes which exist for each calue of ℓ. These curves were plotted using the following nominal physical values:

$R = 1.3$ cm

$h = 0.1$ cm

$E = 7 \times 10^6$ dynes/cm^2 ,

with the other constants being taken as previously. It should be noted that these curves all show the same general characteristics (except $\ell = 6$), that is, all of the curves lie within an envelope bounded by the $m = 0$ and $m = 1$ curves. The fact that for $m > 1$ the curves approach (decrease towards) the $m = 0$ curve seems to defy the principle that the eigenfrequency should increase monotonically with increasing constraints, as reflected by nodal lines and points. In reality this is not true since the $m = 1$ mode actually has the most nodal lines and points. This can readily be seen if the displacements are examined for various modes. Taking for example the $\ell = 2$ modes, it is found that for $m = 0$, v vanishes at $\cos\theta = 0, \pm 1$ and w vanishes at $\cos\theta = \pm 1/\sqrt{3}$. (These are not really nodes but pseudo-nodes in that not all components of the displacement vanish at these points. Nodes only exist at the poles and never occur for the $m = 0,1$ modes). For $m = 1$, u vanishes at $\cos\theta = 0, \pm 1$, v vanishes at $\cos\theta = \pm 1/\sqrt{2}$, and w vanishes at $\cos\theta = 0, \pm 1$. For $m = 2$, u vanishes at $\cos\theta = \pm 1$, v vanishes at $\cos\theta = 0, \pm 1$, and w vanishes at $\cos\theta = \pm 1$. Figure 4.13 shows these nodal lines and points.

As can be seen the $m = 1$ mode does have more points constrained than either $m = 0$ or $m = 2$. But it should also be noted that the $m = 2$ mode involves less constraints than the $m = 0$ mode. This would imply a lower frequency for $m = 2$ than for $m = 0$ which does not appear in the frequency pressure curves. This discrepancy may be attributed to the fact that the expansions for the displacements were truncated after six terms. An expansion with more terms might give better agreement. Figure 4.12 shows that the $\ell = 6$, $m = 5$ mode has a lower frequency than the $\ell = 6$, $m = 0$ mode which would seem to substantiate this premise, since the $m = 0$ mode is more constrained than the $m = 5$ mode. This explanation does not consider the strength of the constraints. The $m = 0$ mode may have weaker constraints than the $m = 2$ mode which would account for its lower frequency.

At a nominal intraocular pressure of 20 mm Hg the asymmetric vibrations exhibit eigenfrequencies of 136 cps for the $n = 2$, $m = 1$ mode and 100 cps for the $n = 2$, $m = 2$ mode. In comparison the axisymmetric mode ($n = 2$, $m = 0$) has a natural frequency of 84 cps and the one degree of freedom model has a corresponding eigenfrequency of 193 cps at 20 mm Hg.

The asymmetric vibrations were also examined with respect to the influence of E and h. Figures 4.14, 4.15, and 4.16 show curves of the eigenfrequency (in cps) versus the intraocular pressure (in mm Hg) of asymmetric vibrations for $\ell = 2,3,4$ with Young's modulus equal to

7×10^5 dynes/cm^2. As can be seen, these curves have the same general appearance as in the case of $E = 7 \times 10^6$ dynes/cm^2, except that the frequencies are lower for corresponding modes, and the dependence on the number of nodal lines (m) is less pronounced. For $n = 2$, $m = 0$ the eigenfrequency at 20 mm Hg is 38 cps.

Some qualitative results which may be extracted from this analysis and the numerical results are:

1- the square of the eigenfrequency appears to be a linear function of the intraocular pressure. That is, the frequency-pressure relation may be written as

$$\sigma_{m\ell} = \frac{d\sigma_{m\ell}}{dP} P + (\sigma_o)_{m\ell} \; ; \tag{4.7.4}$$

2- $$\frac{d\sigma_{m\ell}}{dP} = g_1(R) g_2(\ell) \; , \tag{4.7.4}$$

where $g_1(R)$ and $g_2(\ell)$ are functions of R and ℓ respectively. It should be noted that $d\sigma_{m\ell}/dP$ is independent of m but $d\sqrt{\sigma_{m\ell}}/dP$ is not. The latter is obvious since $(\sigma_o)_{mn}$ is a function of m.

3- $(\sigma_o)_{m\ell}$ may be described by

$$(\sigma_o)_{m\ell} = \sigma_{m\ell}\Big|_{P=0} = E\, G_1(h,R,\ell,m) \tag{4.7.5}$$

$$\approx Eh\, G_2(R,\ell,m) \quad \text{for} \quad \ell \le 4, \tag{4.7.6}$$

where G_1 and G_2 are functions of the variables shown. For the low frequency modes $\ell \le 4$ bending does not play a major role. $d\sigma_{m\ell}/dP$ can be obtained in closed form from the one degree of freedom model and is approximately valid (better than 2%) for all models. From (4.4.10), it can be written as

$$\frac{d\sigma_{m\ell}}{dP} = \frac{n(n+2)(n-1)}{2R^2\left[\rho_1 + \rho_2\left(\frac{n}{n+1}\right) + \frac{\mu n}{R}\right]} . \qquad (4.7.7)$$

V. VARIATION OF PHYSICAL CONSTANTS

Since it is obvious that all eyes are not identical, it is necessary to examine the effects of variations of the constants associated with the corneo-scleral membrane. It has been assumed that the nominal constants associated with the eye are

$R = 1.3$ cm

$h = 0.1$ cm

$E = 7.0 \times 10^6$ dyne/cm^2

$\mu = 0.1$ gm/cm^2

$\rho_1 = \rho_2 = 1.0$ gm/cm^3

$\nu = .5$.

The effects of small variations of these constants on the frequency (and therefore the intraocular pressure determination) will be examined using the axisymmetric shell solution (4.5.19). Since this solution has been obtained in closed form results can be obtained fairly readily.

Figure 5.1 shows the effect of radius variation on the frequency-pressure relation. Here the equilibrium radius was varied $\pm$ 0.1 cm ($\pm$ 7.7%) from a nominal value of 1.3 cm. At 20 mm Hg this radius variation corresponds to a 21.4% variation of frequency in the $n = 2,3$ modes, 21.7% in the $n = 4$ mode, 22.9% in the $n = 5$ mode, and 24.4% in the $n = 6$ mode.

Figure 5.2 shows the effect of a variation of the effective scleral thickness on the frequency-pressure relation. Here the effective thickness was varied $\pm$ 10%) from a nominal value of 1.0 mm. At 20 mm Hg this thickness variation corresponds to an 9.1% variation in the $n = 2,3$

modes, 9.9% in the $n = 4$ mode, 11.6% in the $n = 5$ mode and 13.6% in the $n = 6$ mode.

Figure 5.3 shows the effect of a variation in the modulus of elasticity on the frequency-pressure relation. Here E was varied $\pm 0.5 \times 10^6$ dynes/cm^2 ($\pm$ 7.1%) from a nominal value of 7.0×10^6 dynes/cm^2. At 20 mm Hg this variation in Young's modulus corresponds to a 6.3% variation in the $n = 2$ mode, 5.6% in the $n = 3$ mode, 5.1% in the $n = 4$ mode, 4.9% in the $n = 5$ mode and 4.8% in the $n = 6$ mode.

This problem has also been examined with regard to variations of the scleral density, vitreous density and external tissue density. In each case a variation of $\pm$ 5% was assumed. Here frequency variations at 20 mm Hg amounted to only 0.5% for the $n = 2$ mode and 1.2% for the $n = 6$ mode for variation of the scleral density; 2.5% for the $n = 2$ mode and 2.0% for the $n = 6$ mode for variation of the vitreous density; and 1.7% for the $n = 2$ and $n = 6$ modes for variation of the external tissue density. Since these variations were so small they were not graphically illustrated.

A goal of this analysis is the determination of Young's modulus and an effective thickness of the corneo-scleral membrane by comparison with experiment. Since the scleral thickness varies appreciably (from 0.3 mm to 1.0 mm in the human eye) it will be necessary to introduce an effective thickness. Recent experiments at Ames Research Center by Anliker[17] indicate that the elastic properties of blood vessels in dogs may vary by as much as an order of magnitude depending on the stress imposed on the animals. This indicates that the value of 7×10^6 dynes/cm^2 considered here is at best an estimate of the order of magnitude of E.

Figure 5.4 compares the $n = 2,\ldots,6$ modes for values of the modulus of elasticity differing by a factor of 10. Note that lowering E by an order of magnitude radically changes both the slope and the frequency. At 20 mm Hg the $n = 2$ mode exhibits frequencies of 85 and 38 cps for $E = 7 \times 10^6$ and $E = 7 \times 10^5$ dynes/cm^2 respectively.

Figure 5.5 compares the $n = 2,\ldots,6$ modes for values of the effective thickness, of the sclera, differing by a factor of 10. Comparing this with Fig. 5.4 shows that decreasing either E or h by an order of magnitude produces almost the exact same effect for the $n = 2,3,4$ modes, that is, the curves for $E = 7.0 \times 10^5$ dynes/cm^2 and $h = 0.1$ mm are almost coincident. But the $n = 5,6$ modes do show substantial differences. This is not surprising since bending effects are insignificant for $n \leq 4$.

This similarity in varying E and h for $n \leq 4$ implies that the modulus of elasticity and the effective thickness can only be determined from the frequency spectrum if we also admit modes corresponding to $n > 4$.

VI. EXPERIMENTAL PROGRAM

The objective of the experimental program was to obtain preliminary data concerning the dynamic and static behavior of the eye in order to validate the theoretical considerations described in the previous chapters.

6.1 Dynamic Experiment

The original experimental concept was to excite vibrations of the eye using a sound source (e.g. audio speaker) and determine the resonance frequencies by monitoring the surface deflection optically. Figure 6.1 shows the arrangement of the experimental apparatus devised for this purpose.

The deflection was measured using an MTI KD-45 Fotonic Sensor with a resolution of ten microinches. The instrument employs an 1/8 inch diameter fiber optics bundle to illuminate the object and to conduct the reflected light to a photocell, the output of which is a measure of the relative displacement between the sensor and the reflecting surface. The frequency response of this instrument is d.c. to 60 kc. The signal from the Fotonic Sensor was fed into an oscilloscope whose maximum sensitivity was .001 volt per centimeter. The intraocular pressure was measured using a water column and a hypodermic needle (sizes ranging from #19-25).

The experimental procedure was:

(1) select the infusion pressure by raising the level of the water column;

(2) wait approximately two minutes to allow for a steady state pressure equilibrium;

(3) activate the excitation device (e.g. speaker);

(4) vary the frequency until resonance is observed.

The difficulties encountered in a feasibility experiment on the eye of an anesthetized dog demanded that for an initial study enucleated eyes should be used.

Several experiments were performed with a Jensen 120-W woofer as a sound source. However, it was found that much of the vibratory energy was dissipated in the Fotonic Sensor and its support making it extremely difficult to detect the ocular resonances. By locating the apparatus on a concrete floor, orienting the speaker to maximize the energy transmission to the eye and applying maximum power to the speaker (~ 30 watts) a signal of approximately 15 millivolts could be obtained, with a signal to noise ratio of 3.

Since it was decided that verification of the theory was of primary concern the speaker was replaced by a mechanical vibrator obtained on loan from the Ames Research Center of the NASA. The vibrator consisted of a magnesium tube connected to a ferromagnetic core which was driven by an a.c. excited coil. With the vibrator directly contacting the eye, the amplitude of the exciting vibrations could be controlled so that an adequate resonance signal could be obtained. It was also necessary to limit the vibration amplitude so as not to distort the eye. A measure of the distortion is the change in intraocular pressure when the vibrator is removed from contact with the eye. This was usually about 3 mm H_2O at a nominal pressure of 97 cm H_2O.

Figure 6.2 shows a graph of σ versus the intraocular pressure for a typical set of data obtained by this method. The data will be discussed in the next chapter.

Some experimental observations are:

(1) The material surrounding the eye (fat, tissue, etc.) has extremely good damping properties and must be thoroughly removed to assure a sufficiently strong signal.

(2) In most of the experiments performed the eye was excited near the optic nerve in order to excite axisymmetric modes and make use of a scleral reflecting surface.

(3) The sensitivity of the Fotonic Sensor is a function of the reflectivity of the surface; a better signal was obtained when the sensor was positioned over the sclera rather than the cornea.

(4) Fastening the pressure connection (hypodermic needle) with respect to the eye-support seemed to have little effect on the resonance values.

(5) The resonance frequencies seemed to be lower when the excitation amplitude was increased but no quantitative data was obtained.

(6) To assure that the resonance frequency observed was that of the eye and not that of the eye-vibrator system, the fundamental frequency of the vibrator was examined and found to be higher than 400 cps.

(7) It is very difficult to decrease the pressure in the eye because of the nature of the vitreous. Therefore in all experiments the pressure was increased monotonically.

(8) The eyes used in the experiments were from zero to nine days old (after enucleation). Older eyes showed external decay in spite of refrigeration. Internal decay was visible after about 3 days when a black substance could be observed through the cornea. Dissection showed this to be the decaying retina.

(9) The resonance frequency was measured to an accuracy of $\pm$ 1.5 cps. All pressure readings were within $\pm$1 mm H_2O and assumed steady state conditions.

(10) The output of the Fotonic Sensor is a function of the reflectivity (color, surface finish, etc.) of the object and its orientation and distance from the sensor.

(11) In using this experimental apparatus only the lowest pressure dependent mode could be detected.

It should be noted that this experiment does not simulate the in vivo support of the eye.

6.2 Static Experiment

The purpose of the static experiment was to measure the distensibility of the eye. By assuming the eye to behave like an elastic spherical shell with a uniform wall thickness, Young's modulus could then be calculated. That is, if the geometric parameters (R and h) are known, an effective modulus of elasticity can be determined by measuring either the change in diameter or change in volume associated with a change in intraocular pressure.

To obtain the diameter change the eye was placed on Bausch and Lomb optical comparator of magnification 62.5, and the pressure was varied using a water column. The diameter was measured across the equator of the eye. Whenever the intraocular pressure was increased the equatorial diameter decreased initially and then began to increase continuously after approximately 6 minutes. The diameter continued to increase for more than two hours. The opposite behavior could be observed when the pressure was decreased. This peculiar phenomenon can be attributed in part to an initial change in shape caused by a transient pressure gradient in the polar direction, and in part to the viscoelastic behavior of the sclera. With older eyes the shape change was not very pronounced.

Due to the transient geometric alteration it was decided that the volume would be a better parameter in measuring the distensibility of the eye. Figure 6.3 shows the appratus used to measure volume changes as a function of intraocular pressure and time. The Kontes syringe is accurately ground and gas tight. All members of the hydraulic circuit have much higher values of Young's modulus than the eye so that the corresponding volume change should be negligible.

The experimental procedure was:

(1) the pressure is increased by injecting a known volume of water into the system using the Kontes syringe;

(2) the corresponding pressure rise is measured and held constant by continually injecting more fluid into the system and recording the volume injected as a function of time. By accounting for the volume added to the water column, the change in volume of the eye can be determined.

Figure 6.4 shows a graph of the volume change of the eye versus the time (creep curve) in a representative case at various pressures. The data will be discussed in the next section.

Some noteworthy experimental observations are:

(1) By constantly checking all system joints the leak rate was found to be negligible.

(2) The capillary diameter was non-uniform but the variation was only ±2%. This allowed volume changes in the capillary to be measured to ±1% with pressure changes of 10 cm H_2O.

(3) The Kontes syringe allowed measurements of volume input to ±.02 mℓ.

(4) The pressure could be measured to ±1 mm H_2O.

(5) The eye is obviously viscoelastic and continued to change volume for at least 90 minutes.

6.3 Geometric Parameters

Both external and wall thickness dimensions were measured. The external dimensions were measured using the previously mentioned optical comparator with magnification of 62.5. Of the approximately 20 dog eyes examined the equatorial (scleral) diameter varied from a minimum of 2.136 cm to a maximum of 2.313 cm with a variation in a single eye of about ±.051 cm. The polar (corneal) diameter varied from a minimum of 2.217 cm to a maximum of 2.438 cm. The corneal diameter was more difficult to measure accurately because of the protuberance due to the optic nerve.

Wall thickness measurements were made by dissecting the eye in half through the cornea and measuring the wall thickness using a micrometer. The equatorial (scleral) walls varied between .036 cm and .051 cm with a single eye variation of ±.005 cm. The south polar (near optic nerve) walls varied between .036 cm and .056 cm. The north polar (corneal) walls varied between .089 and .140 cm. Figure 6.5 shows a typical eye and its dimensions.

VII. RESULTS AND DISCUSSION

7.1 Comparison of Theory and Experiment

The free vibration analysis of eyes, described in the earlier chapters, predicts that the frequency squared (σ_{mn}) should be approximately linear with respect to the intraocular pressure irrespective of the excited mode. This theory also predicts that the slope $(d\sigma_{mn}/dP)$ should be independent of m and only a function of n and R. In fact, the slope appears to be independent of the model chosen (to better than 2% from 0 to 100 cm H_2O). That is, for a fixed R and n the values of $d\sigma_{mn}/dP$ for the one, two, and three degree of freedom models is the same, allowing us to obtain a closed form relation from the one degree of freedom model. Therefore, by making use of the slope obtained from the experimental data and assuming a value for n, R can be calculated and compared to its measured value. In addition, the experimental data can be extrapolated back to $P = 0$ to determine $(\sigma_o)_{mn}$ and from this (by using (4.7.6)) m and Eh can be obtained. It should be noted that at least two modes must be detected in order to determine both m and Eh. Also to calculate E and h separately an additional mode is necessary, the symmetric mode number (n) of which is greater than four.

In examining the data graphed in Fig. 6.2 it can be seen that σ_{mn} is linear with respect to Δp (P is a dimensionless value of Δp) to about 35 cm H_2O. At higher pressures the slope decreases and the curve becomes non-linear. Since the normal pressure for a healthy eye is about 25 cm H_2O, it can be seen that under normal physiologic conditions the eye operates in the linear (or elastic) region. In the nonlinear domain the eye is overpressured and glaucoma occurs. In this experiment and the others to be discussed the vibrator was oriented along the symmetry axis (as closely as possible) in order to attempt to excite axisymmetric modes.

In analyzing this data the slope $(d\sigma_{mn}/dP)$ was calculated (from the linear portion of the curve), a value for n was assumed, and with $\rho_2 = 0$, R was calculated from simple theory (4.7.7). It was then assumed that the excited mode was axisymmetric $(m = 0)$, and by extrapolating the data curve back to $\Delta p = 0$ to obtain $(\sigma_o)_{mn}$ and using the measured value of h, E could be calculated.

Figures 7.1, 7.2, 7.3, and 7.4 show data curves for dog eyes enucleated on 9/13/66 (both from the same dog). The data of Figures 7.1 and 7.3 were obtained five days after enucleation while that of figures 7.2 and 7.4 were obtained 8 days after enucleation. The similarity between the curves should be noted. In figures 7.1, 7.2, and 7.4 the data is somewhat irregular at pressures below about 12 cm H_2O. This is probably due to the fact that at these low intraocular pressures the eyes had areas of negative curvature.

Table 7.1 compares the measured and calculated values for the four experiments. An error analysis has been performed to give the bounds shown. The value of R_m shown is an average radius (based on four measurements) measured at the equator less one half of the wall thickness (the middle surface radius). The value of h_m shown is the average thickness of the sclera (obtained from three measurements) and does not include the corneal thickness. It should be noted that the calculated value of R is always (within experimental error) within the accuracy of the measured value when $n = 2$ (ellipsoidal mode).

If it is assumed that the eye is a hollow, elastic, incompressible sphere subject to static internal pressure, Young's modulus can be calculated (using membrane theory[21]) from

$$E = \pi r_o^3 \left[\frac{r_o}{h} - 3 \right] \frac{\Delta p}{\Delta V_o} , \tag{7.1.1}$$

where r_o is the external radius and ΔV_o is the change in volume of the sphere (e.g. the liquid that goes into the eye). Second order h/r_o terms have been neglected.

For a viscoelastic material (7.1.1) can be considered as describing a function that is proportional to the reciprocal of the strain under the condition of constant stress. Figure 7.5 shows this time dependent behavior (experimental) compared to an exponential decay of the form

$$1/\epsilon = \epsilon_1 - \epsilon_2(1 - e^{-t/\tau}) \tag{7.1.2}$$

where ϵ_1 and ϵ_2 are functions of the intraocular pressure and ϵ is the strain. ϵ_1 and ϵ_2 can be calculated from the values of $1/\epsilon$ at $t = 0$ and $t \gg \tau$. The time constant, τ, associated with this behavior is 20 minutes for all of the curves shown.

If Young's modulus is considered to be frequency dependent of the form

$$E = E_1 - \sigma E_o , \tag{7.1.3}$$

where E_1 is a constant as obtained from the elastic considerations (and the experimental data) and E_o is a function of the intraocular pressure, the simple one degree of freedom $(u = v = o)$ elastic analysis can be extrapolated to the axisymmetric $(u = o)$ case and permit comparison with the experimental data. That is, by substituting (7.1.3) in (3.2.11) we obtain

$$\sigma_{mn} = \frac{4\Lambda_1 n + R\Delta p(n+2)(n-1)n}{2R^3\left[\rho_1 + \rho_2 \frac{n}{n+1} + \frac{\mu n}{R} + \frac{2\Lambda_o n}{R^3}\right]} \tag{7.1.4}$$

If E_o is taken to be of the form

$$E_o = \eta(\Delta p)^2 ,$$

where η is a physiologic constant and Δp is in cm H_2O, (7.1.4) can be used to describe the dynamic behavior of the eye. Figure 7.6 shows a comparison of the extrapolated curve from (7.1.4), with $E_1 = 1.2 \times 10^6$ dynes/cm^2 (as determined from the data of Fig. 7.3) and $\eta = 8.0 \times 10^{-6}$, and the vibrational data of Fig. 7.3.

7.2 Comparison with Other Investigations

In 1961, Mackay[23] published data obtained from experimental studies on vibrating rabbit eyes. The eyes (five) were vibrated by placing each in contact with a core driven by a coil fed from an ac source. Mackay hypothesizes that the pressure-frequency relation can be expressed as

$$f = \sqrt{\frac{R\ \Delta p}{2\pi M}} \tag{7.2.1}$$

where f is the fundamental eigenfrequency, R is the radius of the eye and M is the mass of the plunger. Based on this he obviously feels that this is a "system" (eye-vibrator system) resonance rather than an ocular resonance that is being measured. Figure 7.7 shows a simple model that might represent this system. k_v and k_e represent the effective spring constants of the vibrator and eye respectively. M and m_e represent the effective masses of the vibrator and eye respectively. For this system the natural frequency squared may be written as

$$\sigma = \frac{k_v + k_e}{M + m_e} . \tag{7.2.2}$$

From this Mackay concluded that

$$\left.\begin{aligned} k_v &= 0 \\ m_e &= 0 \\ k_e &= 2\pi R \, \Delta p \end{aligned}\right\} . \tag{7.2.3}$$

When rewriting, (7.2.2) becomes

$$\sigma = \sigma_e \left[\frac{1 + k_v/k_e}{1 + M/m_e} \right] , \tag{7.2.4}$$

where

$$\sigma_e = k_e/m_e . \tag{7.2.5}$$

By differentiating (7.2.4) with respect to Δp we obtain

$$\frac{d\sigma}{d(\Delta p)} = \frac{1}{1 + M/m_e} \frac{d\sigma_e}{d(\Delta p)} , \tag{7.2.6}$$

assuming that only k_e is a function of Δp.

This implies that $1 + M/m_e$ acts as a scale factor which relates the rate of change of resonant frequency with respect to the eye-vibrator system to the ocular system.

It should be noted that if $M \ll m_e$ and $k_v = 0$, then

$$\sigma = \sigma_e \, . \tag{7.2.7}$$

Figure 7.8 shows a comparison of Mackay's data, his hypothesized theoretical curve, and a curve calculated from the axisymmetric model (see section 4.5), assuming that $n = 2$, $R = 0.60$ cm and $Eh = 1.6 \times 10^4$ dynes/cm (e.g. $E = 7 \times 10^5$ dynes/cm^2 and $h = .023$ cm). Since the theoretical curve based on section 4.5 does not take into account frequency dependent elastic effects, we can assume (since there is such good agreement with the experimental data) that there is some coupling between the eye and the vibrator. In fact, if the eye-vibrator coupling were strong enough the data might actually show a vibrator resonance as influenced by the eye. It should be pointed out that Mackay's publication made no mention of the magnitude of the geometric parameters of the experimental rabbit eyes, and therefore the values used in this analysis have been assumed.

7.3 Conclusions

A model has been developed to analytically describe the dynamic behavior of a vibrating eye. This model treats the eye as an elastic shell surrounded by and filled with an incompressible, invicid, irrotationally flowing fluid. Equations have been developed which consider both the symmetric and asymmetric vibrational modes and a closed form solution has been obtained for the symmetric case. A frequency dependent elastic model has been proposed and has been directly applied to the one degree of freedom $(u = v = o)$ vibrating system. This model permits extrapolation to the axisymmetric $(u = o)$ and asymmetric systems.

Both static and dynamic experiments have been performed on enucleated dog eyes. The static experiments emphasize the viscoelastic behavior of the sclera, while the vibration experiments indicate that the elastic properties (i.e., Young's modulus) are frequency dependent. The dynamic experiments prove that there exists an intraocular pressure range in which linear elastic theory, as used in the models chosen, describes the dynamic behavior of the eye to within experimental accuracy. This pressure range includes the normal intraocular pressure of a healthy eye but does not seem to extend much above 35-40 cm H_2O.

The static creep experiments imply that there is a time constant associated with the volume change caused by a state of constant stress. This time constant is of the order of 20 minutes.

The dynamic vibration experiments indicate that Young's modulus for the sclera is frequency dependent and may be written in the form

$$E = E_1 - E_o \sigma \ . \tag{7.3.1}$$

This model when extrapolated to the symmetric case shows agreement within experimental accuracy if E_o is described by

$$E_o = \eta(\Delta p)^j , \qquad (7.3.2)$$

where η is a constant depending on the physiologic state of the sclera, and j is approximately 2 or 3 (also depending on the physiologic state).

If one considers the vibration data in light of the structure of the sclera (see section 1.2) a possible explanation appears. That is, at low pressures the lamina fusca, rich in elastic fibers, governs the dynamic behavior of the eye and the experimental data agrees well with linear elastic theory. At higher pressures the sclera proper and episclera, composed of loosely intertwined bundles of connective tissue and few elastic fibers, are added to the dynamic system with their associated frequency dependent elastic properties. It is interesting to consider the possibility that the onset of the nonlinear dynamic behavior might coincide with the onset of glaucoma.

Based on the preliminary experiments discussed here it would seem that the postulated theory, when used in conjunction with the proposed frequency dependent elastic model, may well describe the dynamic behavior of the eye to a first approximation.

7.4 Recommendations

Some suggestions for future study are:

(1) The experimental technique should be modified so that the vibrational studies can be performed in vivo. This is very important since the elastic properties in vivo may be very different from the in

vitro elastic properties discussed in this paper. In addition, the damping properties of the surroundings must be taken into account.

(2) Toward this end the use of sound waves as attempted (see section 6.1) might be pursued. Methods of focusing these waves should be examined such as using an inverted speaker or going to close range small systems using piezoelectric crystals or magnetostrictive materials.

(3) Attempts should be made to experimentally determine the mode shape. This may be done by using multiple Fotonic Sensors to map the surface of the eye during vibration.

(4) A mechanical vibrator should be designed which is force independent, that is, which delivers constant amplitude vibrations independent of external force or frequency. In this way any chance of coupling between the eye and the vibrator would be eliminated.

(5) Attempts at detecting higher modes should be made. This is important since it will allow a firm determination of E_1 and E_o as a function of pressure. This can possibly be done by using the more sensitive Fotonic Sensor (sensitivity of 10^{-6} inches) in conjunction with appropriate filters and amplifiers.

(6) More extensive static experiments should be performed to determine ϵ_1, ϵ_2 and τ as functions of pressure. The experiment might be extended so that both ΔV_o and Δr_o were measured simultaneously to provide a cross check. This data could then be compared to the work of Schwartz[24] where only Δr_o was measured. Measuring only Δr_o does not take into account shape changes (which were discovered in this program and are mentioned in section 6.2) and therefore may produce erroneous results.

(7) The eye should also be examined with regard to the effects of vibration excitation amplitudes and ocular support (such as surrounding the eye with liquid).

(8) The frequency dependent elastic considerations should be extended to the multi-degree of freedom systems and consideration should be taken of the dependence of E_o on Δp.

(9) More sophistication might be added to the analytical model such as viscosity, nonsphericity, attachments (nerves, muscles, etc.), elastic outer material, multilayered sclera, effects of the cornea and lens, and effects of the ocular support.

VIII. APPENDIX A

ASSOCIATED LEGENDRE POLYNOMIALS OF THE FIRST KIND

8.1 Legendre's Equation and Solution

Legendre's equation may be written as

$$(1-\eta^2)\frac{d^2y}{d\eta^2} - 2\eta\frac{dy}{d\eta} + \left[n(n+1) - \frac{m^2}{1-\eta^2}\right]y = 0 \ . \tag{8.1.1}$$

To obtain a solution, consider first the equation with $m = 0$. Assume a series solution of the form

$$y(\eta) = \sum_s \mathcal{a}_s \eta^s \ . \tag{8.1.2}$$

By using (8.1.2), (8.1.1) becomes

$$\sum_s \left\{ s(s-1)\mathcal{a}_s\eta^{s-2} + [n(n+1) - s(s+1)]\mathcal{a}_s\eta^s \right\} = 0 \ . \tag{8.1.3}$$

Since the η^s terms are linearly independent, each coefficient must equal zero separately. This produces

$$(s+1)(s+2)\mathcal{a}_{s+2} + [n(n+1) - s(s+1)]\mathcal{a}_s = 0 \tag{8.1.4}$$

or

$$\mathcal{a}_s = \frac{-(s+1)(s+2)}{(n-s)(n+s+1)}\mathcal{a}_{s+2} \ . \tag{8.1.5}$$

From (8.1.5) it can be seen that $\mathcal{a}_{-1}$ and $\mathcal{a}_{-2}$ are zero if $\mathcal{a}_0$ and $\mathcal{a}_1$ are finite. Also if $\mathcal{a}_s = 0$ then $\mathcal{a}_{s-2} = \mathcal{a}_{s-4} = \ldots = 0$, so that all negative powers of η vanish for finite $\mathcal{a}_0$ and $\mathcal{a}_1$. If $\mathcal{a}_0 = 1$, the even powered series becomes

$$p_n = 1 - \frac{n(n+1)}{2!}\eta^2 + \frac{n(n-2)(n+1)(n+3)}{4!}\eta^4 + \ldots \quad (8.1.6)$$

If $a_1 = 1$, the odd powered series becomes

$$q_n = \eta - \frac{(n-1)(n+2)}{3!}\eta^3 + \frac{(n-1)(n-3)(n+2)(n+4)}{5!}\eta^5 - \ldots \quad (8.1.7)$$

The complete solution to (8.1.1) with $m = 0$ can then be written as

$$y = A_n p_n + B_n q_n \quad \text{for} \quad -1 < \eta < 1 . \quad (8.1.8)$$

By rearranging and normalizing (8.1.6) and (8.1.7) the Legendre polynomial of the first kind is defined by a finite series as

$$P_n(\eta) = \sum_{j=0}^{k} (-1)^j \frac{(2n-2j)!}{2^n(j!)(n-j)!(n-2j)!}\eta^{n-2j} \quad (8.1.9)$$

which is valid for n equal to a positive integer with $k = \frac{1}{2}n$ or $\frac{1}{2}(n-1)$, whichever is an integer. This can be expanded to give the more familiar form

$$P_n(\eta) = \frac{1}{2^n n!}\frac{d^n}{d\eta^n}(\eta^2 - 1)^n . \quad (8.1.10)$$

The second solution of Legendre's equation is also defined from (8.1.6) and (8.1.7) by the infinite series as

$$Q_n(\eta) = 2^n \sum_{j=0}^{\infty} \frac{(n+j)!(n+2j)!}{j!(2n+2j+1)!}\eta^{-(n+2j+1)} . \quad (8.1.11)$$

This series diverges for $|\eta| = 1$ and therefore this part of the solution is only useful for problems which exclude the poles. For this reason it will not be discussed further.

(8.1.10) then is the solution to (8.1.1) with $m = 0$. If (8.1.1) (with $m = 0$) is differentiated m times, and letting $x = d^m y/d\eta^m$, (8.1.1) may be written as

$$(1-\eta^2)\frac{d^2x}{d\eta^2} - 2\eta(m+1)\frac{dx}{d\eta} + (n-m)(n+m+1)x = 0 \ . \tag{8.1.12}$$

Let

$$z = (1-\eta^2)^{m/2}x \ . \tag{8.1.13}$$

When using (8.1.13) in (8.1.12) we obtain

$$(1-\eta^2)\frac{d^2z}{d\eta^2} - 2\eta\frac{dz}{d\eta} + \left[n(n+1) - \frac{m}{1-\eta^2}\right]z = 0 \ . \tag{8.1.14}$$

This is identical with (8.1.1) Legendre's equation, and a solution is therefore

$$y = z = (1-\eta^2)^{m/2}x = (1-\eta^2)^{m/2}\frac{d^m}{d\eta^m}P_n(\eta) \ . \tag{8.1.15}$$

Or the associated Legendre polynomial of the 1st kind may be defined as

$$P_n^m(\eta) = (1-\eta^2)^{m/2}\frac{d^m}{d\eta^m}P_n(\eta) \ . \tag{8.1.16}$$

8.2 Basic Recurrence Relations[18,19,20]

Without proof some useful recurrence relation will be given.

$$(m+n)(1-\eta^2)^{1/2}P_n^{m-1} = P_{n+1}^m - \eta P_n^m \ . \tag{8.2.1}$$

$$P_n^{m+1} = 2m\eta(1-\eta^2)^{-1/2}P_n^m - (m+n)(n-m+1)P_n^{m-1}$$

(continued)

$$= [(n+m+1)\eta P_n^m - (n-m+1)P_{n+1}^m](1-\eta^2)^{-1/2} \tag{8.2.2}$$

$$= [(m-n)\eta P_n^m + (m+n)P_{n-1}^m](1-\eta^2)^{-1/2}$$

$$P_{n-1}^m - \eta P_n^m = (m-n-1)(1-\eta^2)^{1/2} P_n^{m-1} \tag{8.2.3}$$

$$(2n+1)\eta P_n^m = (n+m)P_{n-1}^m + (n-m+1)P_{n+1}^m \tag{8.2.4}$$

$$P_{n+1}^{m+1} - P_{n-1}^{m+1} = (2n+1)(1-\eta^2)^{1/2} P_n^m \tag{8.2.5}$$

$$P_{n-1}^{m+1} - \eta P_n^{m+1} = (m-n)(1-\eta^2)^{1/2} P_n^m \quad . \tag{8.2.6}$$

8.3 Differential Relations

$$\dot{P}_n^m(\eta) = \frac{d}{d\theta} P_n^m(\eta) = \frac{dP_n^m}{d\eta}\frac{d\eta}{d\theta} = - \sin\theta \, P_n^{m'} \tag{8.3.1}$$

where

$$\eta = \cos\theta \tag{8.3.2}$$

and

$$\dot{P}_n^m = - (1-\eta^2)^{1/2} P_n^{m'} \tag{8.3.3}$$

$$\ddot{P}_n^m = \frac{d}{d\theta}\dot{P}_n^m = - \eta P_n^{m'} + (1-\eta^2)P_n^{m''} \tag{8.3.4}$$

$$\dddot{P}_n^m = \frac{d}{d\theta}\ddot{P}_n^m = (1-\eta^2)^{1/2}P_n^{m'} + 3\eta(1-\eta^2)^{1/2}P_n^{m''} - (1-\eta^2)^{\ /2}P_n^{m'''} \tag{8.3.5}$$

$$\ddddot{P}_n^m = \frac{d}{d\theta}\dddot{P}_n^m = \eta P_n^{m'} = \eta P_n^{m'} + (7\eta^2 - 4)P_n^{m''} - 6\eta(1-\eta^2)P_n^{m'''}$$

$$+ (1-\eta^2)^2 P_n^{m''''} \quad . \tag{8.3.6}$$

From the definition of $P_n^m(\eta)$ (8.1.15)

$$P_n^{m'}(\eta) = \frac{d}{d\eta} P_n^m = \frac{d}{d\eta}\left[(1-\eta^2)^{m/2} \frac{d^m}{d\eta^m} P_n\right] = -\mu m(1-\eta^2)^{\frac{m-2}{2}} \frac{d^m}{d\eta^m} P_n$$

$$+ (1-\eta^2)^{\frac{m}{2}} \frac{d^{m+1}}{d\eta^{m+1}} P_n = \frac{-\mu m}{1-\eta^2} P_n^m + (1-\eta^2)^{-\frac{1}{2}} P_n^{m+1} . \qquad (8.3.7)$$

If use is made of (8.2.5) in (8.3.7), we find that

$$(1-\eta^2)P_n^{m'} = -\eta n P_n^m + (m+n)P_{n-1}^m \qquad (8.3.8)$$

or

$$(1-\eta^2)P_n^{m'} = \eta(n+1)P_n^m - (n-m+1)P_{n+1}^m . \qquad (8.3.9)$$

A useful relation for the second derivative of the associated Legendre polynomial can be gotten directly from Legendre's equation. That is

$$(1-\eta^2)P_n^{m''} - 2\eta P_n^{m'} + \left[n(n+1) - \frac{m^2}{1-\eta^2}\right]P_n^m = 0 . \qquad (8.3.10)$$

Differentiation of (8.3.10) produces

$$(1-\eta^2)P_n^{m'''} - 4\eta P_n^{m''} + \left[(n+2)(n-1) - \frac{m^2}{1-\eta^2}\right] P_n^{m'} - 2m^2 \frac{\eta}{(1-\eta^2)^2} P_n^m = 0 . \qquad (8.3.11)$$

It we again differentiate, (8.3.11) becomes

$$(1-\eta^2)^2 P^{m''''} - 8\eta(1-\eta^2)P_n^{m'''} + 2(1-\eta^2)\left[n(n+1) - 7 - \frac{m^2-4}{1-\eta^2}\right]P_n^{m''}$$

$$- 4\eta\left[n(n+1)-1\right] P_n^{m'} + \left[n^2(n+1)^2 - \frac{2m^2\{n(n+1)-1\}}{1-\eta^2}\right.$$

$$\left. + \frac{m^2(m^2-4)}{(1-\eta^2)^2}\right]P_n^m = 0 . \qquad (8.3.12)$$

8.4 More Recurrence Relations

By making use of (8.2.4), other useful recurrence relations can be written as

$$\eta^2 P_n^m = \frac{\eta}{2n+1}\left[(m+n)P_{n-1}^m - (m-n-1)P_{n+1}^m\right]$$

$$= \frac{(m+n)(m+n-1)}{(2n+1)(2n-1)} P_{n-2}^m + \left[\frac{(n-m+1)(n+m+1)}{(2n+1)(2n+3)} + \frac{(m+n)(n-m)}{(2n+1)(2n-1)}\right] P_n^m$$

$$+ \frac{(n-m+1)(n-m+2)}{(2n+1)(2n+3)} P_{n+2}^m$$

$$= S_1 P_{n-2}^m + S_2 P_n^m + S_3 P_{n+2}^m \ . \qquad (8.4.1)$$

$$\eta^3 P_n^m = \frac{(m+n)(m+n-1)(m+n-2)}{(2n+1)(2n-1)(2n-3)} P_{n-3}^m + \left(\frac{m+n}{2n+1}\right)\left[\frac{(n+m-1)(n-m-1)}{(2n-1)(2n-3)}\right.$$

$$\left. + \frac{(n-m+1)(n+m+1)}{(2n+1)(2n+3)} + \frac{(n+m)(n-m)}{(2n+1)(2n-1)}\right] P_{n-1}^m$$

$$+ \left(\frac{n-m+1}{2n+1}\right)\left[\frac{(n-m+1)(n+m+1)}{(2n+1)(2n+3)} + \frac{(m+n)(n-m)}{(2n+1)(2n-1)}\right.$$

$$\left. + \frac{(n-m+2)(n+m+2)}{(2n+3)(2n+5)}\right] P_{n+1}^m + \frac{(n-m+1)(n-m+2)(n-m+3)}{(2n+1)(2n+3)(2n+5)} P_{n+3}^m$$

$$= S_4 P_{n-3}^m + S_5 P_{n-1}^m + S_6 P_{n+1}^m + S_7 P_{n+3}^m \ . \qquad (8.4.2)$$

$$\eta^4 P_n^m = \left(\frac{m+n-3}{2n-5}\right)\frac{(m+n)(m+n-1)(m+n-2)}{(2n+1)(2n-1)(2n-3)} P_{n-4}^m$$

$$+ \left\{\frac{(n-m-2)(m+n)(n+m-1)(n+m-2)}{(2n-5)(2n+1)(2n-1)(2n-3)} + \left(\frac{n+m-1}{2n-1}\right)\left(\frac{m+n}{2n+1}\right)\left[\frac{(n+m-1)(n-m-1)}{(2n-1)(2n-3)}\right.\right.$$

$$\left.\left. + \frac{(n-m-1)(n+m+1)}{(2n+1)(2n+3)} + \frac{(m+n)(n-m)}{(2n+1)(2n-1)}\right]\right\} P_{n-2}^m$$

$$+ \left\{\frac{(n-m)(n+m)}{(2n-1)(2n+1)}\left[\frac{(n+m-1)(n-m-1)}{(2n-1)(2n-3)} + \frac{(n-m+1)(n+m+1)}{(2n+1)(2n+3)}\right.\right.$$

(continued)

$$
\left. + \frac{(m+n)(n-m)}{(2n+1)(2n-1)} \right] + \frac{(n+m+1)(n-m+1)}{(2n+3)(2n+1)} \left[\frac{(n-m+1)(n+m+1)}{(2n+1)(2n+3)} \right.
$$

$$
\left. + \frac{(n+m)(n-m)}{(2n+1)(2n-1)} + \frac{(n-m+2)(n+m++2)}{(2n+3)(2n+5)} \right] \Bigg\} P_n^m
$$

$$
+ \left\{ \frac{(n-m+2)(n-m+1)}{(2n+3)(2n+1)} \left[\frac{(n-m+1)(n+m+1)}{(2n+1)(2n+3)} + \frac{(n+m)(n-m)}{(2n+1)(2n-1)} \right. \right.
$$

$$
\left. \left. + \frac{(n-m+2)(n+m+2)}{(2n+3)(2n+5)} + \frac{(n-m+2)(n-m+3)(n+m+3)(n-m+1)}{(2n+1)(2n+3)(2n+5)(2n+7)} \right\} P_{n+2}^m
$$

$$
+ \frac{(n-m+1)(n-m+2)(n-m+3)(n-m+4)}{(2n+1)(2n+3)(2n+5)(2n+7)} P_{n+4}^m
$$

$$
= S_8 P_{n-4}^m + S_9 P_{n-2}^m + S_{10} P_n^m + S_{11} P_{n+2}^m + S_{12} P_{n+4}^m \,. \tag{8.4.3}
$$

8.5 Integral Relations

The two orthogonality relations relating Legendre polynomials of different degree and different order may be written as

$$
\int_{-1}^{1} P_n^m \, P_\ell^m \, d\eta = \frac{2}{2\ell+1} \, \frac{(\ell+m)!}{(\ell-m)!} \, \delta_{\ell n} \tag{8.5.1}
$$

and

$$
\int_{-1}^{1} \frac{P_n^m \, P_n^\ell}{1-\eta^2} \, d\eta = \frac{(n+\ell)!}{\ell(n-\ell)!} \, \delta_{\ell m} \tag{8.5.2}
$$

where

$$
\left.
\begin{aligned}
\delta_{\ell n} &= 0 \qquad \ell \neq n \\
&= 1 \qquad \ell = n
\end{aligned}
\right\} . \tag{8.5.3}
$$

When making use of (8.4.1), (8.4.2), (8.4.3), (8.2.1) and (8.2.2) some useful integral relations may be derived.

$$I(n)\int_{-1}^{1} \eta^2 \, P_n^m \, P_\ell^m \, d\eta$$

$$= I(n)\int_{-1}^{1}\left[S_1 P_{n-2}^m + S_2 P_n^m + S_3 P_{n+2}^m\right] P_\ell^m \, d\eta$$

$$= \left(\frac{2}{2\ell+1}\right)\frac{(\ell+m)!}{(\ell-m)!}\left[I(n)\left\{S_1\delta_{\ell,n-2} + S_2\delta_{\ell,n} + S_3\delta_{\ell,n+2}\right\}\right]$$

$$= \left(\frac{2}{2\ell+1}\right)\frac{(\ell+m)!}{(\ell-m)!}\left[I(\ell+2)Q_1 + I(\ell)Q_2 + I(\ell-2)Q_3\right] \qquad (8.5.4)$$

where $I(n)$ is some function of n and

$$Q_1 = S_1\delta_{\ell,n-2}$$

$$= \frac{(m+\ell+2)(m+\ell+1)}{(2\ell+5)(2\ell+3)} \qquad (8.5.5)$$

$$Q_2 = \frac{(\ell+m)(\ell-m)}{(2\ell+1)(2\ell-1)} + \frac{(\ell-m+1)(\ell+m+1)}{(2\ell+1)(2\ell+3)} \qquad (8.5.6)$$

$$Q_3 = \frac{(\ell-m)(\ell-m-1)}{(2\ell-3)(2\ell-1)} \quad . \qquad (8.5.7)$$

$$I(n)\int_{-1}^{1} \eta^3 P_n^m \, P_\ell^m \, d\eta$$

$$= I(n)\int_{-1}^{1}\left[S_4 P_{n-3}^m + S_3 P_{n-1}^m + S_6 P_{n+1}^m + S_7 P_{n+3}^m\right] P_\ell^m \, d\eta$$

$$= \left(\frac{2}{2\ell+1}\right)\frac{(\ell+m)!}{(\ell-m)!}\left\{I(n)\left[S_4\delta_{\ell,n-3} + S_5\delta_{\ell,n-1} + S_6\delta_{\ell,n+1} + S_7\delta_{\ell,n+2}\right]\right\}$$

$$= \left(\frac{2}{2\ell+1}\right)\frac{(\ell+m)!}{(\ell-m)!}\left[I(\ell+3)Q_4 + I(\ell+1)Q_5 + I(\ell-1)Q_6 + I(\ell-3)Q_7\right] \qquad (8.5.8)$$

where

$$Q_4 = \frac{(\ell+m+3)(\ell+m+2)(\ell+m+1)}{(2\ell+7)(2\ell+5)(2\ell+3)} \tag{8.5.9}$$

$$Q_5 = \left(\frac{\ell+m+1}{2\ell+3}\right)\left[\frac{(\ell+m)(\ell-m)}{(2\ell+1)(2\ell-1)} + \frac{(\ell-m+2)(\ell+m+2)}{(2\ell+3)(2\ell+5)}\right.$$

$$\left. + \frac{(\ell+m+1)(\ell-m+1)}{(2\ell+3)(2\ell+1)}\right] \tag{8.5.10}$$

$$Q_6 = \left(\frac{\ell-m}{2\ell-1}\right)\left[\frac{(\ell-m)(\ell+m)}{(2\ell+1)(2\ell-1)} + \frac{(\ell+m-1)(\ell-m-1)}{(2\ell-1)(2\ell-3)}\right.$$

$$\left. + \frac{(\ell-m-1)(\ell-m+1)}{(2\ell+3)(2\ell+1)}\right] \tag{8.5.11}$$

$$Q_7 = \frac{(\ell-m-2)(\ell-m-1)(\ell-m)}{(2\ell-5)(2\ell-3)(2\ell-1)} \quad . \tag{8.5.12}$$

$$I(n)\int_{-1}^{1} \eta^4 P_n^m\, P_\ell^m\, d\eta \; -$$

$$= I(n)\int_{-1}^{1}\left[S_8 P_{n-4}^m + S_9 P_{n-2}^m + S_{10} P_n^m + S_{11} P_{n+2}^m + S_{12} P_{n+4}^m\right] P_\ell^m d\eta$$

$$= \left(\frac{2}{2\ell+1}\right)\frac{(\ell+m)!}{(\ell-m)!}\left\{I(n)\left[S_8\delta_{\ell,n-4} + S_9\delta_{\ell,n-2} + S_{10}\delta_{\ell,n}\right.\right.$$

$$\left.\left. + S_{11}\delta_{\ell,n+2} + S_{12}\delta_{\ell,n+4}\right]\right\}$$

$$= \left(\frac{2}{2\ell+1}\right)\frac{(\ell+m)!}{(\ell-m)!}\left[I(\ell+4)Q_8 + I(\ell+2)Q_9 + I(\ell)Q_{10}\right.$$

$$\left. + I(\ell-2)Q_{11} + I(\ell-4)Q_{12}\right] \tag{8.5.13}$$

where

$$Q_8 = \frac{(\ell+m+1)(\ell+m+2)(\ell+m+3)(\ell+m+4)}{(2\ell+3)(2\ell+5)(2\ell+7)(2\ell+9)} \tag{8.5.14}$$

$$Q_9 = \frac{(\ell-m)(\ell+m)(\ell+m+1)(\ell+m+2)}{(2\ell-1)(2\ell+1)(2\ell+3)(2\ell+5)} + \frac{(\ell+m+1)(\ell+m+2)}{(2\ell+3)(2\ell+5)}\left[\frac{(\ell-m+1)(\ell+m+1)}{(2\ell+1)(2\ell+3)}\right.$$

$$\left. + \frac{(\ell+m+2)(\ell-m+2)}{(2\ell+3)(2\ell+5)} + \frac{(\ell+m+3)(\ell-m+3)}{(2\ell+5)(2\ell+7)}\right] \qquad (8.5.15)$$

$$Q_{10} = \frac{(\ell-m)(\ell+m)(\ell+m-1)(\ell-m-1)}{(2\ell-1)^2(2\ell-3)(2\ell+1)} + \frac{(\ell+m+1)(\ell+m+2)(\ell-m+1)(\ell-m+2)}{(2\ell+1)(2\ell+3)^2(2\ell+5)}$$

$$+ \left[\frac{(\ell-m)(\ell+m)}{(2\ell+1)(2\ell-1)} + \frac{(\ell+m+1)(\ell-m+1)}{(2\ell+1)(2\ell+3)}\right]^2 \qquad (8.5.16)$$

$$Q_{11} = \frac{(\ell-m)(\ell-m-1)}{(2\ell-1)(2\ell-3)^2}\left[\frac{(\ell+m-2)(\ell-m-2)}{(2\ell-5)} + \frac{(\ell+m-1)(\ell-m-1)}{(2\ell-1)}\right]$$

$$+ \frac{(\ell-m)(\ell-m-1)}{(2\ell-3)(2\ell-1)(2\ell+1)}\left[\frac{(\ell-m)(\ell+m)}{(2\ell-1)} + \frac{(\ell+m+1)(\ell-m+1)}{(2\ell+3)}\right] \qquad (8.5.17)$$

$$Q_{12} = \frac{(\ell-m)(\ell-m-1)(\ell-m-2)(\ell-m-3)}{(2\ell-1)(2\ell-3)(2\ell-5)(2\ell-7)} \, . \qquad (8.5.18)$$

A useful formula that will not be proved generally, may be written as

$$\int_{-1}^{1} \eta^a P_n^m P_\ell^m d\eta = \int_{-1}^{1} \eta^a P_{n+1}^m P_\ell^m d\eta \qquad (8.5.19)$$

where a is a positive (or zero) integer. As an example let $a = 4$. Then from (8.4.3)

$$\eta^4 P_n^m = S_8(n)P_{n-4}^m + S_9(n)P_{n-2}^m + S_{10}(n)P_n^m + S_{11}(n)P_{n+2}^m + S_{12}(n)P_{n+4}^m \qquad (8.5.20)$$

and

$$\eta^4 P_{n+1}^m = S_8(n+1)P_{n-3}^m + S_9(n+1)P_{n-1}^m + S_{10}(n+1)P_{n+1}^m + S_{11}(n+1)P_{n+3}^m$$

$$+ S_{12}(n+1)P_{n+5}^m \, . \qquad (8.5.21)$$

On multiplying by $P_\ell^m d\eta$ and integrating from -1 to $+1$ we obtain

$$\int_{-1}^{1} \eta^4 P_n^m P_\ell^m d\eta = \left(\frac{2}{2\ell+1}\right) \frac{(\ell+m)!}{(\ell-m)!} \Big[S_8(n)\delta_{\ell,n-4} + S_9(n)\delta_{\ell,n-2}$$

$$+ S_{10}(n)\delta_{\ell,n} + S_{11}(n)\delta_{\ell,n+2} + S_{12}(n)\delta_{\ell,n+4} \Big]$$

$$= \left(\frac{2}{2\ell+1}\right) \frac{(\ell+m)!}{(\ell-m)!} \Big[S_8(\ell+4) + S_9(\ell+2) + S_{10}(\ell) + S_{11}(\ell-2)$$

$$+ S_{12}(\ell-4) \Big] \tag{8.5.22}$$

and

$$\int_{-1}^{1} \eta^4 P_{n+1}^m P_\ell^m d\eta = \left(\frac{2}{2\ell+1}\right) \frac{(\ell+m)!}{(\ell-m)!} \Big[S_8(n+1)\delta_{\ell,n-3} + S_9(n+1)\delta_{\ell,n-1}$$

$$+ S_{10}(n+1)\delta_{\ell,n+1} + S_{11}(n+1)\delta_{\ell,n+3} + S_{12}(n+1)\delta_{\ell,n+5} \Big]$$

$$= \left(\frac{2}{2\ell+1}\right) \frac{(\ell+m)!}{(\ell-m)!} \Big[S_8(\ell+4) + S_9(\ell+2) + S_{10}(\ell)$$

$$+ S_{11}(\ell-2) + S_{12}(\ell-4) \Big] . \tag{8.5.23}$$

IX. APPENDIX B

DETAILS OF THE COMPLETE SHELL MODEL SOLUTION

The complete equations of motion (4.2.10), (4.2.11), and (4.2.12) will now be examined. First it is best to define separately many of the terms contained in the equations and eliminate the derivations with respect to θ. When using (8.3.3), (8.3.4), (8.3.5), (8.3.6), (8.3.9), (8.3.10), (8.3.11) and (8.3.12) the following terms can be defined:

$$
\begin{aligned}
I_7 &= \ddddot{P}{}_n^m + 2\dddot{P}{}_n^m \cot\theta - \ddot{P}{}_n^m(\cot^2\theta + m^2 \csc^2\theta) \\
&\quad + \dot{P}{}_n^m \cot\theta(3 + \cot^2\theta - m^2 \csc^2\theta) \\
&= (1-\eta^2)P^{m''''} - 8\eta(1-\eta^2)P_n^{m'''} + [12\eta^2 - m(m-1)-4]P_n^{m''} \\
&\quad + 2m(m-1)\frac{\eta}{1-\eta^2}P_n^{m'} + \frac{m}{1-\eta^2}\left[n(n+1) - \frac{m^2}{1-\eta^2}\right]P_n^m \\
&= \left[\frac{4m^2(n+2)}{(1-\eta^2)^2} - \frac{m^2(n+1)(n+4)}{1-\eta^2} + n(n+1)(n+2)(n-1)\right]P_n^m \\
&\quad - 4m^2(n-m+1)\frac{\eta}{(1-\eta^2)^2}P_{n+1}^m \;. \qquad (9.1.1)
\end{aligned}
$$

$$
I_8 = \ddot{P}{}_n^m + \dot{P}{}_n^m \cot\theta = (1-\eta^2)P_n^{m''} - 2\eta P_n^{m'} = \left[\frac{m^2}{1-\eta^2} - n(n+1)\right]P_n^m \;. \qquad (9.1.2)
$$

$$
\begin{aligned}
I_9 &= \left\{\ddot{P}{}_n^m - 3\cot\theta\,\dot{P}{}_n^m + (4-m^2)\csc^2\theta\,P_n^m\right\} \\
&= \left\{(1-\eta^2)P_n^{m''} + 2\eta P_n^{m'} + \frac{4-m^2}{1-\eta^2}P_n^m\right\}
\end{aligned}
$$

(continued)

$$= \left\{ \left[\frac{4(n+2)}{1-\eta^2} - (n+1)(n+4) \right] P_n^m - 4(n-m+1) \frac{\eta}{1-\eta^2} P_{n+1}^m \right\} . \qquad (9.1.3)$$

$$I_{10} = \dddot{P}_n^m \sin\theta + \ddot{P}_n^m \cos\theta + \dot{P}_n^m \left[\sin\theta(1 - \cot^2\theta) - m^2 \csc\theta \right]$$

$$+ 2m^2 P_n^m \cot\theta \csc\theta$$

$$= -(1-\eta^2) \left[(1-\eta^2) P_n^{m'''} - 4\eta P_n^{m''} - \frac{m^2}{1-\eta^2} P_n^{m'} - \frac{2m^2\eta}{(1-\eta^2)^2} P_n^m \right]$$

$$= (n-1)(n+2) \left[(n+1)\eta P_n^m - (n-m+1) P_{n+1}^m \right] . \qquad (9.1.4)$$

$$I_{11} = -\dot{P}_n^m \sin\theta = (1-\eta^2) P_n^{m'}$$

$$= (n+1)\eta P_n^m - (n-m+1) P_{n+1}^m$$

$$= \left(\frac{n+1}{2n+1} \right) \left[(n+m) P_{n-1}^m - \frac{n(n-m+1)}{(n+1)} P_{n+1}^m \right] . \qquad (9.1.5)$$

$$I_{12} = \dddot{P}_n^m \sin\theta + \ddot{P}_n^m \cos\theta - \dot{P}_n^m \left(\cot^2\theta \sin\theta + \frac{m^2}{2} \csc\theta \right)$$

$$= -(1-\eta^2) \left[(1-\eta^2) P_n^{m'''} - 4\eta P_n^{m''} + \left\{ 1 - \frac{m^2}{2(1-\eta^2)} \right\} P_n^{m'} \right]$$

$$= \left\{ (n+1)[(n-1)(n+2)+1] - \frac{m^2(n+5)}{2(1-\eta^2)} \right\} \eta P_n^m$$

$$- (n-m+1) \left[(n-1)(n+2)+1 - \frac{m^2}{2(1-\eta^2)} \right] P_{n+1}^m . \qquad (9.1.6)$$

$$I_{13} = \csc\theta \left[\dot{P}_n^m (1+\nu) - 4 P_n^m \cot\theta \right]$$

$$= -(1+\nu) P_n^{m'} - \frac{4\eta}{1-\eta^2} P_n^m$$

(continued)

$$= -\left[(n+5)+\nu(n+1)\right] \frac{\eta}{1-\eta^2} P_n^m + (1+\nu)(n-m+1) \frac{1}{1-\eta^2} P_{n+1}^m \ . \qquad (9.1.7)$$

$$I_{14} = \ddot{P}_n^m + \dot{P}_n^m \cot\theta + (2-m^2 \csc^2\theta) P_n^m$$

$$= (1-\eta^2) P_n^{m''} - 2\eta P_n^{m'} + \left(2 - \frac{m^2}{1-\eta^2}\right) P_n^m$$

$$= -(n+2)(n-1) P_n^m \ . \qquad (9.1.8)$$

$$I_{15} = \ddot{P}_n^m + 3\dot{P}_n^m \cot\theta = (1-\eta^2) P_m^{m''} - 4\eta P_n^{m'}$$

$$= \left[\frac{m^2-2(n+1)}{1-\eta^2} - (n+1)(n-2)\right] P_n^m + 2(n-m+1) \frac{\eta}{1-\eta^2} P_{n+1}^m \ . \qquad (9.1.9)$$

$$I_{16} = \ddot{P}_n^m - \dot{P}_n^m \cot\theta = (1-\eta^2) P_n^{m''}$$

$$= \left[\frac{m^2+2(n+1)}{1-\eta^2} - (n+1)(n+2)\right] P_n^m - 2(n-m+1) \frac{\eta}{1-\eta^2} P_{n+1}^m \ . \qquad (9.1.10)$$

$$I_{17} = \ddot{P}_n^m - \dot{P}_n^m \cot\theta + 2(1-m^2 \csc^2\theta) P_n^m$$

$$= (1-\eta^2) P_n^{m''} + 2\left(1 - \frac{m^2}{1-\eta^2}\right) P_n^m$$

$$= \left[\frac{2(n+1)-m^2}{1-\eta^2} - n(n+3)\right] P_n^m - 2(n-m+1) \frac{\eta}{1-\eta^2} P_{n+1}^m \ . \qquad (9.1.11)$$

$$I_{18} = \ddot{P}_n^m - \dot{P}_n^m \cot\theta + 2P_n^m$$

$$= (1-\eta^2) P_n^{m''} + 2P_n^m$$

$$= \left[\frac{m^2+2(n+1)}{1-\eta^2} - n(n+3)\right] P_n^m - 2(n-m+1) \frac{\eta}{1-\eta^2} P_{n+1}^m \ . \qquad (9.1.12)$$

By rewriting (4.2.10), (4.2.11), and (4.2.12) using the previously defined I_i $(i = 1,\ldots,18)$ and by making use of the orthogonality of the $\sin m\varphi$ and $\cos m\varphi$ terms we obtain, for each m,

$$\sum_n \Bigg\{ A_{mn} \left[\left\{ 2(1+k)(1+\nu) - M_n\sigma \right\} P_n^m + k\left\{ I_1 + I_2(\nu+P/k) \right\} \right]$$

$$+ B_{mn}\Big[(1+k)(1+\nu)I_8 - kI_7 \Big]$$

$$+ C_{mn}\left(\frac{m}{1-\eta^2}\right)\left[(1+k)(1+\nu)P_n^m - kI_9 \right] \Bigg\} = 0 \qquad (9.1.13)$$

$$\sum_n \Bigg\{ A_{mn}\Big[kI_{10} + (1+\nu)(1+k)I_{11} \Big]$$

$$- B_{mn}(1+k)\left[I_{12} - I_{11}\left\{ \nu\left(\frac{m^2}{2(1-\eta^2)} - 1 \right) + \frac{m_s\sigma}{1+k} \right\} \right]$$

$$- C_{mn}\left[\frac{m(1+k)}{2} I_{13} \right] \Bigg\} = 0 \qquad (9.1.14)$$

$$\sum_n \Bigg\{ A_{mn}\Big[kmI_{14} - m(1+\nu)(1+k)P_n^m \Big]$$

$$- B_{mn}\left(\frac{1+k}{2}\right) m\Big[I_{15} + \nu I_{16} \Big]$$

$$+ C_{mn}\left[\left(\frac{1+k}{2}\right)\Big(I_{17} - \nu I_{18} \Big) + m_s\sigma P_n^m \right] \Bigg\} = 0 \; . \qquad (9.1.15)$$

Since the final objective is to reduce these equations of motion to a series of algebraic equations, the next step is to put these equations into a form in which the orthogonality of the P_n^m's can be taken advantage of. This requires reducing all of the terms to forms which can be integrated simply after being multiplied by $P_\ell^m \, d\eta$. To do this it is necessary to multiply (4.7.1) by $(1-\eta^2)^2$ and (4.7.2) by $(1-\eta^2)$ to produce

$$(1-\eta^2)^2 \left\{ [I_1 + I_2(\nu+P/k)]k + [2(1+k)(1+\nu) - M_n\sigma]P_n^m \right\}$$
$$= \left[L_1 + L_2\eta^2 + L_3\eta^4 \right] P_n^m \tag{9.1.16}$$

where

$$L_1 = 2(1+k)(1+\nu) - M_n\sigma + (n+2)(n-1)[n(n+1)+(1+\nu) + P/k]k$$

$$L_2 = -2L_1 \tag{9.1.17}$$

$$L_3 = L_1 \; .$$

$$(1-\eta^2)^2 I_8(1+k)(1+\nu) = \left[L_4 + L_5\eta^2 + L_6\eta^4 \right] P_n^m \tag{9.1.18}$$

where

$$\left.\begin{aligned} L_4 &= [m^2 - n(n+1)](1+k)(1+\nu) \\ L_5 &= [2n(n+1) - m^2](1+k)(1+\nu) \\ L_6 &= - n(n+1)(1+k)(1+\nu) \quad . \end{aligned}\right\} \tag{9.1.19}$$

$$(1-\eta^2)I_7 = \left[L_7 + L_8\eta^2 + L_9\eta^4 \right] P_n^m + L_{10}P_{n+2}^m \tag{9.1.20}$$

where

$$\begin{aligned} L_7 = {} & 4m^2(n+2)-m^2(n+1)(n+4)+n(n+1)(n+2)(n-1) \\ & - 4m^2(n-m+1)(n+m+1)/(2n+3) \end{aligned}$$

(continued)

$$
\left.
\begin{aligned}
L_8 &= m^2(n+1)(n+4)-2n(n+1)(n+2)(n-1) \\
L_9 &= n(n+1)(n+2)(n-1) \\
L_{10} &= -\,4m^2(n-m+1)(n-m+2)/(2n+3) \quad .
\end{aligned}
\right\} \tag{9.1.21}
$$

$$
(1-\eta^2)m\left[(1+k)(1+\nu)P_n^m - kI_9\right] = \left[L_{11} + \eta^2 L_{12}\right]P_n^m + L_{13}P_{n+2}^m \tag{9.1.22}
$$

where

$$
\begin{aligned}
L_{11} &= m(1+k)(1+\nu) - km[4(n+2)-(n+1)(n+4) \\
&\qquad - 4(n-m+1)(n+m+1)/(2n+3)] \\
L_{12} &= -\,m(1+k)(1+\nu) - km(n+1)(n+4) \\
L_{13} &= 4km(n-m+1)(n-m+2)/(2n+3) \quad .
\end{aligned} \tag{9.1.23}
$$

$$
(1-\eta^2)I_{11} = L_{14}P_{n-1}^m + L_{15}\eta^3 P_n^m + \left(L_{16} + \eta^2 L_{17}\right)P_{n+1}^m \tag{9.1.24}
$$

where

$$
\left.
\begin{aligned}
L_{14} &= (n+1)(n+m)/(2n+1) \\
L_{15} &= -(n+1) \\
L_{16} &= -\,n(n-m+1)/(2n+1) \\
L_{17} &= n-m+1 \quad .
\end{aligned}
\right\} \tag{9.1.25}
$$

$$
(1-\eta^2)I_{12} = L_{18}P_{n-1}^m + L_{19}\eta^3 P_n^m + \left[L_{20} + L_{21}\eta^2\right]P_{n+1}^m \tag{9.1.26}
$$

where

$$\left.\begin{aligned}
L_{18} &= (m+n)\left[(n+1)\{(n-1)(n+2)+1\} - \frac{m^2}{2}(n+5)\right]\Big/(2n+1) \\
L_{19} &= -(n+1)[(n-1)(n+2)+1] \\
L_{20} &= (n-m+1)[\frac{m^2}{2}(n-4)-n\{(n-1)(n+2)+1\}]/(2n+1) \\
L_{21} &= (n-m+1)[(n-1)(n+2)+1] \ .
\end{aligned}\right\} \qquad (9.1.27)$$

$$(1-\eta^2)I_{13} = L_{22}P^m_{n-1} + L_{23}P^m_{n+1} \qquad (9.1.28)$$

where

$$\left.\begin{aligned}
L_{22} &= -(n+n)[(n+5)+\nu(n+1)]/(2n+1) \\
L_{23} &= (n-m+1)[n(1+\nu)-4]/(2n+1) \ .
\end{aligned}\right\} \qquad (9.1.29)$$

$$(1-\eta^2)I_{15} = \left[L_{24} + \eta^2 L_{25}\right]P^m_n + L_{26}P^m_{n+2} \qquad (9.1.30)$$

where

$$\left.\begin{aligned}
L_{24} &= \frac{m^2(2n+1)-(n+1)\{(2n+2)(n-1)+n\}}{2n+3} \\
L_{25} &= (n+1)(n-2) \\
L_{26} &= 2(n-m+1)(n-m+2)/(2n+3) \ .
\end{aligned}\right\} \qquad (9.1.31)$$

$$(1-\eta^2)I_{16} = \left[L_{27} + \eta^2 L_{28}\right]P^m_n + L_{29}P^m_{n+2} \qquad (9.1.32)$$

where

$$L_{27} = [m^2(2n+5)-(n+1)(n+2)]/(2n+3)$$

(continued)

$$\left.\begin{aligned} L_{28} &= (n+1)(n+2) \\ L_{29} &= -2(n-m+1)(n-m+2)/(2n+3) \quad . \end{aligned}\right\} \tag{9.1.33}$$

$$(1-\eta^2)I_{17} = \left[L_{30} + \eta^2 L_{31}\right]P_n^m + L_{32}P_{n+2}^m \tag{9.1.34}$$

where

$$\left.\begin{aligned} L_{30} &= [2(n+1)(n+2)-n(n+3)(2n+3)-m^2(2n+1)]/(2n+3) \\ L_{31} &= n(n+3) \\ L_{32} &= -2(n-m+1)(n-m+2)/(2n+3) \quad . \end{aligned}\right\} \tag{9.1.35}$$

$$(1-\eta^2)I_{18} = \left[L_{33} + \eta^2 L_{34}\right]P_n^m + L_{35}P_{n+2}^m \tag{9.1.36}$$

where

$$\left.\begin{aligned} L_{33} &= [m^2(2n+5)+2(n+1)(n+2)-n(n+3)(2n+3)]/(2n+3) \\ L_{34} &= n(n+3) \\ L_{35} &= -2(n-m+1)(n-m+2)/(2n+3) \quad . \end{aligned}\right\} \tag{9.1.37}$$

$$(1-\eta^2)\left[kmI_{14} - m(1+\nu)(1+k)P_n^m\right] = L_{36}(1-\eta^2)P_n^m \tag{9.1.38}$$

where

$$L_{36} = -km(n+2)(n-1)-m(1+\nu)(1+k) \quad . \tag{9.1.39}$$

$$\begin{aligned} &(1-\eta^2)[kI_{10} + (1+\nu)(1+k)I_{11}] \\ &\qquad = L_{37}P_{n-1}^m + L_{38}\eta^3 P_n^m + \left[L_{39} + \eta^2 L_{40}\right]P_{n+1}^m \end{aligned} \tag{8.1.40}$$

where

$$\left.\begin{aligned}
L_{37} &= L_{41}L_{14} \\
L_{41} &= k(n-1)(n+2)+(1+\nu)(1+k) \\
L_{38} &= L_{41}L_{15} \\
L_{39} &= L_{41}L_{16} \\
L_{40} &= L_{41}L_{17} \quad .
\end{aligned}\right\} \tag{9.1.41}$$

$$(1-\eta^2)I_{11}\left\{\nu\left(\frac{m^2}{2(1-\eta^2)} - 1\right) + \frac{m_s\sigma}{1+k}\right\}$$
$$= L_{42}P^m_{n-1} + L_{43}\eta^3P^m_n + \left[L_{44} + \eta^2L_{45}\right]P^m_{n+1} \tag{9.1.42}$$

where

$$\begin{aligned}
L_{42} &= \left(\frac{m_s\sigma}{1+k} - \nu\right)L_{14} + \frac{\nu m^2}{2}\,\frac{(n+1)(n+m)}{(2n+1)} \\
L_{43} &= \left(\frac{m_s\sigma}{1+k} - \nu\right)L_{15} \\
L_{44} &= \left(\frac{m_s\sigma}{1+k} - \nu\right)L_{16} - \frac{\nu m^2(n-m+1)n}{2(2n+1)} \\
L_{45} &= \left(\frac{m_s\sigma}{1+k} - \nu\right)L_{17} \quad .
\end{aligned} \tag{9.1.43}$$

$$(1-\eta^2)\left[kmI_{14} - m(1+k)(1+\nu)P^m_n\right] = L_{46}(1-\eta^2)P^m_n \tag{9.1.44}$$

where

$$L_{46} = -m[k(n+2)(n-1)+(1+k)(1+\nu)] \ . \tag{9.1.45}$$

In making use of (9.1.16) to (9.1.39), the equations of motion become (for each m)

$$\sum_n \Bigg\{ A_{mn} \left[(1-2\eta^2 + \eta^4) L_1 P_n^m \right] + B_{mn} \Bigg[\Big\{ (L_4 - kL_7) + (L_5 - kL_8)\eta^2$$

$$+ (L_6 - kL_9)\eta^4 \Big\} P_n^m - kL_{10} P_{n+2}^m \Bigg] + C_{mn} \left[\left(L_{11} + \eta^2 L_{12} \right) P_n^m \right.$$

$$\left. + L_{13} P_{n+2}^m \right] \Bigg\} = 0 \,, \tag{9.1.46}$$

$$\sum_n \Bigg\{ A_{mn} \left[L_{37} P_{n-1}^m + L_{38} \eta^3 P_n^m + \left(L_{39} + \eta^2 L_{40} \right) P_{n+1}^m \right]$$

$$- B_{mn} \Bigg[(1+k) \Big\{ (L_{18} - L_{42}) P_{n-1}^m + (L_{19} - L_{43}) \eta^3 P_n^m$$

$$+ (L_{20} - L_{44}) P_{n+1}^m + (L_{21} - L_{45}) \eta^2 P_{n+1}^m \Big\} \Bigg]$$

$$- C_{mn} \left[\frac{m(1+k)}{2} \left\{ L_{22} P_{n-1}^m + L_{23} P_{n+1}^m \right\} \right] \Bigg\} = 0 \,, \tag{9.1.47}$$

and

$$\sum_n \Bigg\{ A_{mn} \left[L_{46} (1-\eta^2) P_n^m \right]$$

$$+ B_{mn} \Bigg[\frac{m(1+k)}{2} \Big\{ (L_{24} + \nu L_{27}) P_n^m + (L_{25} + \nu L_{28}) \eta^2 P_n^m$$

$$+ (L_{26} + \nu L_{29}) P_{n+2}^m \Big\} \Bigg]$$

$$+ C_{mn} \Bigg[\left(\frac{1+k}{2} \right) \Bigg\{ \left(L_{30} - \nu L_{33} + \frac{2m_s \sigma}{1+k} \right) P_n^m + \left(L_{31} - \nu L_{34} + \frac{2m_s \sigma}{1+k} \right) \eta^2 P_n^m$$

$$+ (L_{32} - \nu L_{35}) P_{n+2}^m \Bigg\} \Bigg] \Bigg\} = 0 \,. \tag{9.1.48}$$

The equations of motion are now in a form such that if they are multiplied by $P_\ell^m \, d\eta$ and integrated from -1 to $+1$, the integrals can all be obtained in closed form by making use of (8.5.1) through (8.5.19). The equations of motion are thereby transformed into

$$
\begin{aligned}
& A_{m,\ell-4}J^1_{m\ell} + A_{m,\ell-2}J^2_{m\ell} + A_{m,\ell}J^3_{m\ell} + A_{m,\ell+2}J^4_{m\ell} + A_{m,\ell+4}J^5_{m\ell} \\
& + B_{m,\ell-4}J^6_{m\ell} + B_{m,\ell-2}J^7_{m\ell} + B_{m,\ell}J^8_{m\ell} + B_{m,\ell+2}J^9_{m\ell} + B_{m,\ell+4}J^{10}_{m\ell} \\
& + C_{m,\ell-2}J^{11}_{m\ell} + C_{m,\ell}J^{12}_{m\ell} + C_{m,\ell+2}J^{13}_{m\ell} = 0
\end{aligned}
\qquad (9.1.49)
$$

where

$$
\begin{aligned}
J^1_{m\ell} &= Q_{12}L_1\delta_{\ell,n+4} \\
J^2_{m\ell} &= (Q_{11} - 2Q_3)L_1\delta_{\ell,n+2} \\
J^3_{m\ell} &= (1 - 2Q_2 + Q_{10})L_1\delta_{\ell,n} \\
J^4_{m\ell} &= (Q_9 - 2Q_1)L_1\delta_{\ell,n-2} \\
J^5_{m\ell} &= Q_8L_1\delta_{\ell,n-4} \\
J^6_{m\ell} &= (L_6 - kL_9)Q_{12}\delta_{\ell,n+4} \\
J^7_{m\ell} &= [(L_5 - kL_8)Q_3 + (L_6 - kL_9)Q_{11} - kL_{10}]\delta_{\ell,n+2} \\
J^8_{m\ell} &= [L_4 - kL_7 + (L_5 - kL_8)Q_2 + (L_6 - kL_9)Q_{10}]\delta_{\ell,n} \\
J^9_{m\ell} &= [(L_5 - kL_8)Q_1 + (L_6 - kL_9)Q_9]\delta_{\ell,n-2}
\end{aligned}
\qquad \text{(continued)}
$$

$$J^{10}_{m\ell} = (L_6 - kL_9)Q_8\delta_{\ell,n-4}$$

$$J^{11}_{m\ell} = (L_{12}Q_3 + L_{13})\delta_{\ell,n+2}$$

$$J^{12}_{m\ell} = (L_{12}Q_2 + L_{11})\delta_{\ell,n}$$

$$J^{13}_{m\ell} = L_{12}Q_1\delta_{\ell,n-2}\ , \qquad (9.1.50)$$

and

$$A_{m,\ell-3}J^{14}_{m\ell} + A_{m,\ell-1}J^{15}_{m\ell} + A_{m,\ell+1}J^{16}_{m\ell} + A_{m,\ell+3}J^{17}_{m\ell} + B_{m,\ell-3}J^{18}_{m\ell}$$

$$+ B_{m,\ell-1}J^{19}_{m\ell} + B_{m,\ell+1}J^{20}_{m\ell} + B_{m,\ell+3}J^{21}_{m\ell} + C_{m,\ell-1}J^{22}_{m\ell} + C_{m,\ell+1}J^{23}_{m\ell} = 0 \qquad (9.1.51)$$

where

$$J^{14}_{m\ell} = [L_{38}Q_7 + L_{40}Q_3]\delta_{\ell,n+3}$$

$$J^{15}_{m\ell} = [L_{39} + L_{38}Q_6 + L_{40}Q_2]\delta_{\ell,n+1}$$

$$J^{16}_{m\ell} = [L_{37} + L_{38}Q_5 + L_{40}Q_1]\delta_{\ell,n-1}$$

$$J^{17}_{m\ell} = L_{38}Q_4\delta_{\ell,n-3}$$

$$J^{18}_{m\ell} = (1+k)[(L_{43} - L_{19})Q_7 + (L_{45} - L_{21})Q_3]\delta_{\ell,n+3}$$

$$J^{19}_{m\ell} = (1+k)[L_{44} - L_{20} + (L_{43} - L_{19})Q_6 + (L_{45} - L_{21})Q_2]\delta_{\ell,n+1}$$

$$J^{20}_{m\ell} = (1+k)[L_{42} - L_{18} + (L_{43} - L_{19})Q_5 + (L_{45} - L_{21})Q_1]\delta_{\ell,n-1}$$

$$J^{21}_{m\ell} = (1+k)(L_{43} - L_{19})Q_4\delta_{\ell,n-3}$$

(continued)

$$J_{m\ell}^{22} = -\frac{m(1+k)}{2} L_{23}\delta_{\ell,n+1}$$

$$J_{m\ell}^{23} = -\frac{m(1+k)}{2} L_{22}\delta_{\ell,n-1} ,$$

and

$$A_{m,\ell-2}J_{m\ell}^{24} + A_{m,\ell}J_{m\ell}^{25} + A_{m,\ell+2}J_{m\ell}^{26} + B_{m,\ell-2}J_{m\ell}^{27} + B_{m,\ell}J_{m\ell}^{28}$$

$$+ B_{m,\ell-2}J_{m\ell}^{29} + C_{m,\ell-2}J_{m\ell}^{30} + C_{m,\ell}J_{m\ell}^{31} + C_{m,\ell+2}J_{m\ell}^{32} = 0 \qquad (9.1.53)$$

where

$$J_{m\ell}^{24} = -L_{46}Q_3\delta_{\ell,n+2}$$

$$J_{m\ell}^{25} = L_{46}[1 - Q_2]\delta_{\ell,n}$$

$$J_{m\ell}^{26} = - L_{46}Q_1\delta_{\ell,n-2}$$

$$J_{m\ell}^{27} = \frac{m(1+k)}{2} [L_{26} + \nu L_{29} + Q_3[L_{25} + \nu L_{28})]\delta_{\ell,n+2}$$

$$J_{m\ell}^{28} = \frac{m(1+k)}{2} [L_{24} + \nu L_{27} + Q_2(L_{25} + \nu L_{28})]\delta_{\ell,n}$$

$$J_{m\ell}^{29} = \frac{m(1+k)}{2} [Q_1(L_{25} + \nu L_{28})]\delta_{\ell,n-2}$$

$$J_{m\ell}^{30} = (\frac{1+k}{2})[L_{32} - \nu L_{35} + Q_3(L_{31} - \nu L_{34} + \frac{2m_s\sigma_{mn}}{1+k})]\delta_{\ell,n+2}$$

$$J_{m\ell}^{31} = (\frac{1+k}{2})[L_{30} - \nu L_{33} + \frac{2m_s\sigma}{(1+k)} + Q_2(L_{31} - \nu L_{34} + \frac{2m_s\sigma_{mn}}{1+k})]\delta_{\ell,n}$$

$$J_{m\ell}^{32} = (\frac{1+k}{2})Q_1(L_{31} - \nu L_{34} + \frac{2m_s\sigma_{mn}}{1+k})\delta_{\ell,n-2} . \qquad (9.1.54)$$

Equations (9.1.49), (9.1.51), and (9.1.53) each constitute an infinite set (one equation for each value of ℓ, with $\ell = 1,2,\ldots$) of linear homogeneous algebraic equations for each value of $m(m = 0,1,\ldots,\ell)$. In order for a nontrivial solution for the A's, B's, and C's to exist, the determinant of their coefficients must vanish. This determinantal equation constitutes the frequency equation for each value of m.

In order to solve these equations for the eigenfrequencies, a computer program was developed. This program computes the $J^i_{m\ell}$'s $(i = 1,2,\ldots,32)$ for values of m and ℓ, evaluates the determinant for varied values of σ and plots the value of the determinant as a function of σ. The curve crosses the abscissa (determinant equal zero) at the eigenfrequencies.

The previous description is, of course, not workable unless the determinant is truncated at some finite order. And, in fact, to calculate the first ℓ frequencies requires the continuous evaluation of a determinant of order 3ℓ.

As an example of a calculation the $\ell = 1$ and $\ell = 2$ modes will be examined. It should be noted that the $\ell = 1$ equations are only valid for $m = 0,1$ and to examine the $m = 2$ mode (for $\ell = 1,2$) it is necessary to eliminate the $\ell = 1$ equations (in the determinant) and replace them by the $\ell = 3$ equations.

The equations for $\ell = 1$ and $\ell = 2$ can be written as

$$A_{m,1}J^3_{m,1} + A_{m,3}J^4_{m,1} + A_{m,5}J^5_{m,1} + B_{m,1}J^8_{m,1} + B_{m,3}J^9_{m,1} + B_{m,5}J^{10}_{m,1}$$

$$+ C_{m,1}J^{12}_{m,1} + C_{m,3}J^{13}_{m,1} = 0 \qquad (9.1.55)$$

$$A_{m,2}J^{16}_{m,1} + A_{m,4}J^{17}_{m,1} + B_{m,2}J^{20}_{m,1} + B_{m,4}J^{21}_{m,1} + C_{m,2}J^{23}_{m,1} = 0 \quad (9.1.56)$$

$$A_{m,1}J^{25}_{m,1} + A_{m,3}J^{26}_{m,1} + B_{m,1}J^{28}_{m,1} + B_{m,3}J^{29}_{m.1} + C_{m,1}J^{31}_{m,1}$$

$$+ C_{m,3}J^{32}_{m,1} = 0 \quad (9.1.57)$$

$$A_{m,2}J^{3}_{m,2} + A_{m,4}J^{4}_{m,2} + A_{m,6}J^{5}_{m,2} + B_{m,2}J^{8}_{m,2} + B_{m,4}J^{9}_{m,2}$$

$$+ B_{m,6}J^{10}_{m,2} + C_{m,2}J^{12}_{m,2} + C_{m,4}J^{13}_{m,2} = 0 \quad (9.1.58)$$

$$A_{m,1}J^{15}_{m,2} + A_{m,3}J^{16}_{m,2} + A_{m,5}J^{17}_{m,2} + B_{m,1}J^{19}_{m,2} + B_{m,2}J^{20}_{m,2}$$

$$+ B_{m,5}J^{21}_{m,2} + C_{m,1}J^{22}_{m,2} + C_{m,3}J^{23}_{m,2} = 0 \quad (9.1.59)$$

$$A_{m,2}J^{25}_{m,2} + A_{m,4}J^{26}_{m,2} + B_{m,2}J^{28}_{m,2} + B_{m,4}J^{29}_{m,2} + C_{m,2}J^{31}_{m,2}$$

$$+ C_{m,4}J^{32}_{m,2} = 0 \ . \quad (9.1.60)$$

If we neglect the terms for which $\ell > 2$, the 6×6 frequency determinant may be written as

$$\begin{vmatrix} J^{3}_{m,1} & 0 & J^{8}_{ml} & 0 & J^{12}_{ml} & 0 \\ 0 & J^{16}_{m,1} & 0 & J^{20}_{ml} & 0 & J^{23}_{m,1} \\ J^{25}_{m,1} & 0 & J^{28}_{m,1} & 0 & J^{31}_{m,1} & 0 \end{vmatrix}$$

(continued)

$$\begin{vmatrix} 0 & J^{3}_{m,2} & 0 & J^{8}_{m,2} & 0 & J^{12}_{m,2} \\ J^{15}_{m,2} & 0 & J^{19}_{m,2} & 0 & J^{22}_{m,2} & 0 \\ 0 & J^{25}_{m,2} & 0 & J^{28}_{m,2} & 0 & J^{31}_{m,2} \end{vmatrix} . \qquad (9.1.61)$$

It should be noted that every alternate element of this determinant vanishes, which means that the 6×6 determinant reduces to the product of two 3×3 determinants. This is true of any even determinant whose alternate terms are zero. That is, under these conditions, a $2i \times 2i$ determinant reduces to the product of two $i \times i$ determinants.

By rewriting (9.1.61) as the product of two 3×3 determinants we obtain

$$\begin{vmatrix} J^{3}_{m,1} & J^{8}_{m,1} & J^{12}_{m,1} \\ J^{25}_{m,1} & J^{28}_{m,1} & J^{31}_{m,1} \\ J^{15}_{m,2} & J^{18}_{m,2} & J^{22}_{m,2} \end{vmatrix} \times \begin{vmatrix} J^{16}_{m,1} & J^{20}_{m,1} & J^{23}_{m,1} \\ J^{3}_{m,2} & J^{8}_{m,2} & J^{12}_{m,2} \\ J^{25}_{m,2} & J^{28}_{m,2} & J^{31}_{m,2} \end{vmatrix} . \qquad (9.1.62)$$

$J^{3}_{m,1}$, $J^{31}_{m,1}$, $J^{18}_{m,2}$, $J^{20}_{m,1}$, $J^{3}_{m,2}$, and $J^{31}_{m,2}$ contain σ -terms, and therefore must be evaluated for each value of σ before the determinants can be evaluated.

Equations (9.1.49), (9.1.51) and (9.1.53) have been solved using $\ell = 1,2,\ldots,6$ and $m = 0,1,\ldots 5$, that is for each value of m an 18×18 (in reality two 9×9 determinants) had to be evaluated several hundred times.

X. APPENDIX C

VISCOSITY CONSIDERATIONS

To give some idea as to the effect of viscosity a simplified analysis will be presented. In following the analysis by Lamb[13], the velocity potential of the inner medium for any fundamental mode may be written as

$$\Phi_{1mn}(r,\theta,\varphi,t) = D_{mn} r^{n} \cos m\varphi \, P_{n}^{m} \cos \sqrt{\sigma_{mn}}\, t \; . \tag{10.1.1}$$

For an incompressible, irrotationally flowing fluid the kinetic energy contained in a sphere of radius r may be written as

$$T = -\frac{\rho_1}{2} \iint \Phi_1 \frac{\partial \Phi_1}{\partial r} r^2 d\gamma \tag{10.1.2}$$

where γ denotes the solid angle. By making use of (10.1.1) in (10.1.2) we find that

$$T = -\frac{\rho_1}{2} \iint D_{mn}^2 r^{2n+1} n \cos^2 m\varphi (P_n^m)^2 \cos^2 \sqrt{\sigma_{mn}}\, t \, d\gamma \; . \tag{10.1.3}$$

Since the system has been considered to be conservative, the energy must be constant which implies that the potential energy may be written as

$$V = -\frac{\rho_1}{2} \iint D_{mn}^2 r^{2n+1} n \cos^2 m\varphi (P_n^m)^2 \sin^2 \sqrt{\sigma_{mn}}\, t \, d\gamma \, . \tag{10.1.4}$$

The dissipation in a liquid sphere, of viscosity μ, based on the assumption of irrotational flow is

$$E_D = -\mu \iint \frac{\partial q^2}{\partial r} r^2 d\gamma = -\mu r^2 \frac{\partial}{\partial r} \iint q^2 d\gamma . \tag{10.1.5}$$

The kinetic energy of the fluid contained between two spherical surfaces of radii r and $r+\delta r$ can be gotten from (10.1.2) and from the definition of kinetic energy. By equating these, we obtain

$$\frac{1}{2} \rho_1 \left[\iint q^2 r^2 d\gamma \right] \delta r = \frac{-1}{2} \rho_1 \left[\frac{\partial}{\partial r} \iint \Phi_1 \frac{\partial \Phi_1}{\partial r} r^2 d\gamma \right] \delta r \tag{10.1.6}$$

which implies that

$$\iint q^2 d\gamma = \frac{-1}{r^2} \frac{\partial}{\partial r} \iint \Phi_1 \frac{\partial \Phi_1}{\partial r} r^2 d\gamma . \tag{10.1.7}$$

If use is made of (10.1.1) in (10.1.7), we find that

$$\iint q^2 d\gamma = -n(2n+1) \iint D^2_{mn} r^{2n-2} \cos^2 m\varphi (P^m_n)^2 \cos^2 \sqrt{\sigma_{mn}}\, t \, d\gamma . \tag{10.1.8}$$

And from (10.1.5) the dissipation becomes

$$E_D = 2\mu n(2n+1)(n-1) \iint D^2_{mn} r^{2n-1} \cos^2 m\varphi (P^m_n)^2 \cos^2 \sqrt{\sigma_{mn}}\, t \, d\gamma . \tag{10.1.9}$$

Or the mean value per unit time may be written as

$$\overline{E}_D = \mu n(2n+1)(n-1) \iint D^2_{mn} r^{2n-1} \cos^2 m\varphi (P^m_n)^2 d\gamma . \tag{10.1.10}$$

If it is assumed that the effect of viscosity may be represented by a gradual variation of the coefficient D_{mn}, then

$$\overline{E}_D = \frac{d}{dt} (T + V) . \tag{10.1.11}$$

Or by making use of (10.1.10), (10.1.3) and (10.1.4) in (10.1.11) produces, for a sphere of radius R

$$\frac{d}{dt} D_{mn} = - \frac{\mu}{\rho_1} \frac{(n-1)(2n+1)}{R^2} D_{mn} , \tag{10.1.12}$$

the solution of which may be written in the form

$$D_{mn} = D_{mn_o} e^{-t/\tau} , \tag{10.1.13}$$

where D_{mn_o} is a constant and τ is defined by

$$\tau = \frac{R^2\rho_1}{\mu} \frac{1}{(n-1)(2n+1)} . \tag{10.1.14}$$

This result indicates that if the vitreous body is considered to have a viscosity approximating water $(\mu \sim .01 \frac{\text{dyne-sec}}{\text{cm}^2})$, then a spherical liquid mass, of radius 1.3 cm and density 1.0 gm/cm^3, will have a decay time for the fundamental (n=2) mode of

$$\tau = 33.8 \text{ sec}$$

This implies that even if the viscosity of the vitreous body is two orders of magnitude greater than that of water the decay time will still be of the order of .35 seconds which corresponds to 35 cycles (assuming a natural frequency of approximately 100 cps).

While it must be realized that this is only a very elementary model of the viscous effects (and does not include the viscous effects of the external tissue), it does imply that in this early model viscosity can be neglected.

XI. APPENDIX D

MODE SHAPES

The mode shapes for $n = 1,2,3,4$ for the axisymmetric shell model will be examined here. From (4.2.1) and (4.2.5) the radial and tangential displacements for any axisymmetric mode can be written as

$$w_n(\theta,t) = A_n \, e^{i\sqrt{\sigma_n}\,t} \, P_n(\cos\theta) \tag{11.1.1}$$

$$v_n(\theta,t) = B_n \, e^{i\sqrt{\sigma_n}\,t} \, \frac{d}{d\theta} P_n(\cos\theta) \, . \tag{11.1.2}$$

The Legendre polynomials for $n = 1,2,3,4$ are

$$P_1(\cos\theta) = \cos\theta \tag{11.1.3}$$

$$P_2(\cos\theta) = \frac{1}{2}\,(3\cos^2\theta - 1) \tag{11.1.4}$$

$$P_3(\cos\theta) = \frac{1}{2}\,(5\cos^3\theta - 3\cos\theta) \tag{11.1.5}$$

$$P_4(\cos\theta) = \frac{1}{8}\,(35\cos^4\theta - 30\cos^2\theta + 3) \tag{11.1.6}$$

and their derivatives with respect to θ are

$$\frac{dP_1}{d\theta} = -\sin\theta \tag{11.1.7}$$

$$\frac{dP_2}{d\theta} = -3\sin\theta\cos\theta \tag{11.1.8}$$

$$\frac{dP_3}{d\theta} = -\frac{3}{2}\sin\theta(5\cos^2\theta - 1) \tag{11.1.9}$$

$$\frac{dP_4}{d\theta} = -\frac{5}{2}\sin\theta\cos\theta(7\cos^2\theta - 3) \, . \tag{11.1.10}$$

Using the nominal physical constants $R = 1.3$ cm, $h = 0.1$ cm, $E = 7.0 \times 10^6$ dyne/cm^2, and $\nu = 0.5$ at $P = 0$, the eigenfrequencies for the first four mode numbers $(n = 1,2,3,4)$ as computed in section (4.5) are

$$\left.\begin{aligned}
\sigma_1 &= 0 \quad \text{and} \quad 9.328 \times 10^6 \\
\sigma_2 &= 0.3128 \times 10^6 \quad \text{and} \quad 31.87 \times 10^6 \\
\sigma_3 &= 0.5522 \times 10^6 \quad \text{and} \quad 65.50 \times 10^6 \\
\sigma_4 &= 0.8418 \times 10^6 \quad \text{and} \quad 110.2 \times 10^6 \ .
\end{aligned}\right\} \qquad (11.1.11)$$

To obtain a relation between A_n and B_n we make use of (4.5.13)

$$A_n[2(1+k)(1+\nu)+k(n+2)(n-1)\{n(n+1)+(1+\nu)+ P/k\} - M_n\sigma]$$

$$- B_n[(1+k)(1+\nu)+k(n+2)(n-1)]n(n+1) = 0 \ . \qquad (11.1.12)$$

A_n and B_n are related as

$$\left.\begin{aligned}
A_1 &= B_1 \quad \text{for} \quad \sigma_1 = 0 \\
B_1 &= -\ 7.984A_1 \quad \text{for} \quad \sigma_1 = 9.328 \times 10^6
\end{aligned}\right\} \qquad (11.1.13)$$

$$\left.\begin{aligned}
B_2 &= 0.2760A_2 \quad \text{for} \quad \sigma_2 = 0.3128 \times 10^6 \\
B_2 &= -\ 5.587A_2 \quad \text{for} \quad \sigma_2 = 31.87 \times 10^6
\end{aligned}\right\} \qquad (11.1.14)$$

$$\left.\begin{aligned}
B_3 &= 0.1433A_3 \quad \text{for} \quad \sigma_3 = 0.5522 \times 10^6 \\
B_3 &= -\ 4.242A_3 \quad \text{for} \quad \sigma_3 = 65.50 \times 10^6
\end{aligned}\right\} \qquad (11.1.15)$$

$$\left.\begin{aligned} B_4 &= +\,0.07798A_4 \quad \text{for} \quad \sigma_4 = 0.8418 \times 10^6 \\ B_4 &= -\,3.398A_4 \quad \text{for} \quad \sigma_4 = 110.2 \times 10^6 \;. \end{aligned}\right\} \tag{11.1.16}$$

By making use of (11.1.13), (11.1.14), (11.1.15), (11.1.16), and the Legendre polynomials and their derivatives in (11.1.1) and (11.1.2), we obtain for the radial and tangential displacements

$$\left.\begin{aligned} w_1(\theta,t) &= A_1 \cos\theta \\ v_1(\theta,t) &= -\,A_1 \sin\theta \end{aligned}\right\} \sigma = 0 \tag{11.1.17}$$

$$\left.\begin{aligned} w_1(\theta) &= A_1 \cos\theta \\ v_1(\theta) &= 7.984A_1 \sin\theta \end{aligned}\right\} \sigma = 9.328 \times 10^6 \tag{11.1.18}$$

$$\left.\begin{aligned} w_2(\theta) &= \frac{A_2}{2}\,(3\cos^2\theta - 1) \\ v_2(\theta) &= -\,0.8280A_2 \sin\theta\cos\theta \end{aligned}\right\} \sigma = 0.3128 \times 10^6 \tag{11.1.19}$$

$$\left.\begin{aligned} w_2(\theta) &= \frac{A_2}{2}\,(3\cos^2\theta - 1) \\ v_2(\theta) &= 16.76\,A_2 \sin\theta\cos\theta \end{aligned}\right\} \sigma = 31.87 \times 10^6 \tag{11.1.20}$$

$$\left.\begin{aligned} w_3(\theta) &= \frac{A_3}{2}\cos\theta(5\cos^2\theta - 3) \\ v_3(\theta) &= -\,0.2150\,A_3 \sin\theta(5\cos^2\theta - 1) \end{aligned}\right\} \sigma = 0.5522 \times 10^6 \tag{11.1.21}$$

$$\left.\begin{aligned} w_3(\theta) &= \frac{A_3}{2} \cos\theta(5\cos^2\theta - 3) \\ v_3(\theta) &= 6.363\ A_3 \sin\theta(5\cos^2\theta - 1) \end{aligned}\right\} \sigma = 65.50 \times 10^6 \qquad (11.1.22)$$

$$\left.\begin{aligned} w_4(\theta) &= \frac{A_4}{8} (35\cos^4\theta - 30\cos^2\theta + 3) \\ v_4(\theta) &= -\ 0.1950\ A_4 \sin\theta\cos\theta(7\cos^2\theta - 3) \end{aligned}\right\} \sigma = 0.8418 \times 10^6 \qquad (11.1.23)$$

$$\left.\begin{aligned} w_4(\theta) &= \frac{A_4}{8} (35\cos^4\theta - 30\cos^2\theta + 3) \\ v_4(\theta) &= 8.494\ A_4 \sin\theta\cos\theta(7\cos^2\theta - 3). \end{aligned}\right\} \sigma = 110.2 \times 10^6 \qquad (11.1.24)$$

It should be noted that w_1 and v_1 for $\sigma = 0$ are time independent which implies a continuous linear motion.

In order to obtain an effective plot of these mode shapes, the Calcomp plotter associated with the B5500 computer was used. By making use of the Stanford University Computation Center Library Program No. 159 the graphs of the mode shapes were obtained. Since the Calcomp plotter only understands cartesian coordinates it was necessary to transform the aforementioned relations. This was done as follows:

A point on the equilibrium surface of the sclera (circular cross-section) can be written in vector form as

$$\vec{R} = R\sin\theta\ \hat{i} + R\cos\theta\ \hat{k} \qquad (11.1.25)$$

where $\hat{i}$ and $\hat{k}$ are unit vectors in the x and z -directions respectively.

The displacements in vector notation can be written as

$$\vec{w}_n = w_n \sin\theta\,\hat{i} + w_n \cos\theta\,\hat{k} \tag{11.1.26}$$

and

$$\vec{v}_n = v_n \cos\theta\,\hat{i} - v_n \sin\theta\,\hat{k}\ . \tag{11.1.27}$$

The displaced surface (2-dimensional) is then

$$\vec{R}_{dn} = \vec{R} + \vec{w}_n + \vec{v}_n \tag{11.1.28}$$

or using (11.1.25), (11.1.26) and (11.1.27)

$$\vec{R}_{dn} = [(R + w_n)\sin\theta + v_n \cos\theta]\hat{i}$$

$$+ [(R + w_n)\cos\theta - v_n \sin\theta]\hat{k}\ . \tag{11.1.29}$$

When making use of (11.1.17) through (11.1.24) in (11.1.29), the displaced surfaces for each mode may be written as:

for $\sigma_1 = 0$

$$\vec{R}_{d_1} = R \sin\theta\,\hat{i} + (R\cos\theta + A_1)\hat{k} \tag{11.1.30}$$

for $\sigma_1 = 9.328 \times 10^6$

$$\vec{R}_{d_1} = \sin\theta[R + 8.98\ A_1 \cos\theta]\hat{i}$$

$$+ [R\cos\theta + A_1(1 - 8.98 \sin^2\theta)]\hat{k} \tag{11.1.31}$$

for $\sigma_2 = 0.3128 \times 10^6$

$$\vec{R}_{d_2} = \sin\theta[R + A_2\{0.67 \cos^2\theta - 0.50\}]\hat{i}$$

$$+ \cos\theta[R + A_2\{1.00 - 0.67 \sin^2\theta\}]\hat{k} \tag{11.1.32}$$

for $\sigma_2 = 31.87 \times 10^6$

$$\vec{R}_{d_2} = \sin\theta[R + A_2\{18.26\cos^2\theta - .50\}]\hat{i}$$

$$+ \cos\theta[R + A_2\{1.00 - 18.26\sin^2\theta\}]\hat{k} \qquad (11.1.33)$$

for $\sigma_3 = 0.5522 \times 10^6$

$$\vec{R}_{d_3} = \sin\theta[R + A_3\cos\theta\{1.43\cos^2\theta - 1.29\}]\hat{i}$$

$$+ [R\cos\theta + A_3\{1.43\cos^4\theta - .21\cos^2\theta - .22\}]\hat{k} \qquad (11.1.34)$$

for $\sigma_3 = 65.50 \times 10^6$

$$\vec{R}_{d_3} = \sin\theta[R + A_3\cos\theta\{34.32\cos^2\theta - 7.86\}]\hat{i}$$

$$+ [R\cos\theta + A_3\{34.32\cos^4\theta - 39.68\cos^2\theta + 6.63\}]\hat{k} \qquad (11.1.35)$$

for $\sigma_4 = 0.8418 \times 10^6$

$$\vec{R}_{d_4} = \sin\theta[R + A_4\{3.01\cos^4\theta - 3.17\cos^2\theta + .38\}]\hat{i}$$

$$+ \cos\theta[R + A_4\{3.01\cos^4\theta - 1.80\cos^2\theta - .21\}]\hat{k} \qquad (11.1.36)$$

for $\sigma_4 = 110.2 \times 10^6$

$$\vec{R}_{d_4} = \sin\theta[R + A_4\{63.43\cos^4\theta - 29.23\cos^2\theta + .38\}]\hat{i}$$

$$+ \cos\theta[R + A_4\{63.43\cos^4\theta - 88.69\cos^2\theta + 25.86\}]\hat{k}\,. \qquad (11.1.37)$$

By examining the $\sigma_1 = 0$ mode equation (11.1.30) and comparing it to the equilibrium equation (11.1.25), it can be seen that the difference between the equations is a displacement A_1 in the $\hat{k}$ -direction. That is every point of the equilibrium surface is displaced a distance A_1 in the $\hat{k}$ -direction, or more simply, this describes a translation in the $\hat{k}$ -direction.

Figs. 12.1a through 12.1h show the mode shapes for the first four mode numbers $(n = 1,2,3,4)$. These figures depict the maximum and minimum displacements during oscillation. The low frequency modes are the most familiar. That is, for $n = 1$ a translation is observed, and for $n = 2,3,4$ the familiar two, three, and four lobed figures are seen to emerge.

The high frequency modes though are not at all familiar. An examination of them shows very sharp bends (although the bends are greatly exaggerated in the figures in order that they show up distinctly) which would seem to account for the high frequencies associated with these modes. The sharp bends are due to the large tangential displacement associated with the high frequency modes.

BIBLIOGRAPHY

1. Nickerson, J. L., Paradijeff, A., and Feinhandler, H. S., "A Study of the Effects of Externally Applied Sinusoidal Forces on the Eye", AMRL-TDR-63-120.

2. Hayashi, D. T. and Anliker, M., "Model Studies on the Migratory Behavior of Detached Retinas", Investigative Ophthalmology 3:678, 1964.

3. Silvis, J. W., "The Response of a Simulated Detached Retina to Various Dynamic Forces", Engineer's Thesis, Department of Aeronautics and Astronautics, Stanford University, August 1965.

4. Magid, E. B. and Coermann, R. R., "The Reaction of the Human Body to Extreme Vibrations," Proceedings of the Institute of Environmental Science, pp. 135-153, 1960.

5. Posner, A., "What Do We Mean by Intraocular Pressure", The Eye, Ear, Nose and Throat Monthly, 41:285-6, April, 1962.

6. Goldmann, H., Transactions of the Second Conference on Glaucoma, New York; Josiah Macy, Jr. Foundation, 1956.

7. Schiotz, H., "Ein niur Tonometer", Arch. Augenheilk, 52:401-424, 1905.

8. Mackay, R. S. and Marg, E., "Fast, Automatic Electronic Tonometers Based on Exact Theory", Acta Ophthal (Kbh) 37:495-507, 1959.

9. Kestenbaum, A., Applied Anatomy of the Eye, New York: Grune and Stratton, 1963.

10. Newell, F. W., Ophthalmology, St. Louis: C. V. Mosby, 1965.

11. Vaughan, D., Cook, R., and Asbury, T., General Ophthalmology, Los Altos: Lange Medical Publications, 1962.

12. Landau, L. D., and Lifshitz, E.M., Fluid Mechanics, London; Pergamon Press, 1959.

13. Lamb, H., Hydrodynamics, 6th Ed., New York: Dover, 1932.

14. Strutt, J. W., The Theory of Sound, 2nd Ed., New York: Dover, 1945.

15. Flügge, W., Stresses in Shells, Berlin: Springer, 1960.

16. Lamb, H., "On the Vibrations of a Spherical Shell", Proc. Lond. Math Soc 14:50-56, 1882.

17. Anliker, M., Personal Communication, 1966.

18. Smythe, W. R., Static and Dynamic Electricity, 2nd Ed., New York: McGraw-Hill, 1950.

19. Robin, L., Functions Spheriques de Legendre et Fonctions Spheriodales, Tome 11, Paris: Gauthier-Villars, 1958.

20. Hobson, E. W., The Theory of Spherical and Ellipsoidal Harmonics, Cambridge: University Press, 1931.

21. Love, A. E. H., The Mathematical Theory of Elasticity, New York: Dover, 1944.

22. Lee, E. H., "Viscoelasticity", Handbook of Engineering Mechanics, Ed. Flügge, W., New York: McGraw-Hill, 1962.

23. Mackay, S. R., "Electronics in Clinical Research", Proc. IRE, Vol. 50, No. 5, 1962, p. 1177-1189.

24. Schwartz, N. J., "A Theoretical and Experimental Study of the Mechanical Behavior of the Cornea with Application to the Measurement of Intraocular Pressure", Ph.D. Thesis, University of California, Berkeley, Aug. 1965.

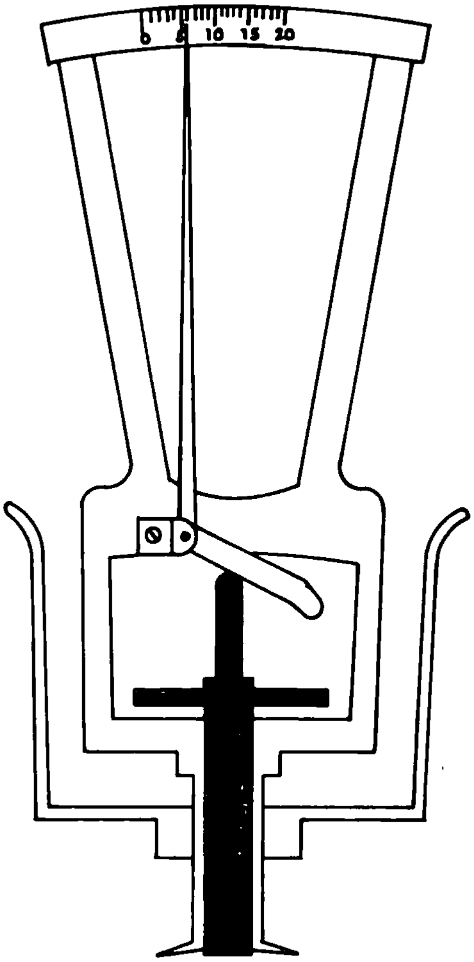

FIGURE 1.1. SCHIOTZ TONOMETER

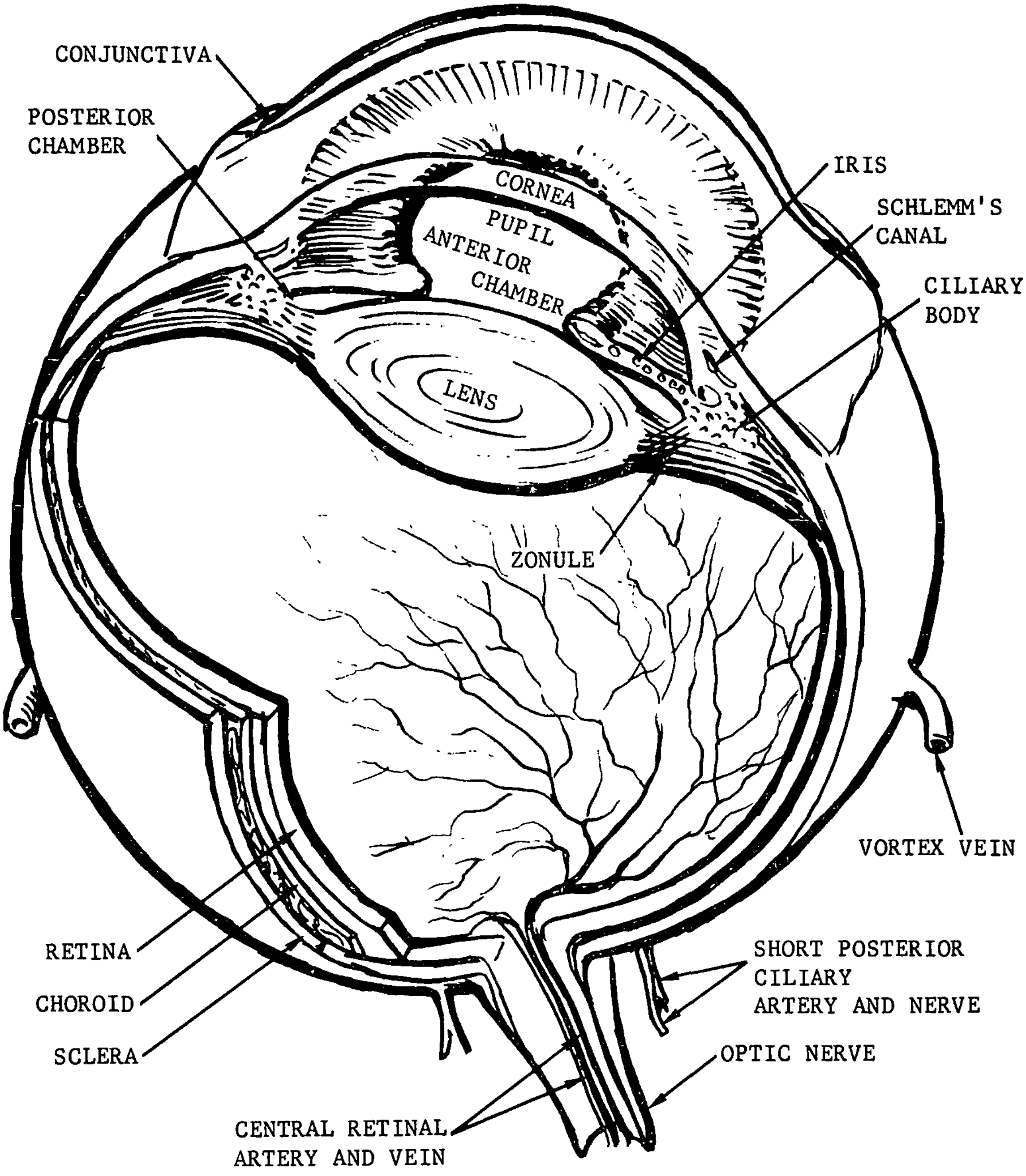

FIGURE 1.2. HUMAN EYE

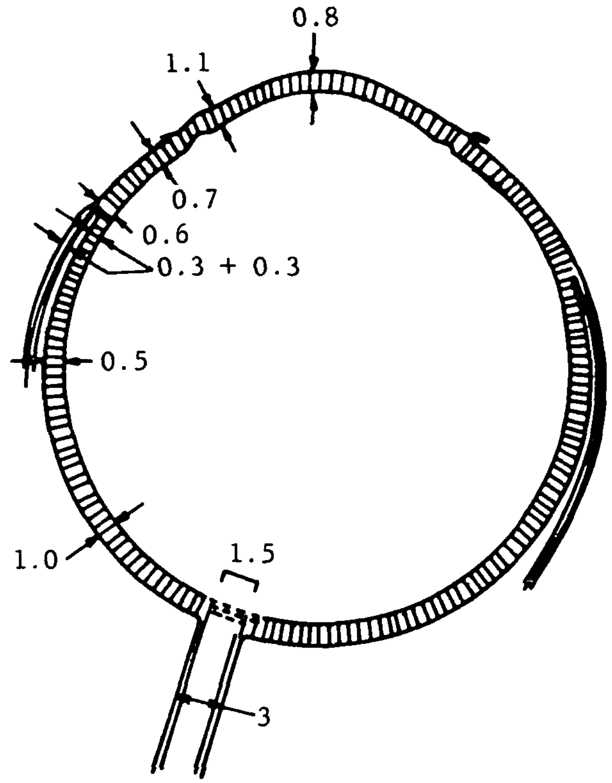

FIGURE 1.3. CROSS-SECTION OF HUMAN EYE IN MM

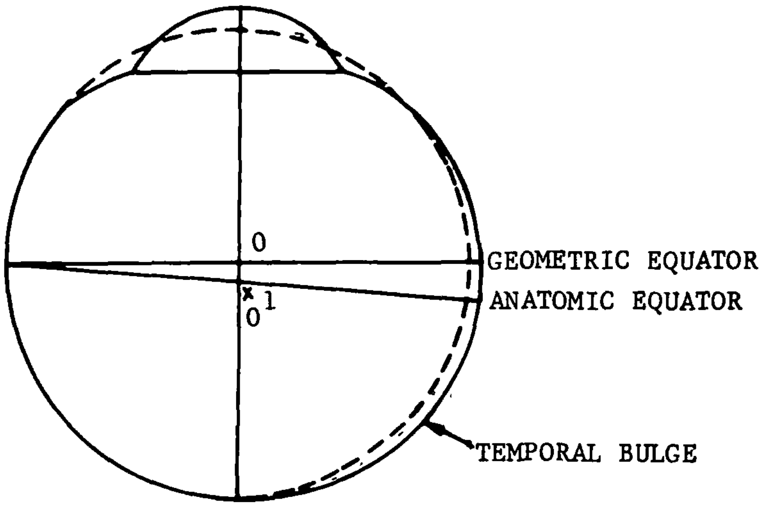

--- THEORETICAL SCLERAL CIRCLE
—— ACTUAL DEVIATIONS FROM THE IDEAL
0 = GEOMETRIC CENTER OF SCLERAL SPHERE
0^1 = THE APPROXIMATE CENTER OF THE SCLERAL BULGE

FIGURE 1.4. DEVIATIONS FROM THE SCLERAL SPHERE

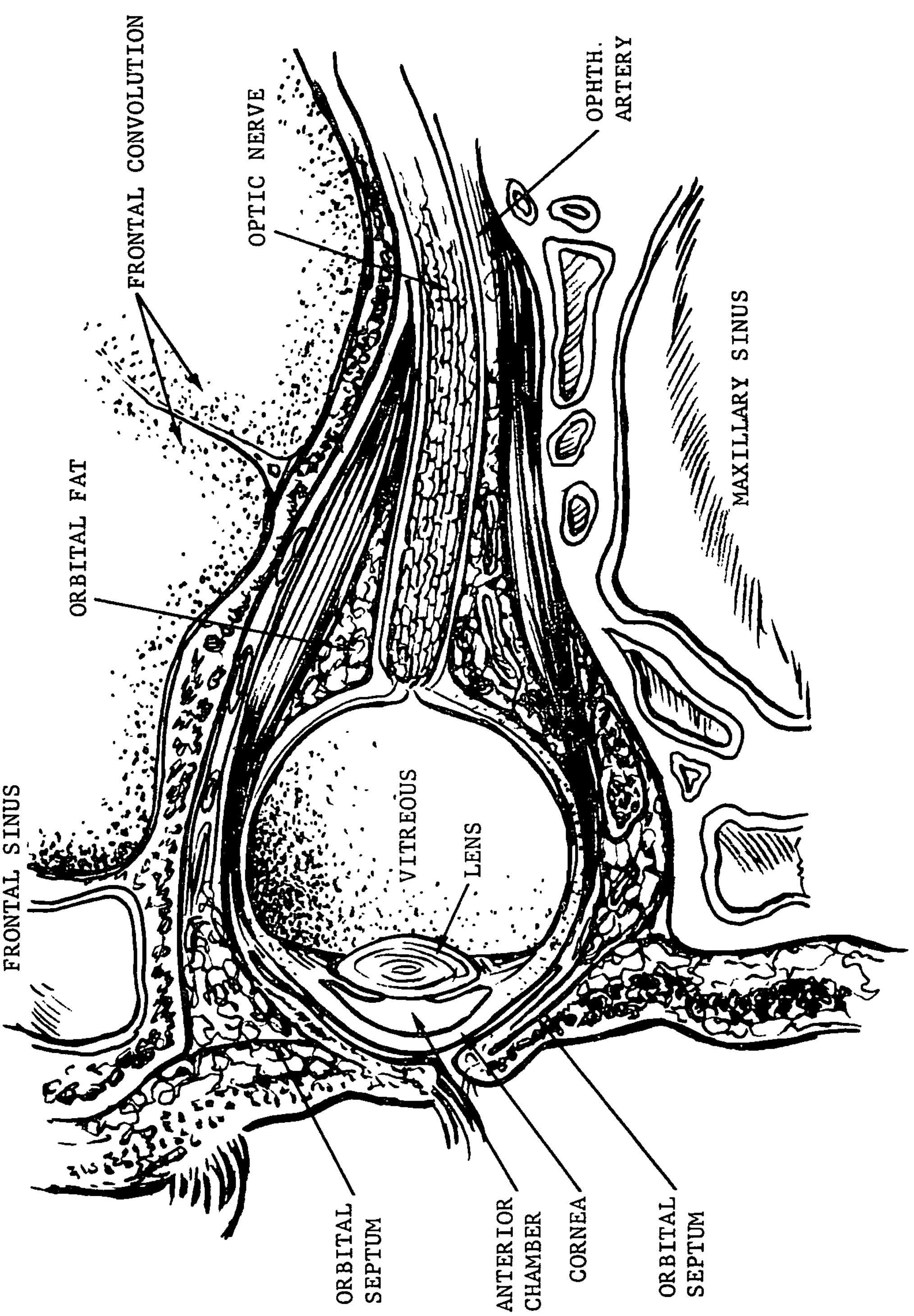

FIGURE 1.5. ORBITAL ANATOMY

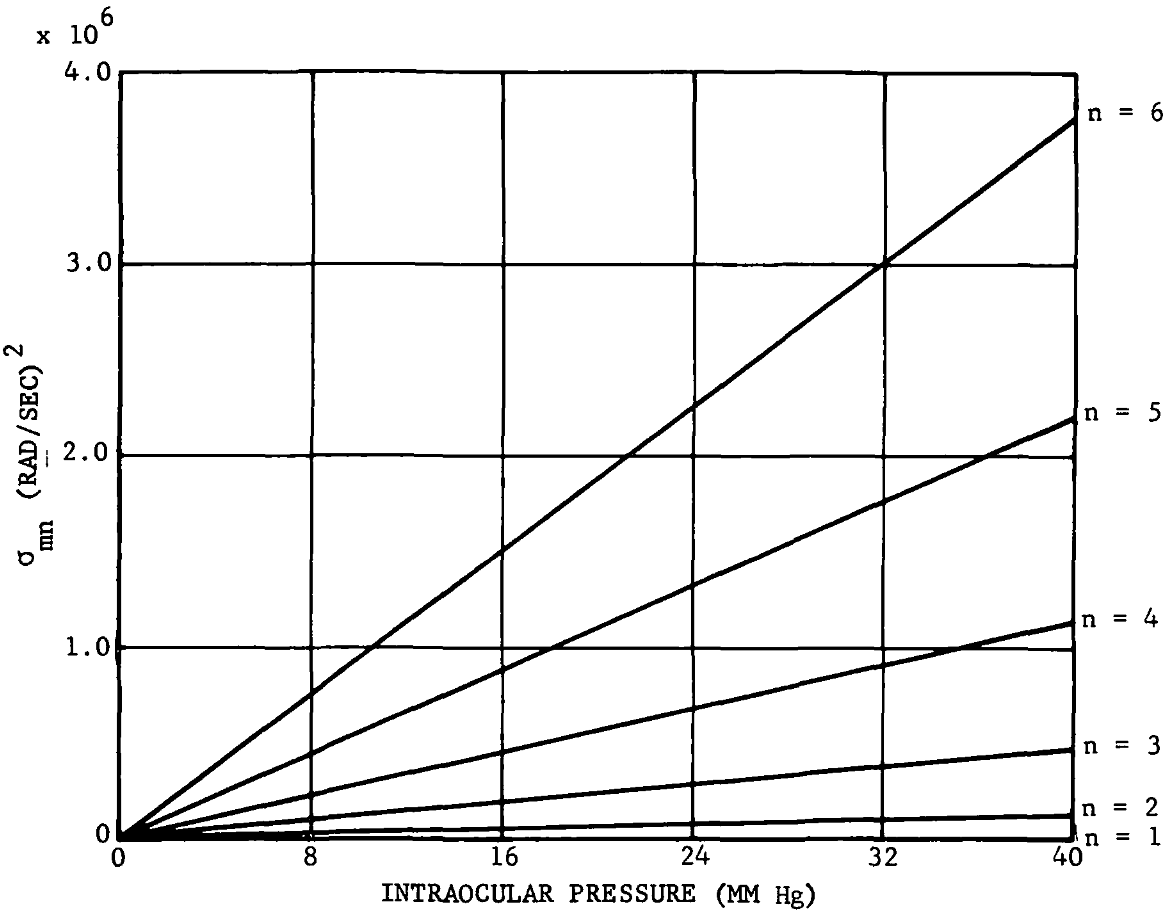

FIGURE 3.1. SPHERICAL DROPLET: $\mu = 0$, $\rho_2 = 0$

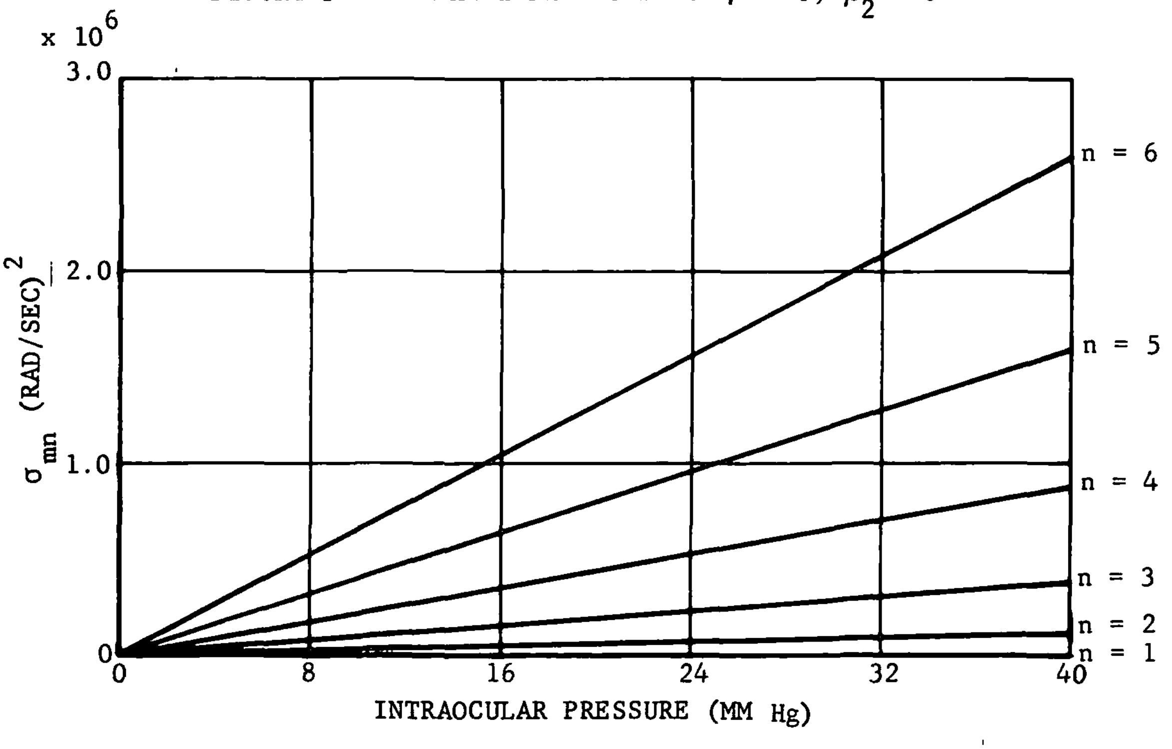

FIGURE 3.2. SPHERICAL DROPLET WITH SHELL INERTIA: $\rho_2 = 0$

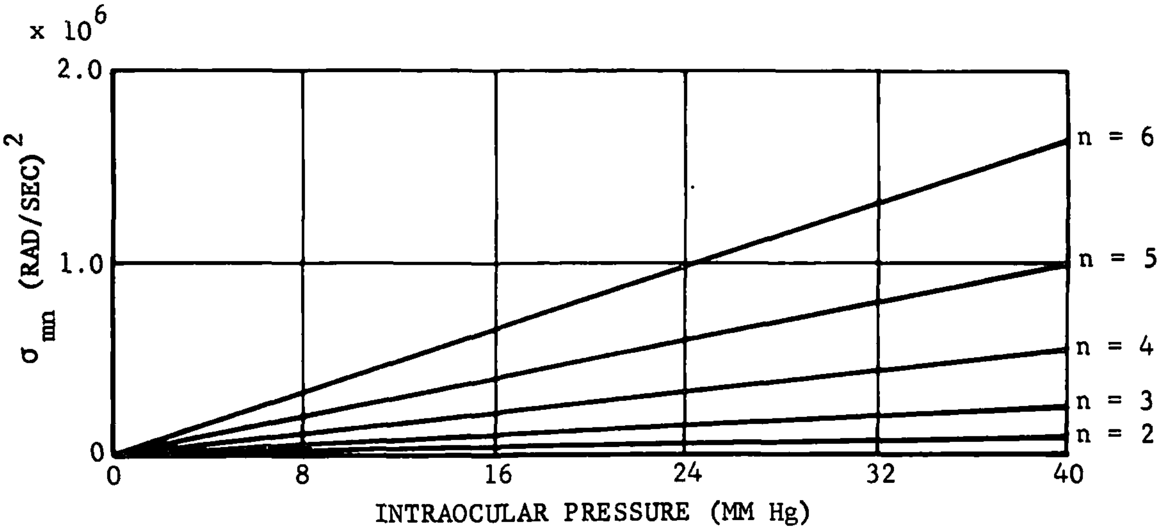

FIGURE 3.3. SPHERICAL DROPLET WITH SHELL INERTIA AND EXTERNAL MEDIUM

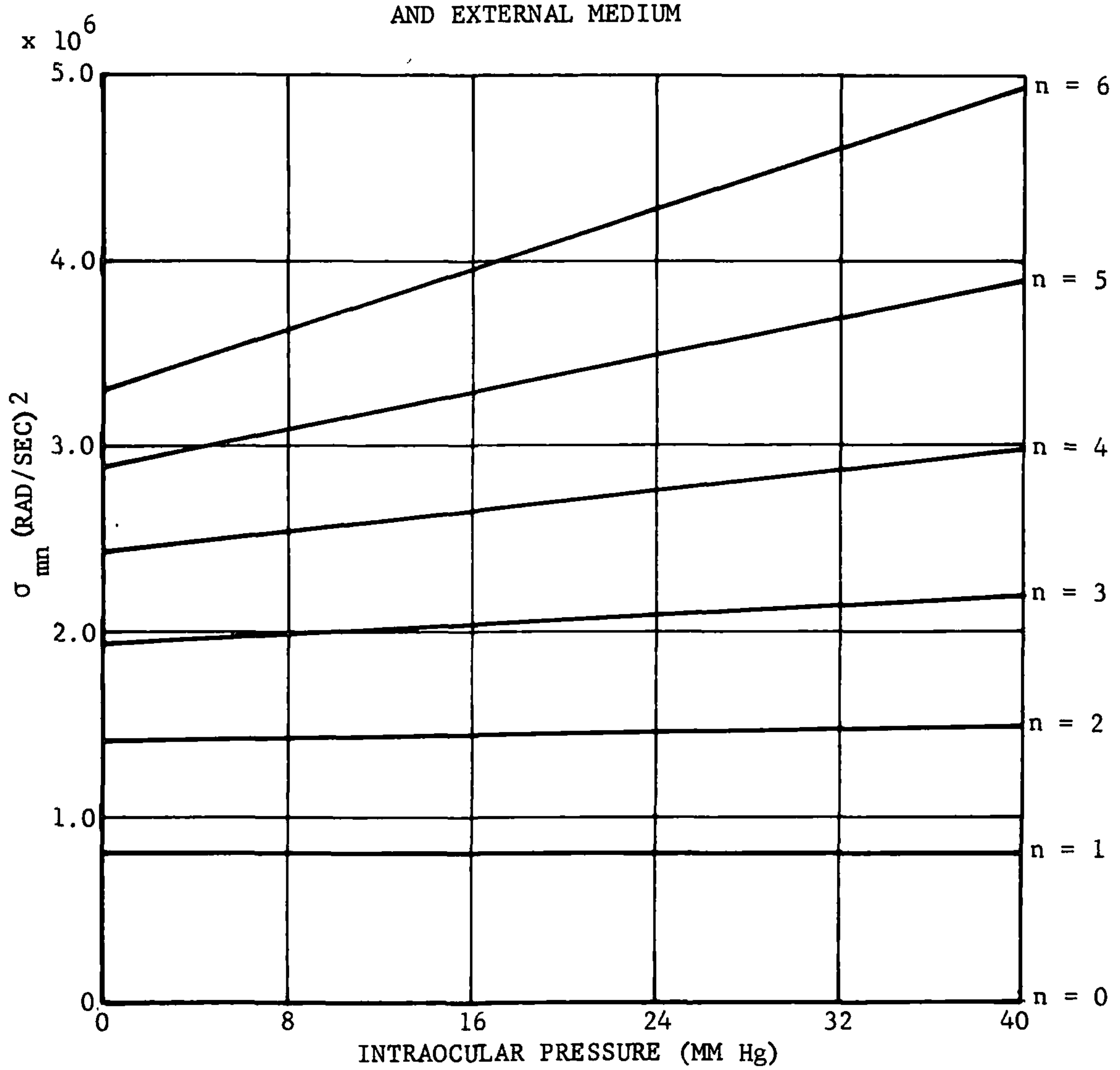

FIGURE 3.4. ONE DEGREE OF FREEDOM MEMBRANE MODEL

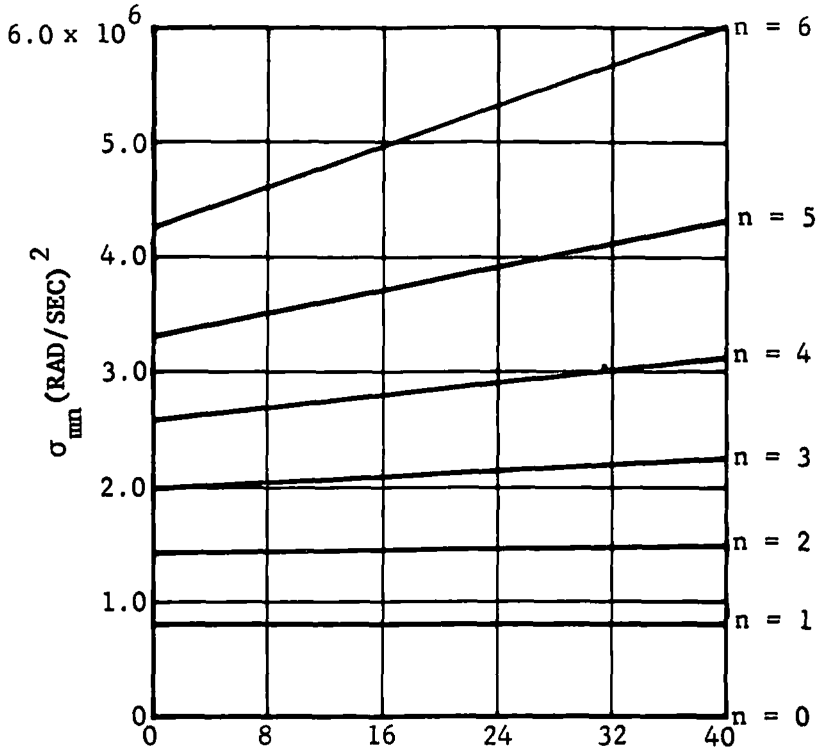

FIGURE 4.1. ONE DEGREE OF FREEDOM SHELL MODEL

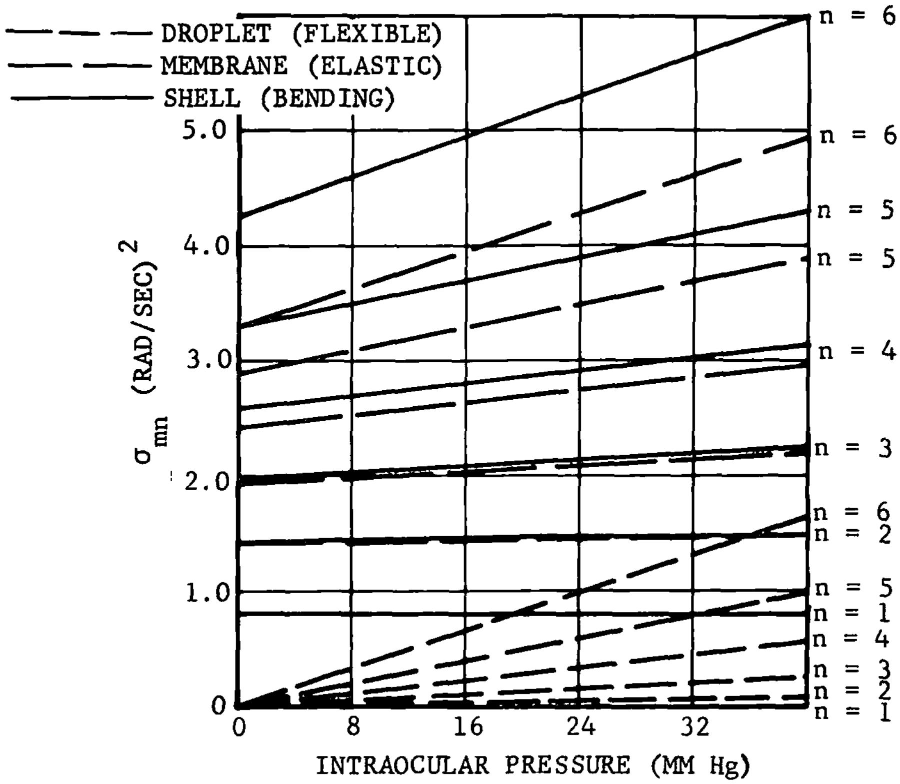

FIGURE 4.2. COMPARISON OF ONE DEGREE OF FREEDOM MODELS

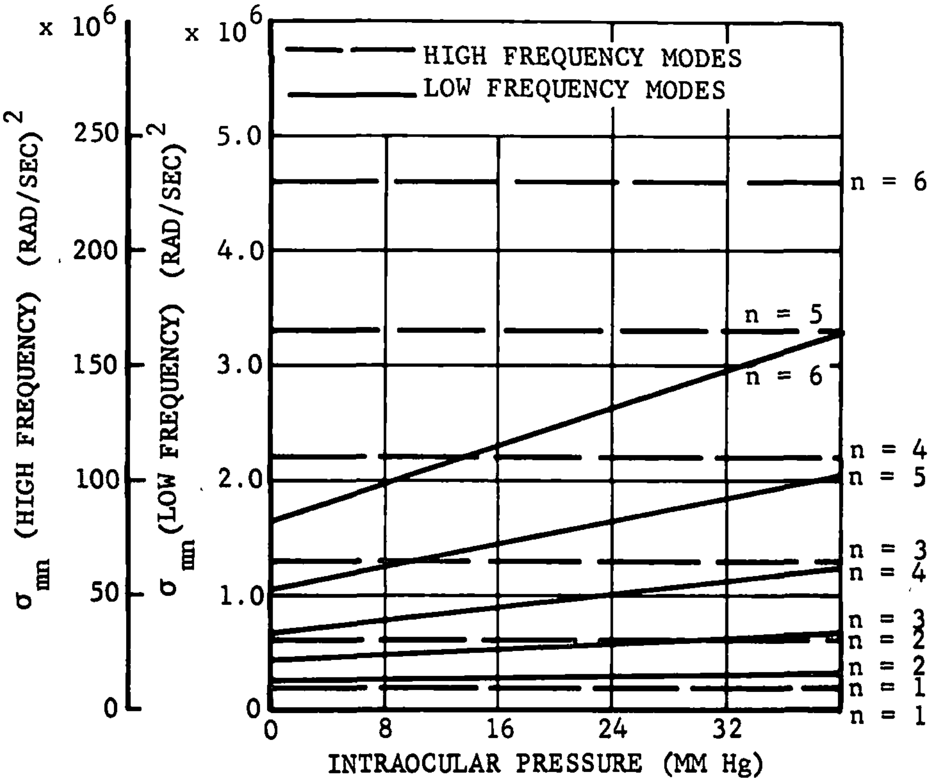

FIGURE 4.3. AXISYMMETRIC (TWO DEGREE OF FREEDOM SHELL MODEL)

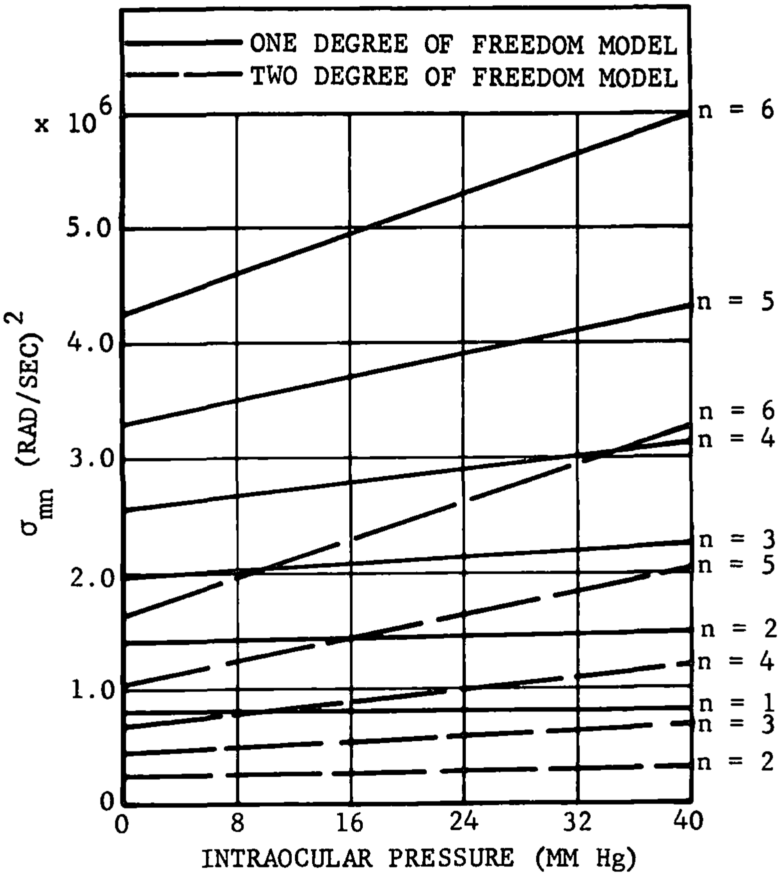

FIGURE 4.4. SHELL MODEL COMPARISON

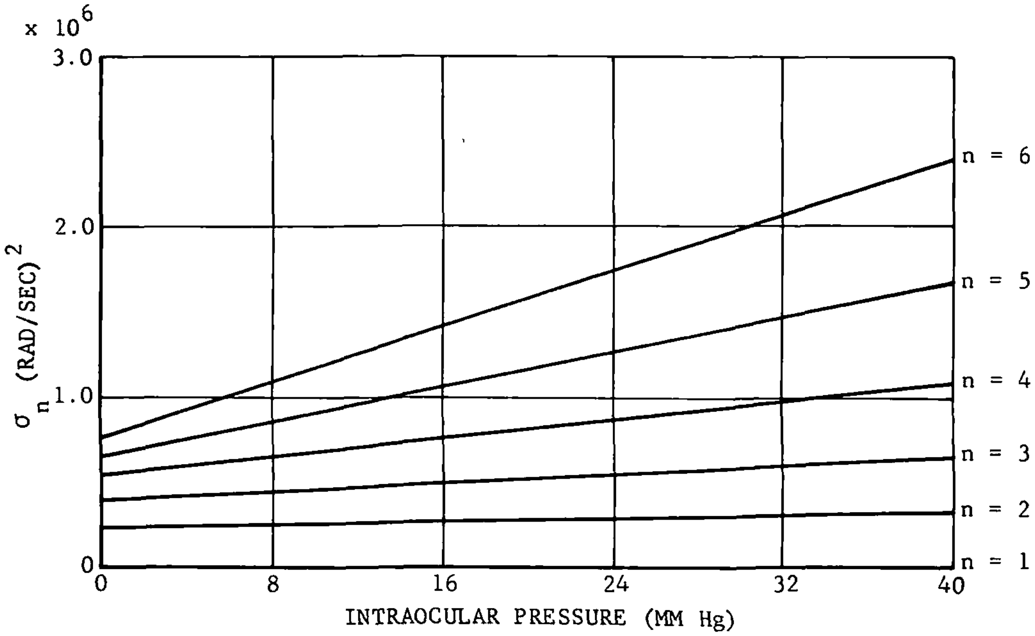

FIGURE 4.5. TWO DEGREE OF FREEDOM MEMBRANE MODEL (k = 0)

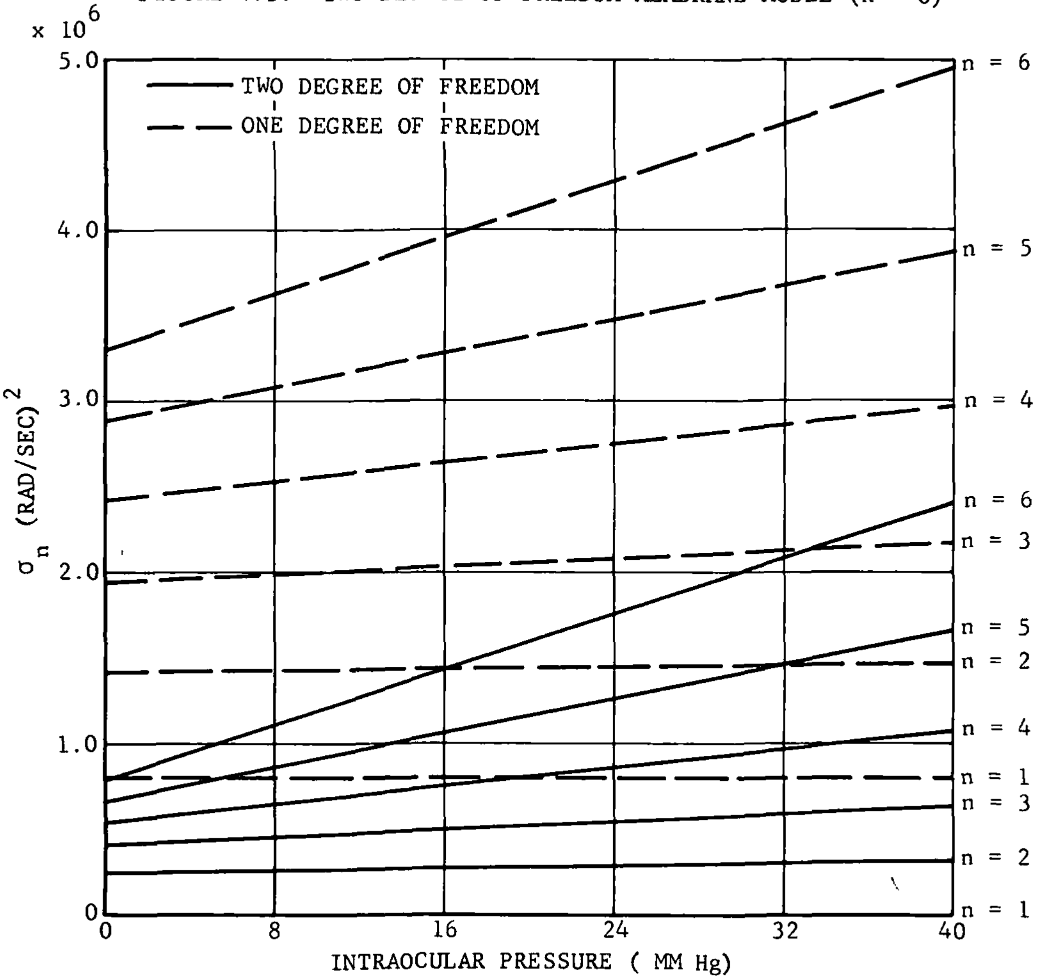

FIGURE 4.6. MODEL MEMBRANE COMPARISON

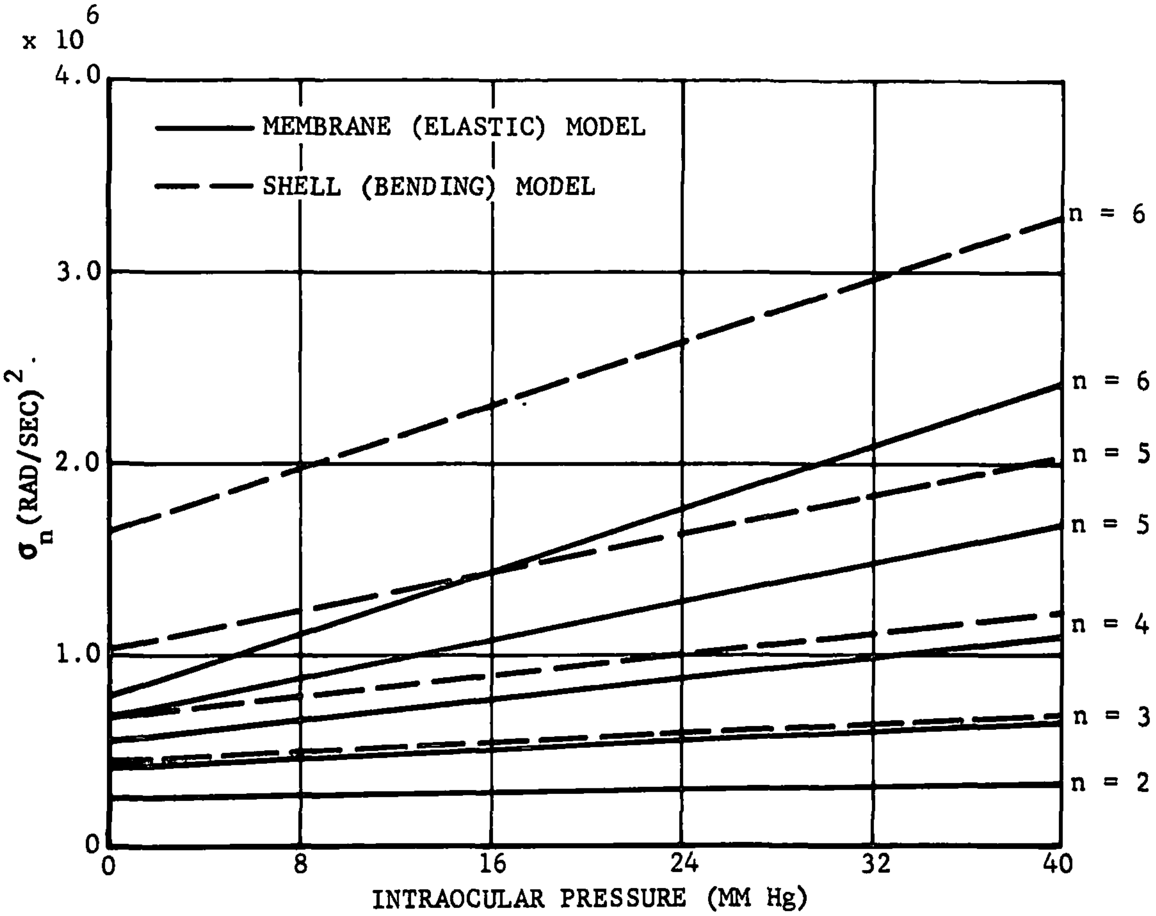

FIGURE 4.7. TWO DEGREE OF FREEDOM COMPARISON

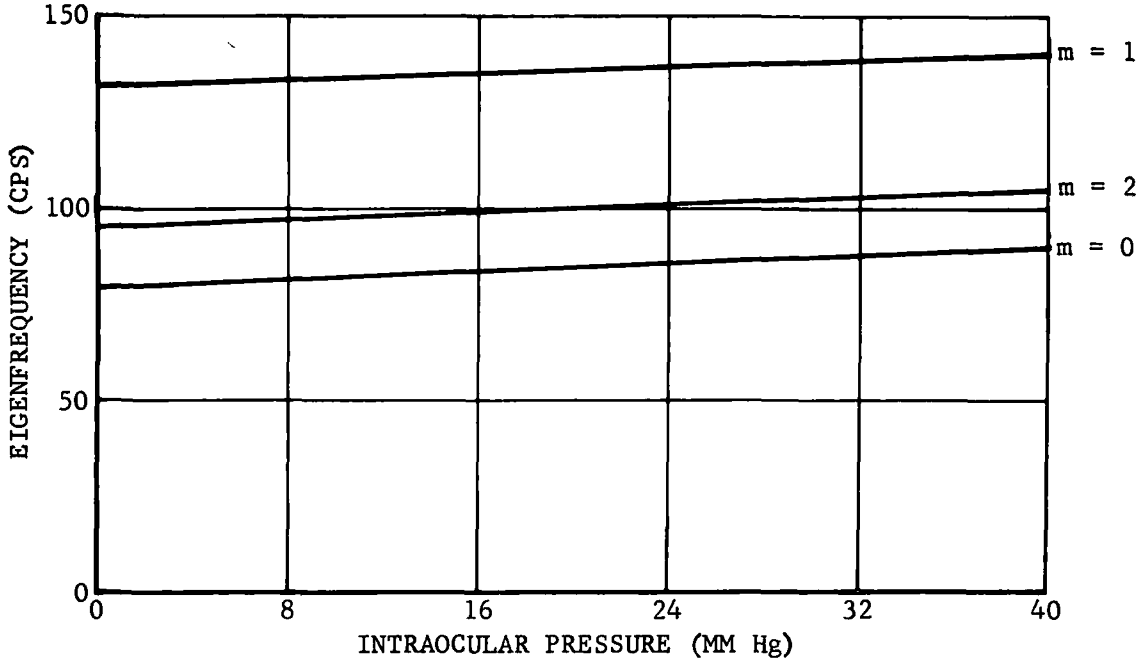

FIGURE 4.8. SYMMETRIC AND ASYMMETRIC MODES:
$n = 2$, $E = 7 \times 10^6$ DYNES/CM^2

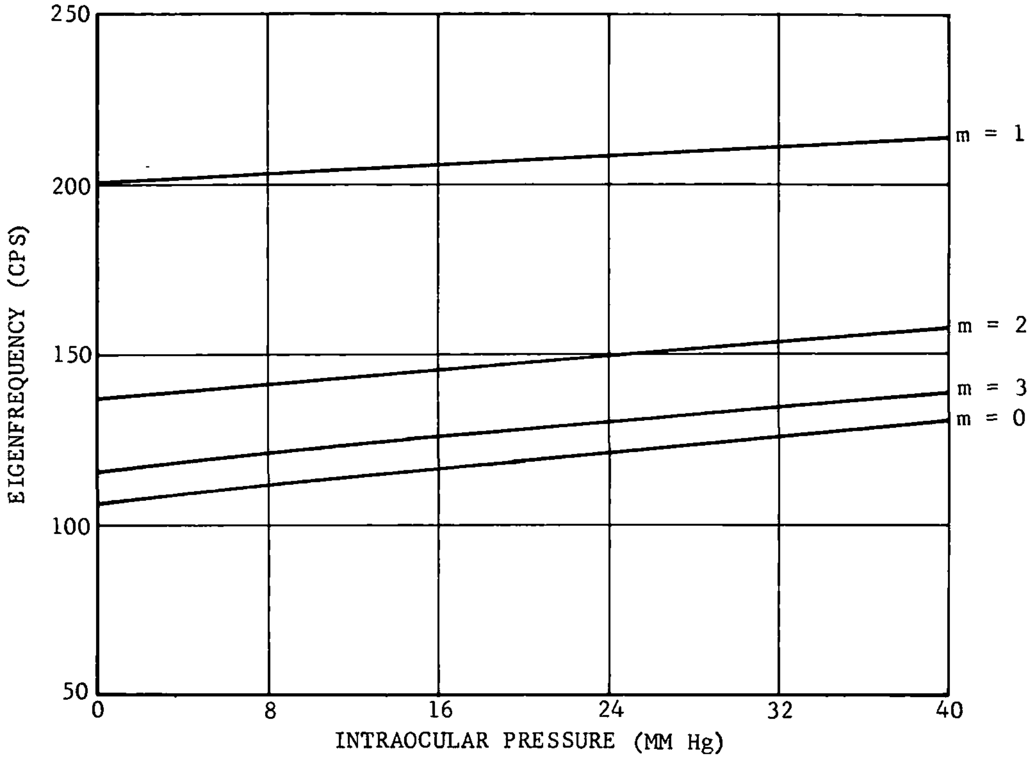

FIGURE 4.9. SYMMETRIC AND ASYMMETRIC MODES:
$n = 3$, $E = 7 \times 10^6$ DYNES/CM^2

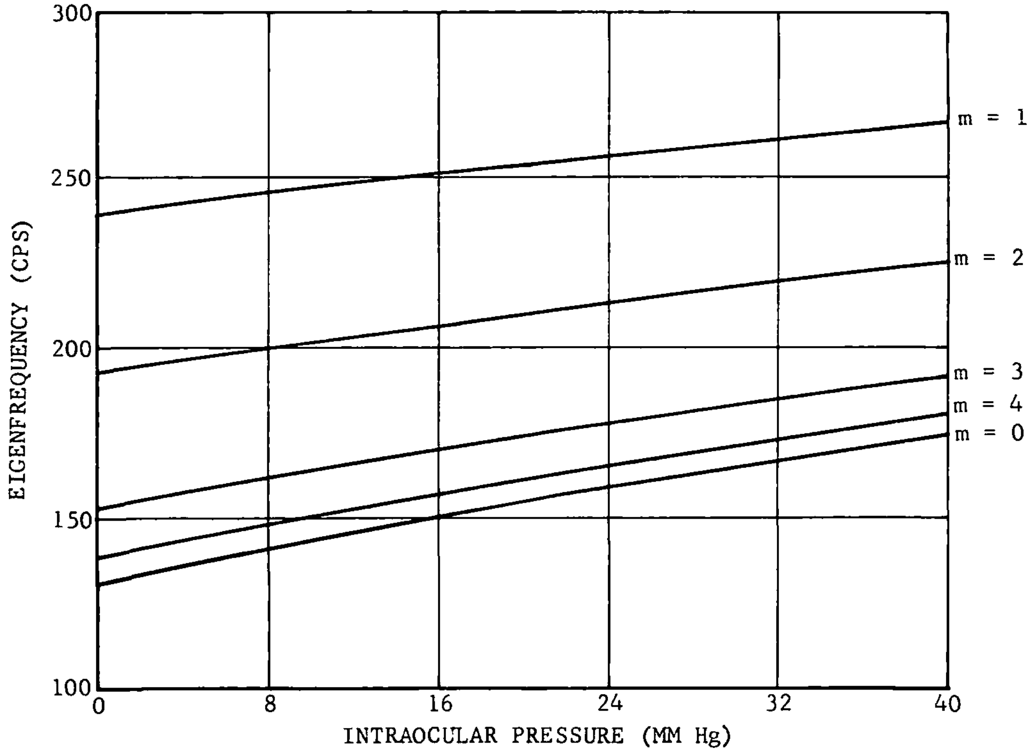

FIGURE 4.10. SYMMETRIC AND ASYMMETRIC MODES:
$n = 4$, $E = 7 \times 10^6$ DYNES/CM^2

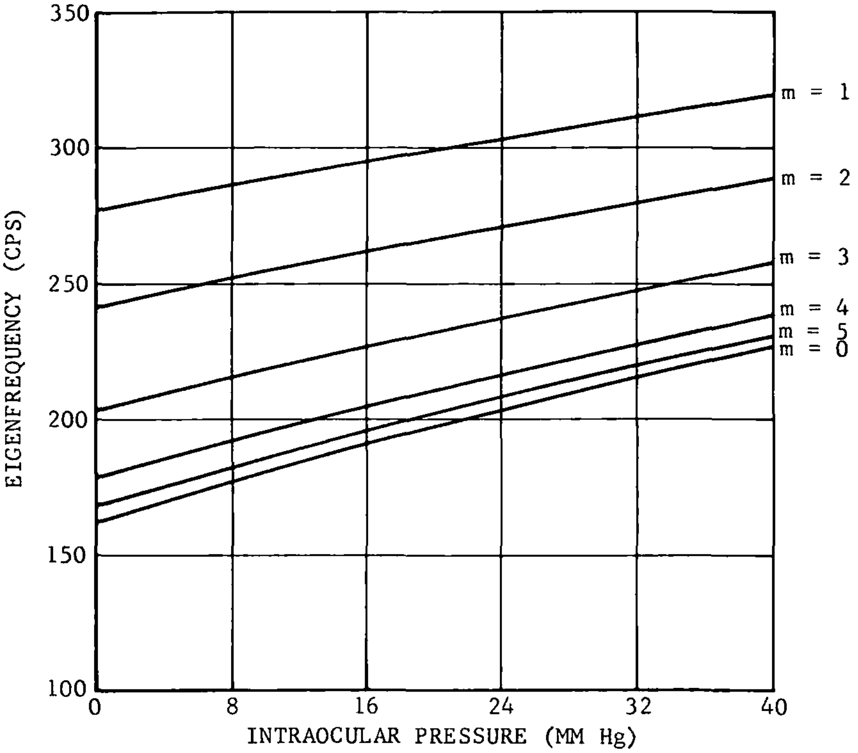

FIGURE 4.11. SYMMETRIC AND ASYMMETRIC MODES:
$n = 5$, $E = 7 \times 10^6$ DYNES/CM^2

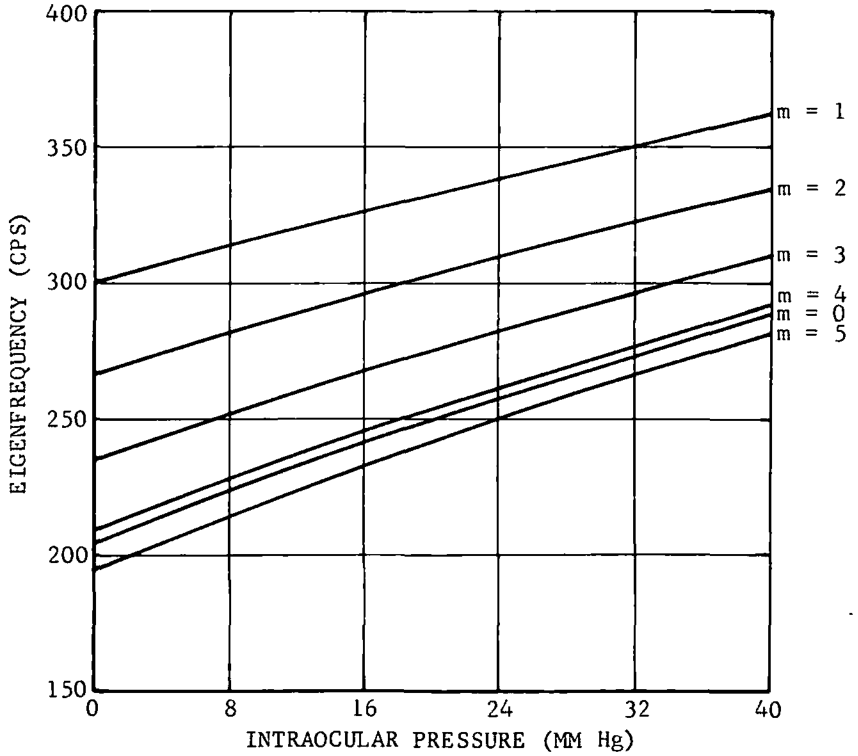

FIGURE 4.12. SYMMETRIC AND ASYMMETRIC MODES:
$n = 6$, $E = 7 \times 10^6$ DYNES/CM^2

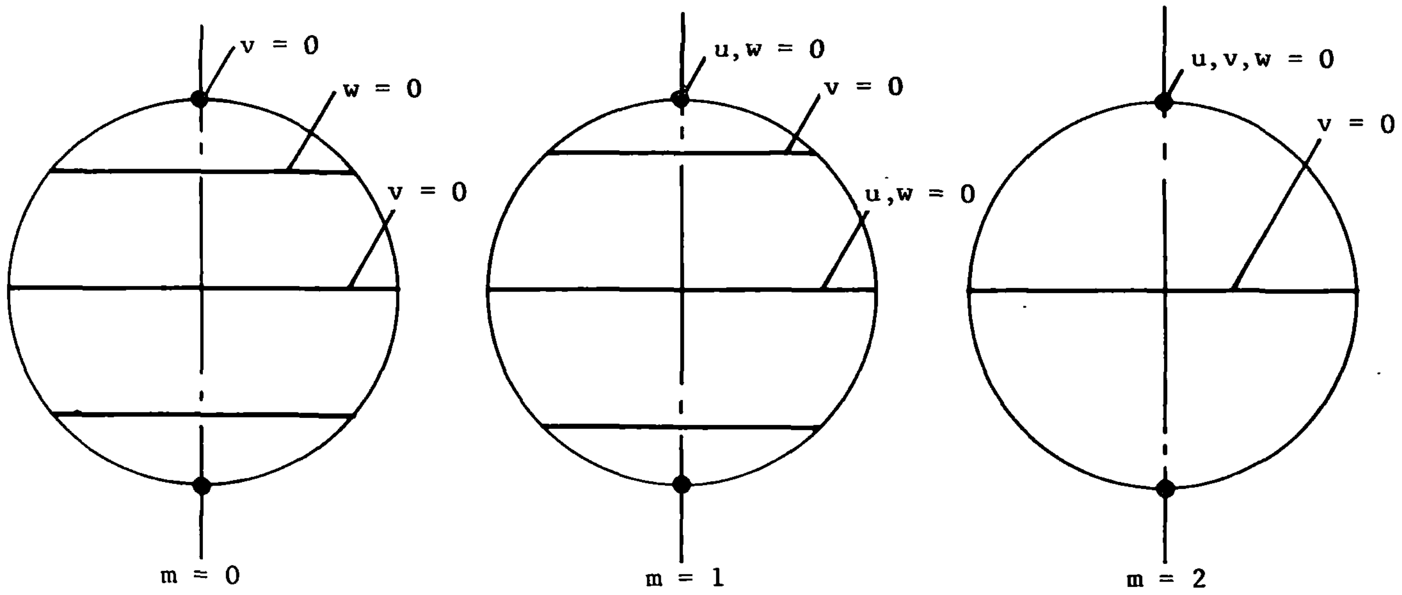

FIGURE 4.13. NODAL LINES AND POINTS: $n = 2$; $m = 0,1,2$

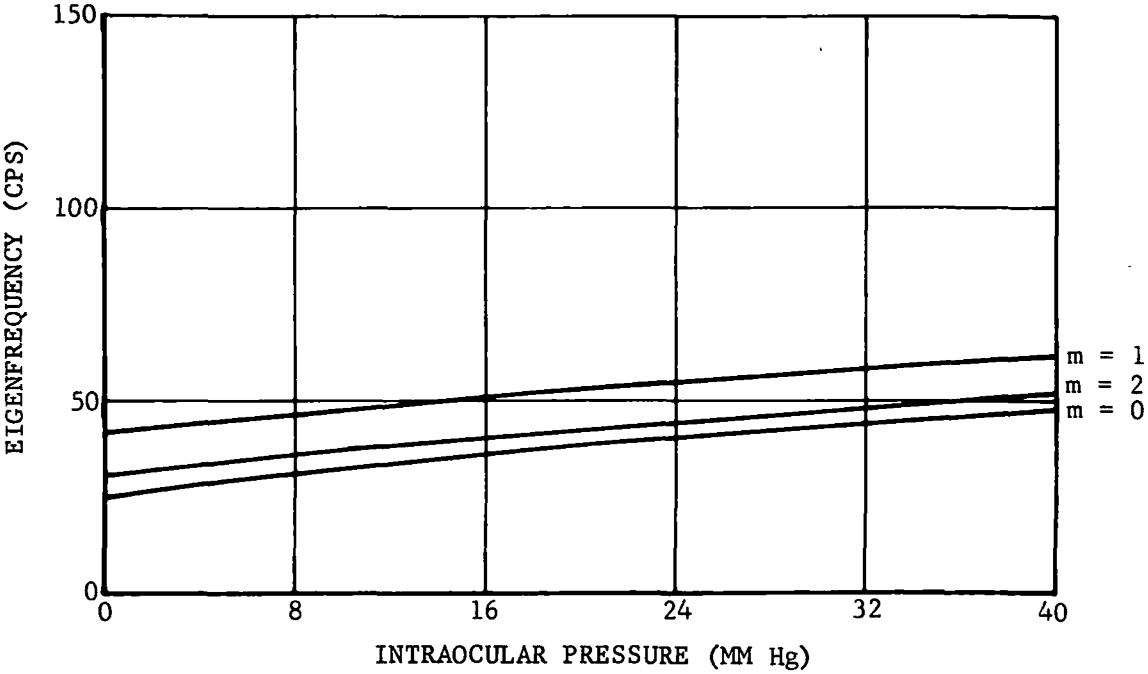

FIGURE 4.14. SYMMETRIC AND ASYMMETRIC MODES:
$n = 2$, $E = 7\times10^5$ DYNES/CM^2

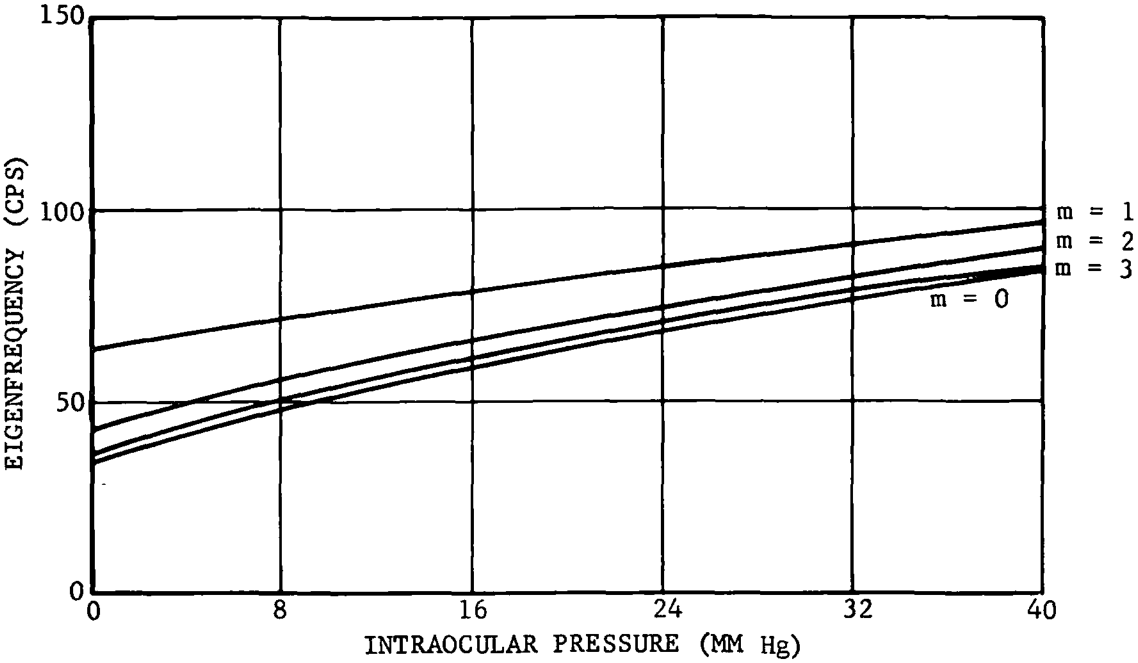

FIGURE 4.15. SYMMETRIC AND ASYMMETRIC MODES: $n = 3$, $E = 7 \times 10^5$ DYNES/CM^2

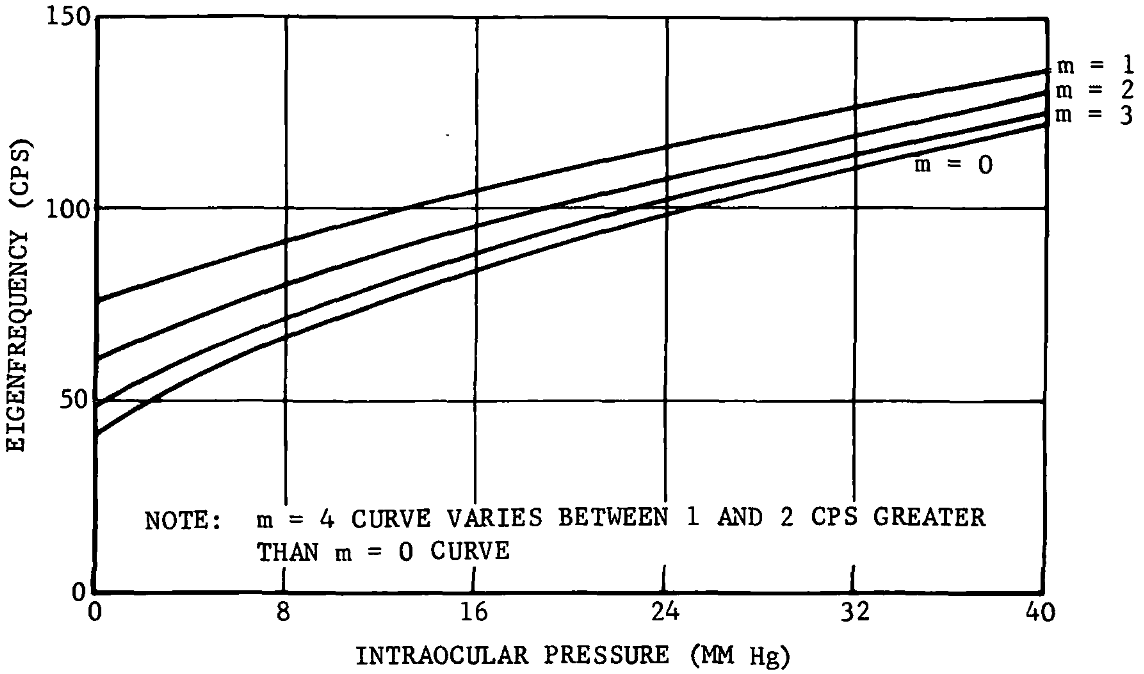

FIGURE 4.16. SYMMETRIC AND ASYMMETRIC MODES: $n = 4$, $E = 7 \times 10^5$ DYNES/CM^2

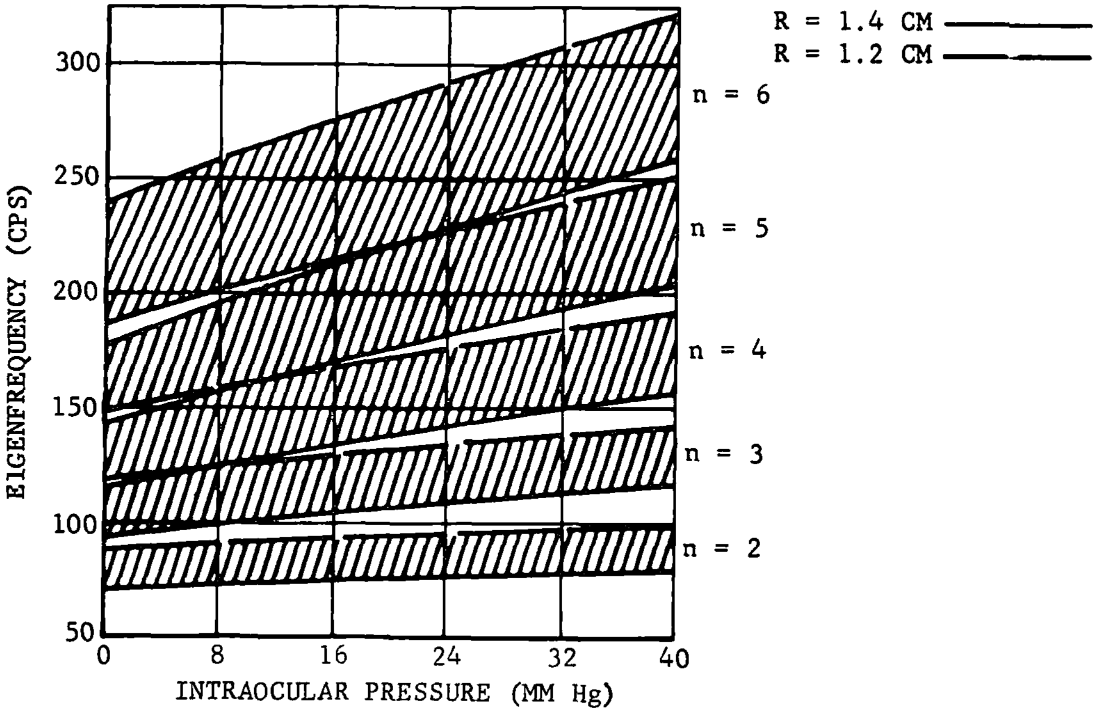

FIGURE 5.1. EFFECT OF RADIUS VARIATION

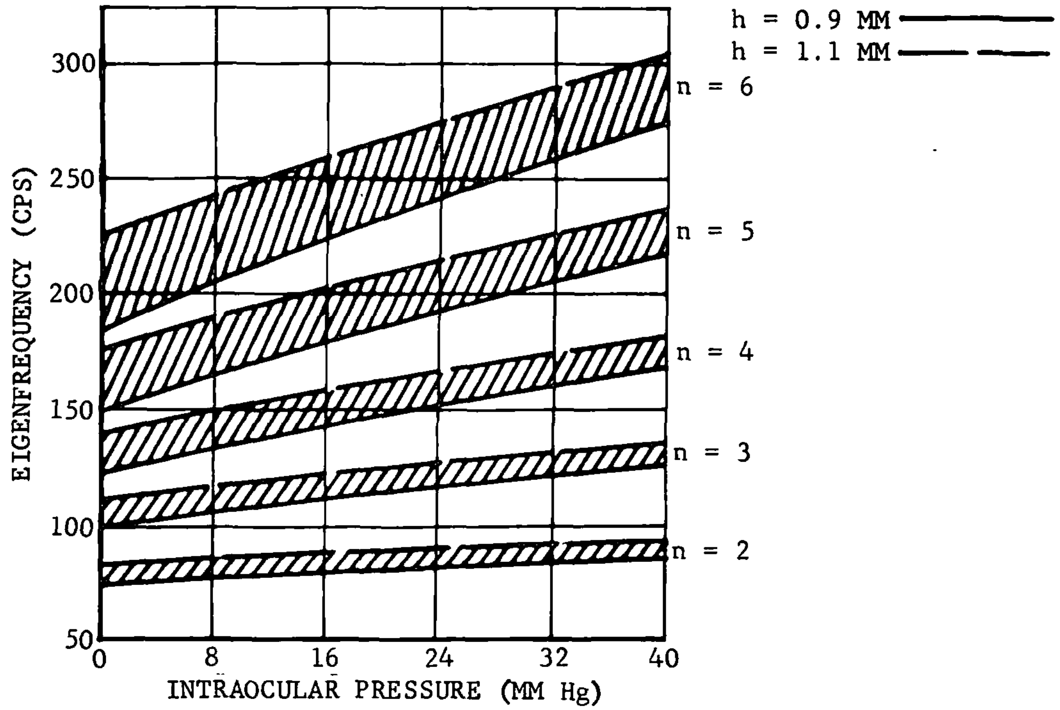

FIGURE 5.2. EFFECT OF CORNEO-SCLERAL THICKNESS VARIATION

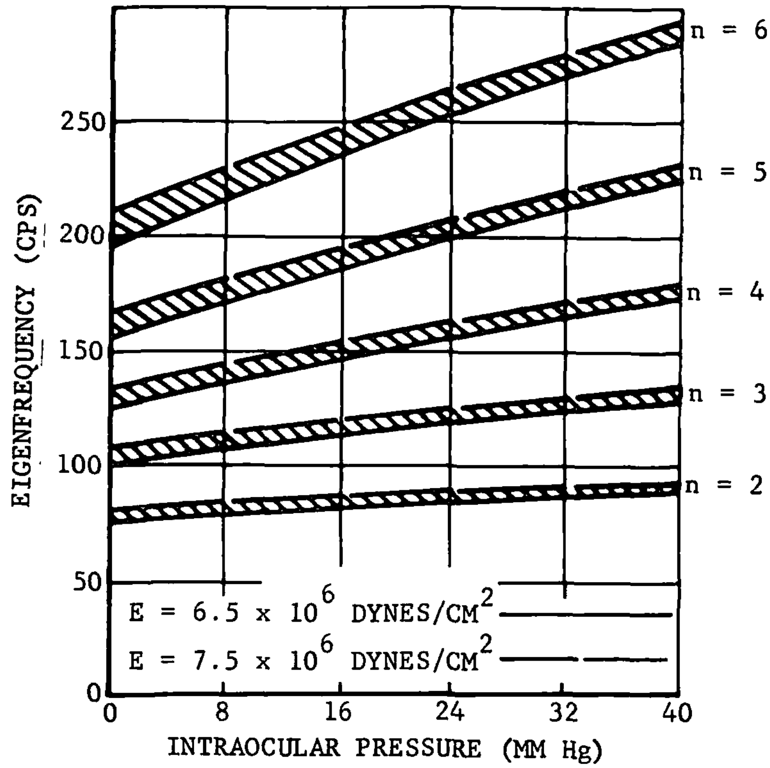

FIGURE 5.3. EFFECT OF YOUNG'S MODULUS VARIATION

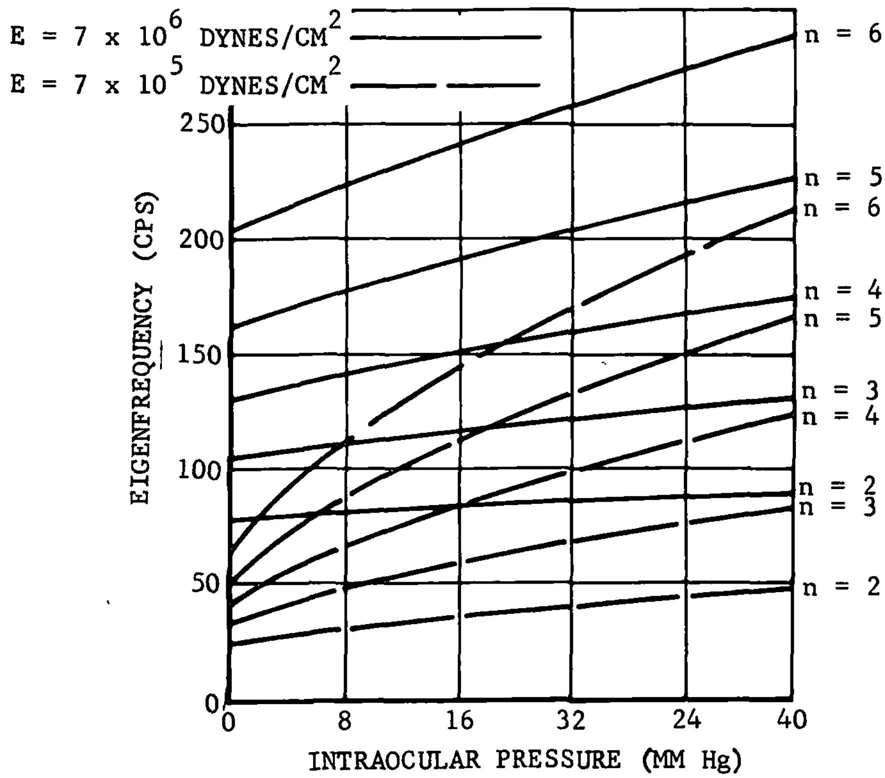

FIGURE 5.4. EFFECT OF YOUNG'S MODULUS

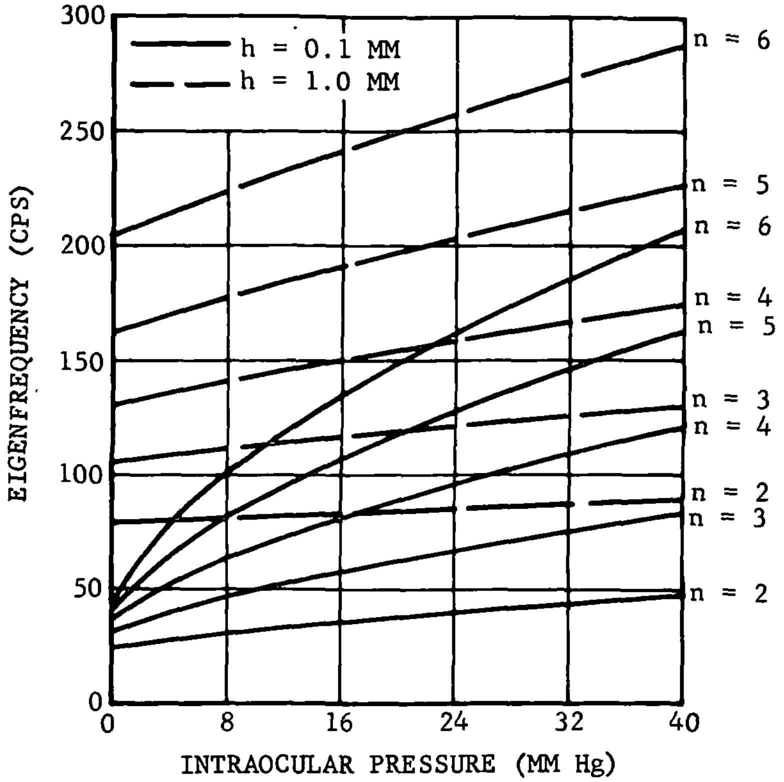

FIGURE 5.5. EFFECT OF CORNEO-SCLERAL MEMBRANE THICKNESS

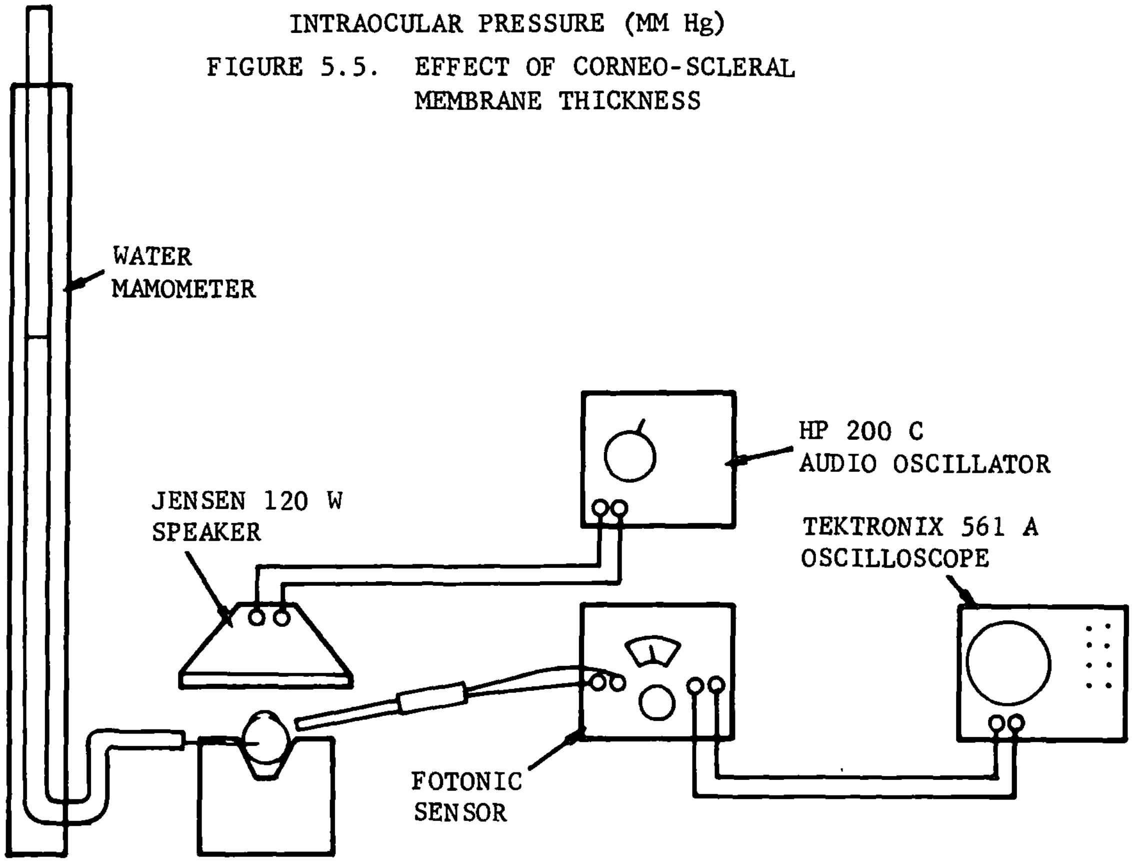

FIGURE 6.1. DYNAMIC EXPERIMENTAL APPARATUS

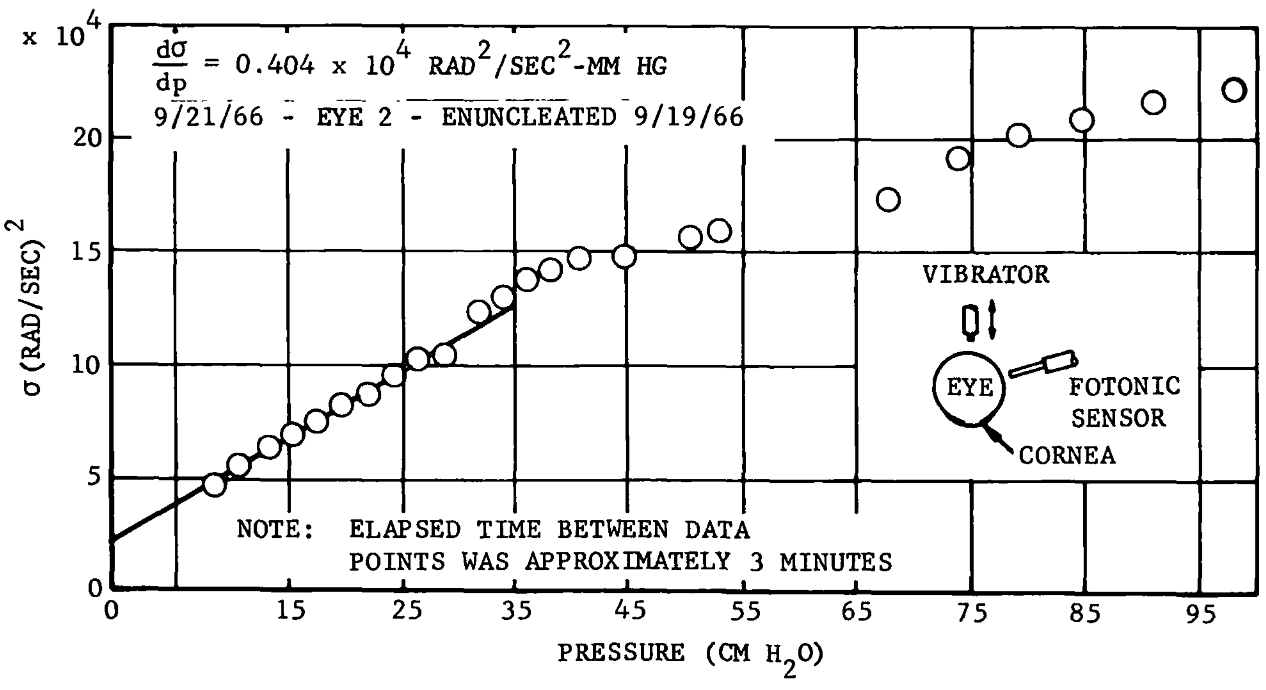

FIGURE 6.2. TYPICAL VIBRATION DATA FOR A DOG EYE

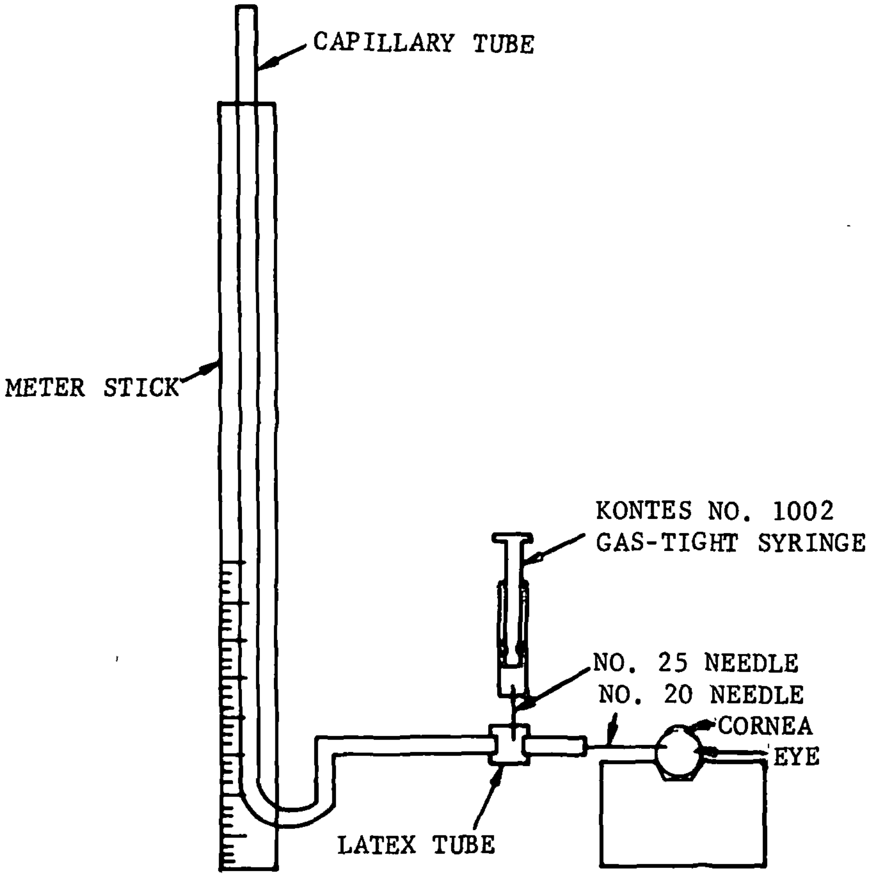

FIGURE 6.3. STATIC EXPERIMENTAL APPARATUS

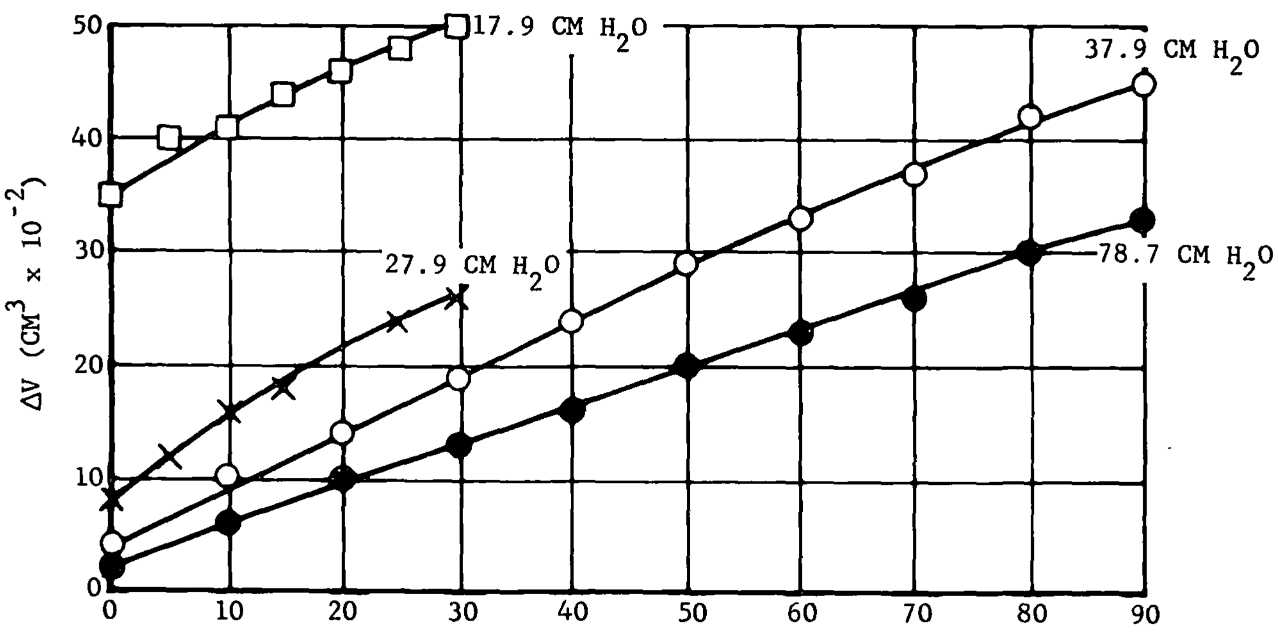

FIGURE 6.4. OCULAR CREEP CURVE

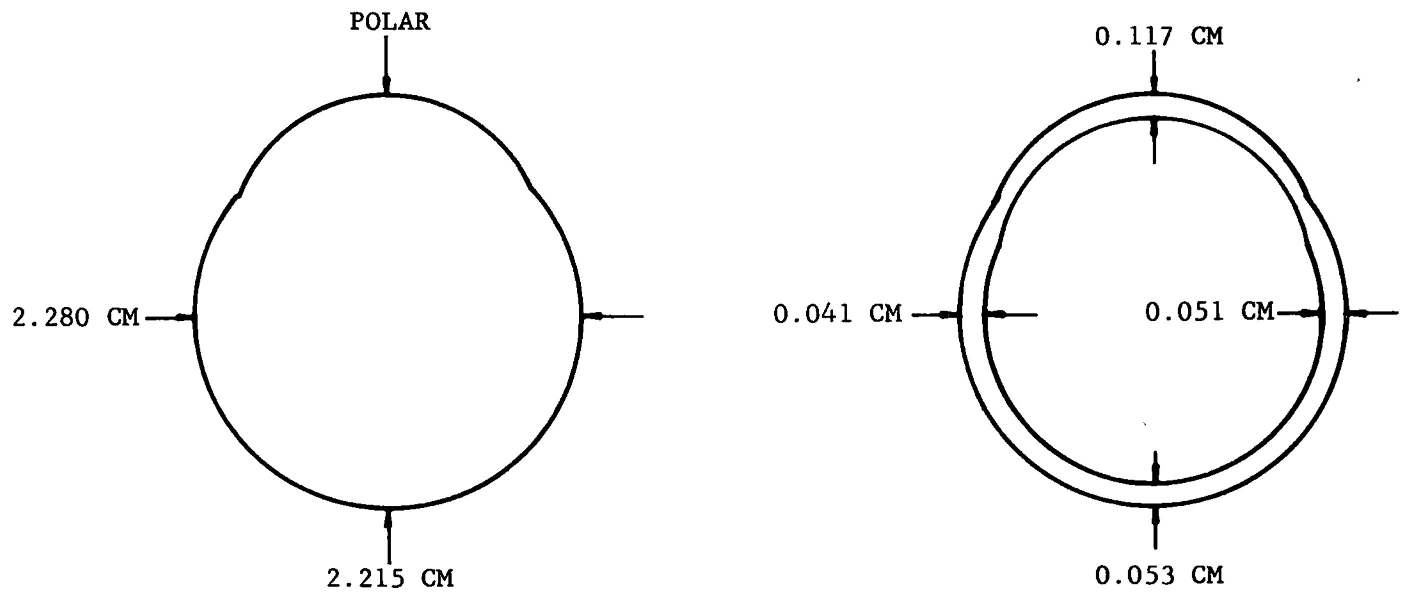

FIGURE 6.5. TYPICAL DOG EYE

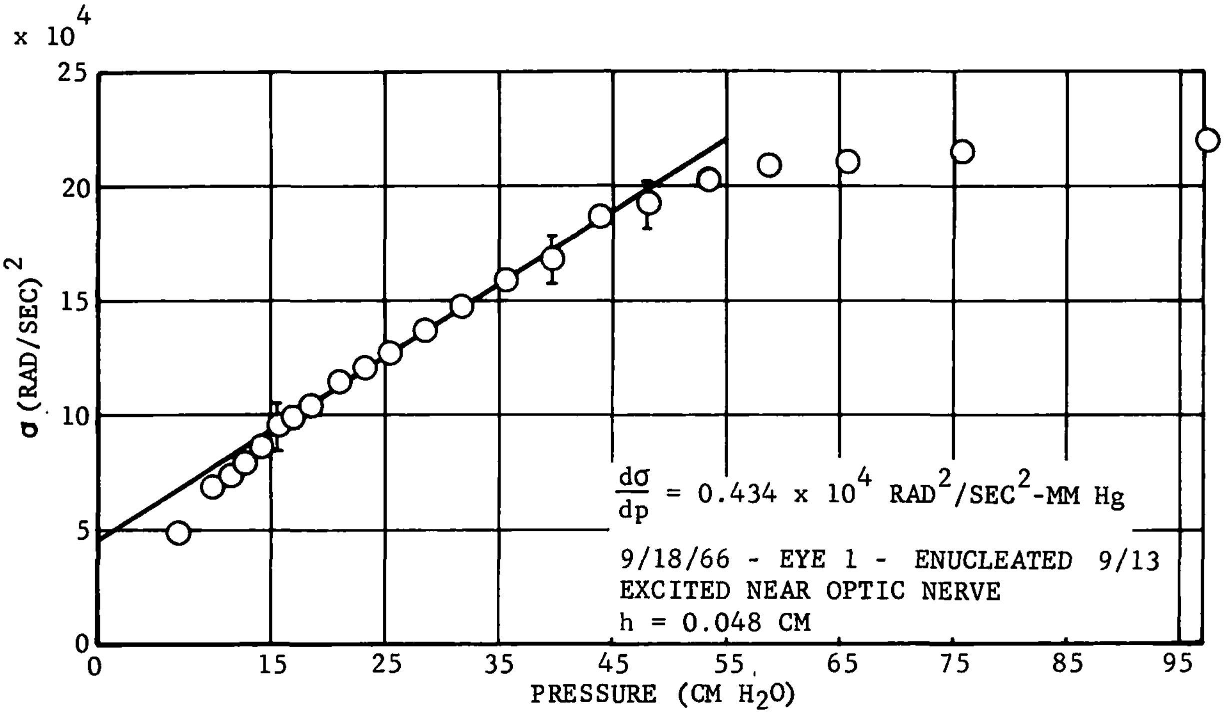

FIGURE 7.1. VIBRATION DATA FOR AN ENUCLEATED DOG EYE (5 DAYS OLD) - EYE 1

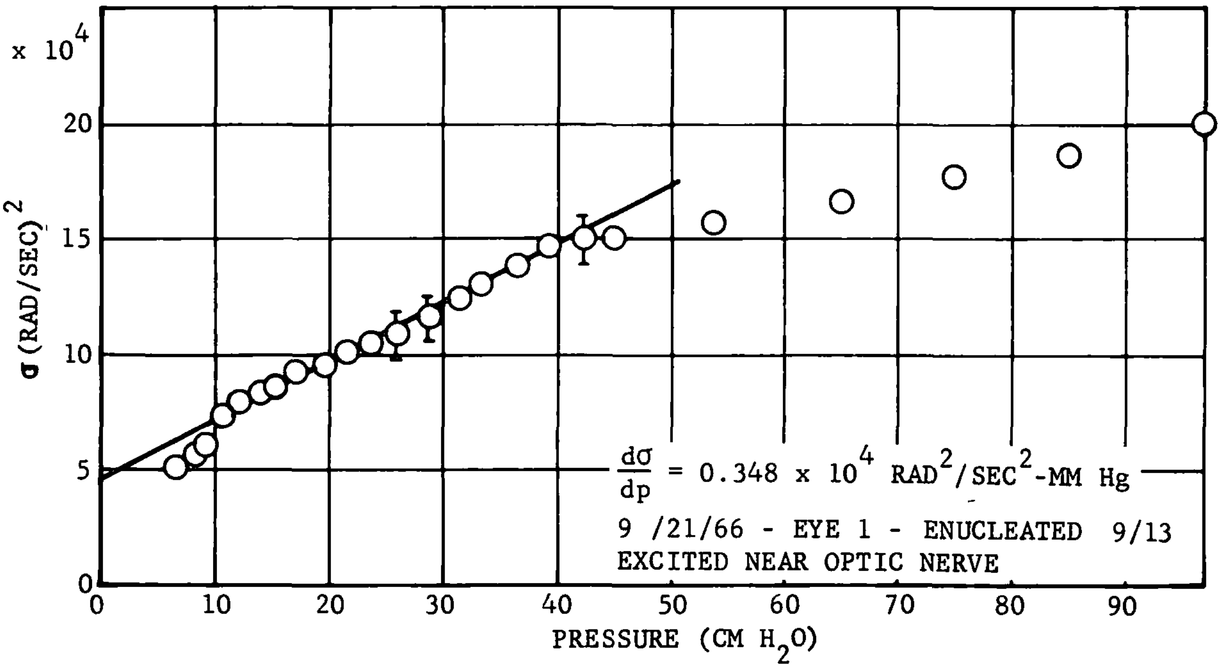

FIGURE 7.2. VIBRATION DATA FOR ENUCLEATED DOG EYE (8 DAYS OLD) - EYE 1

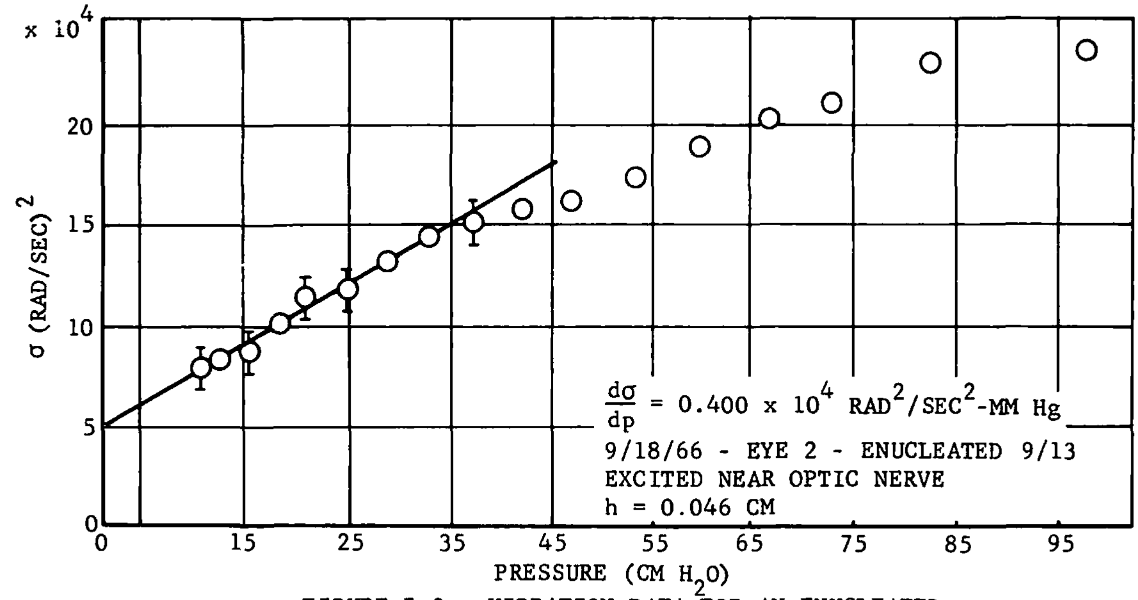

FIGURE 7.3. VIBRATION DATA FOR AN ENUCLEATED DOG EYE (5 DAYS OLD) - EYE 2

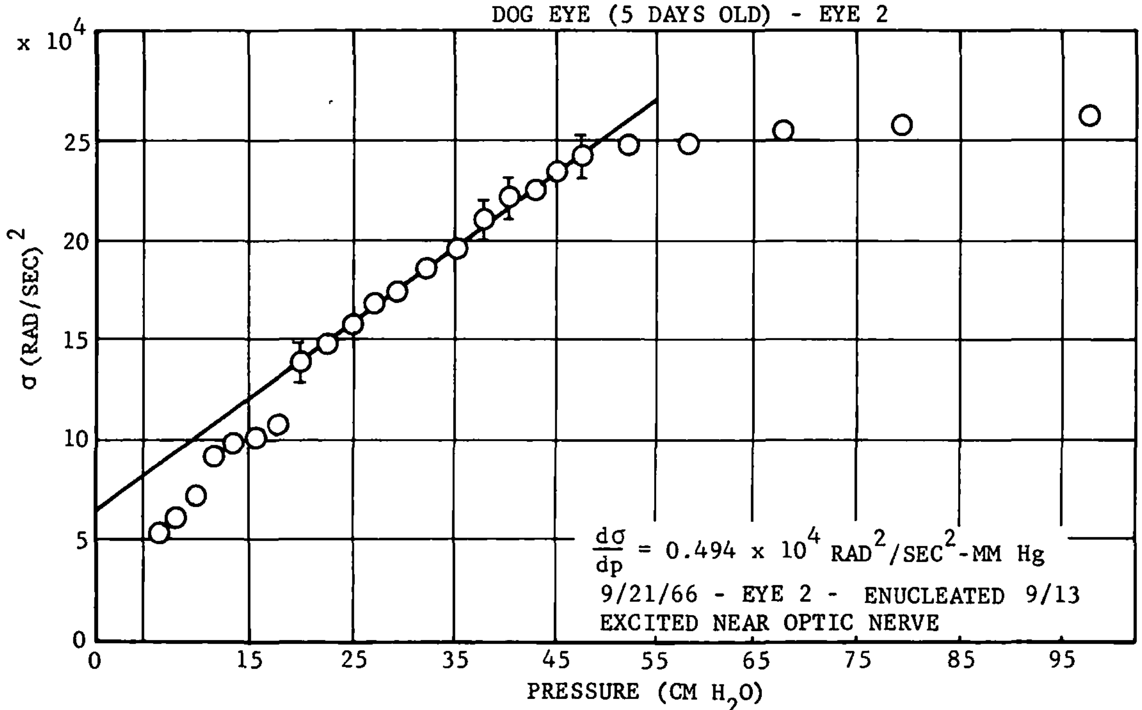

FIGURE 7.4. VIBRATION DATA FOR AN ENUCLEATED DOG EYE (8 DAYS OLD) - EYE 2

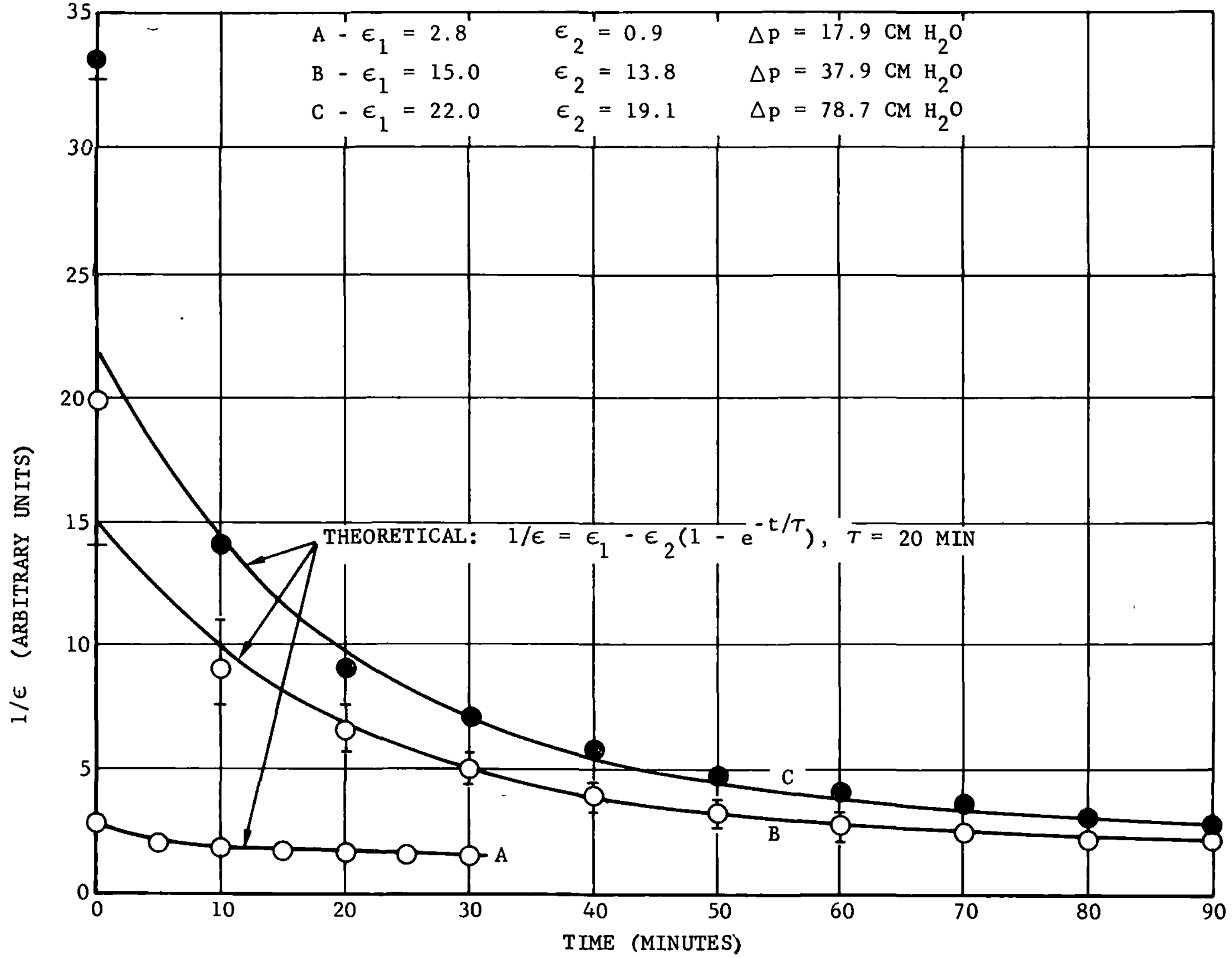

FIGURE 7.5. VISCOELASTIC BEHAVIOR

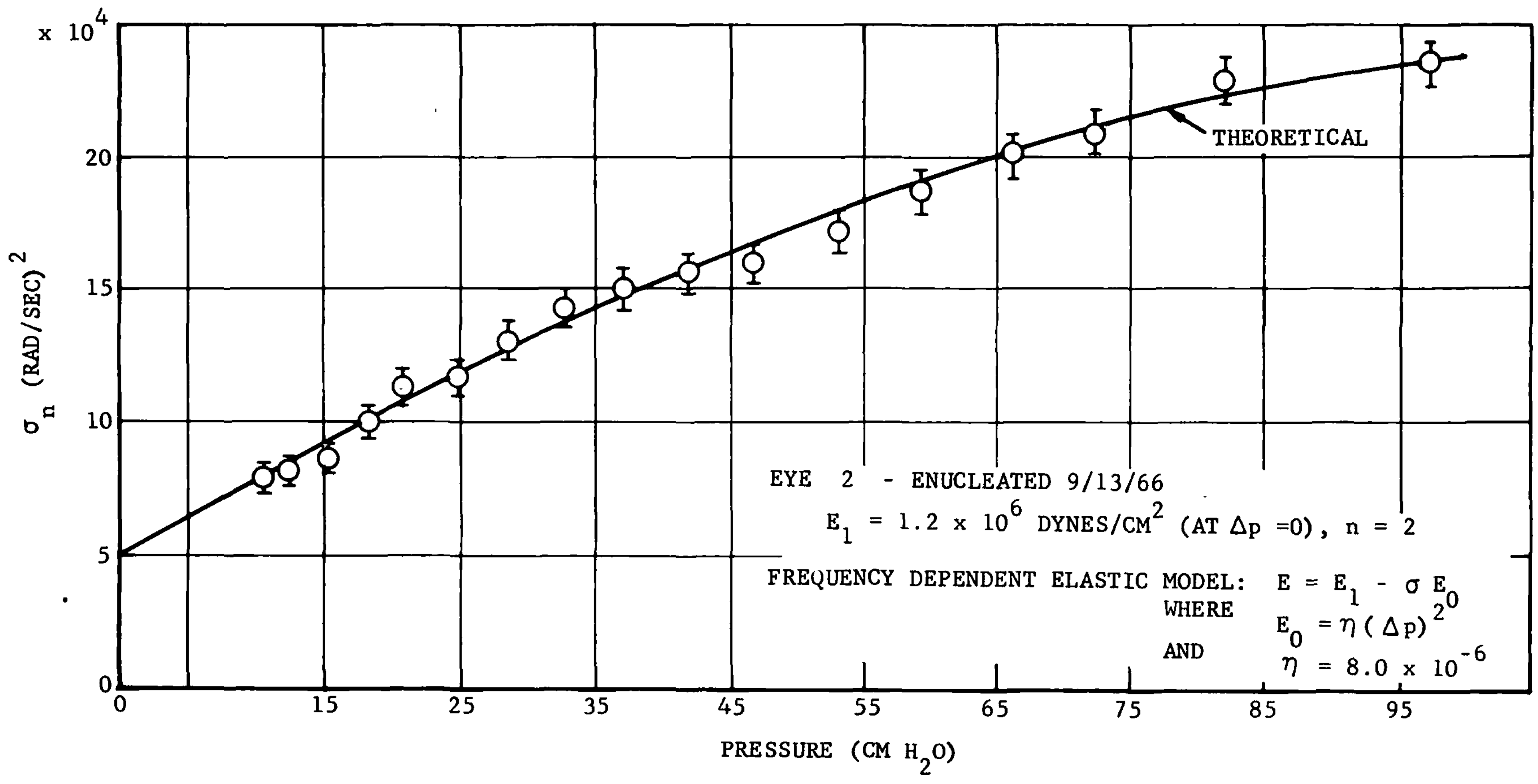

FIGURE 7.6. FREQUENCY-PRESSURE DEPENDENT YOUNG'S MODULUS MODEL: COMPARISON WITH EXPERIMENTAL DATA

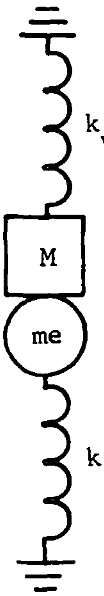

FIGURE 7.7. SPRING-MASS MODEL FOR EYE-VIBRATOR SYSTEM

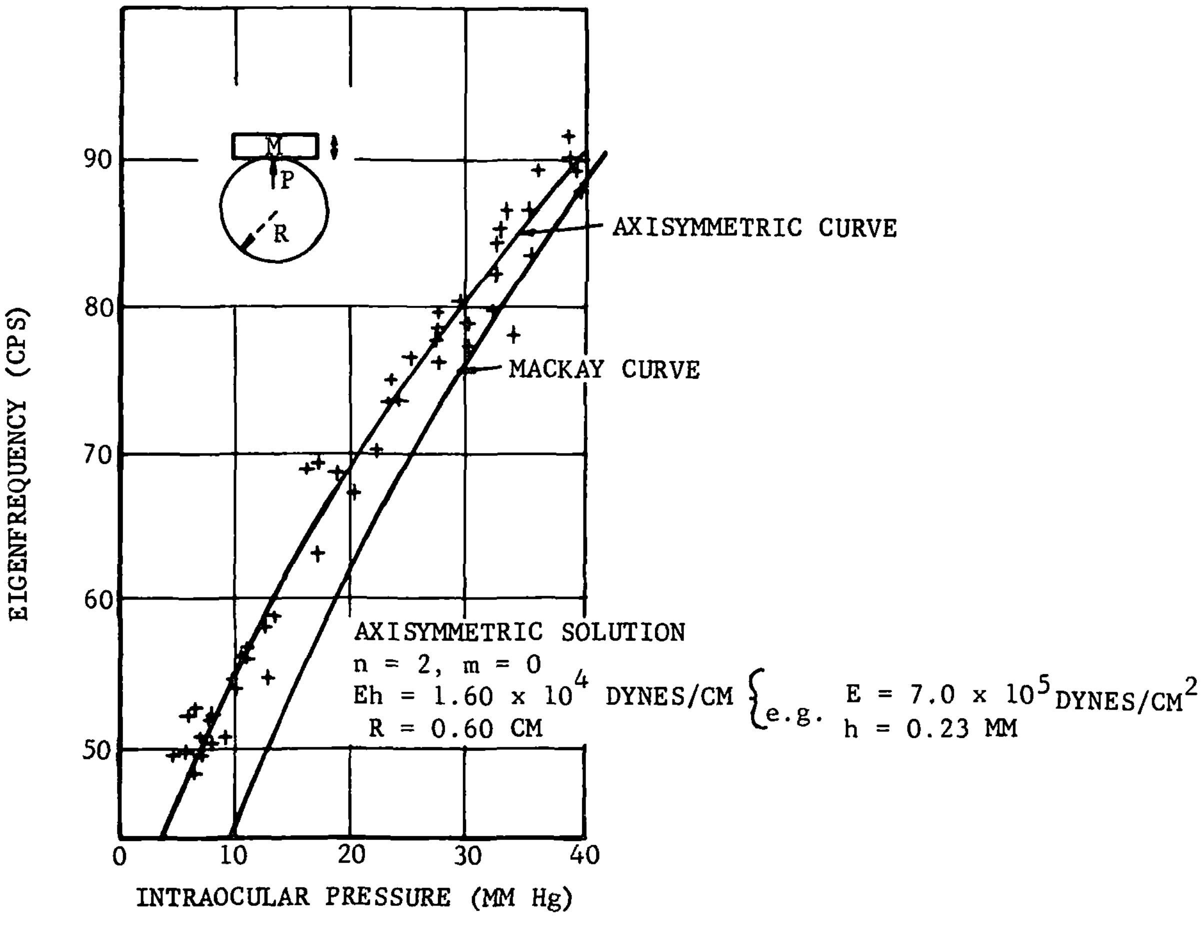

FIGURE 7.8. COMPARISON WITH MACKAY'S DATA

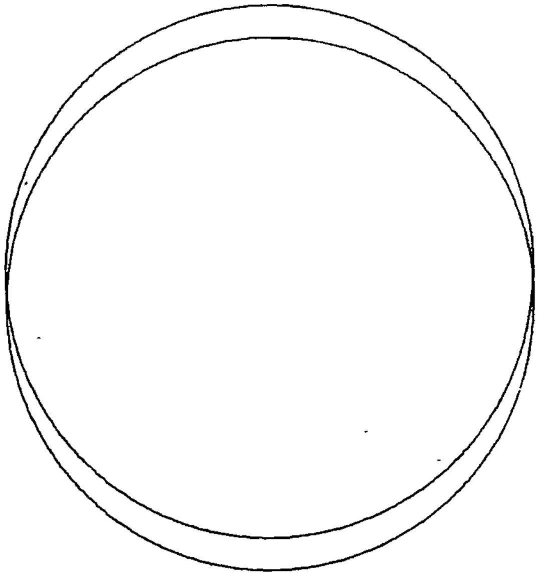

$n = 1,\ f = 0$
$v_1(\theta) = -A_1 \sin\theta$
$w_1(\theta) = A_1 \cos\theta$
FIGURE 12.1 a

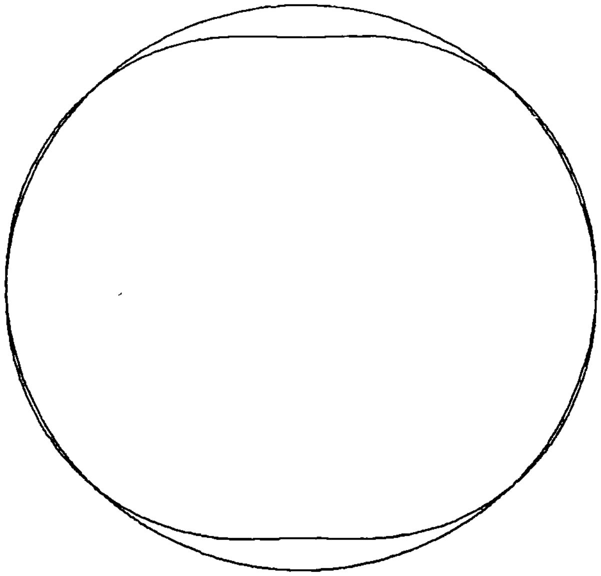

$n = 1,\ f = 486$ CPS
$v_1(\theta) = 7.98\ A_1 \sin\theta$
$w_1(\theta) = A_1 \cos\theta$
FIGURE 12.1 b

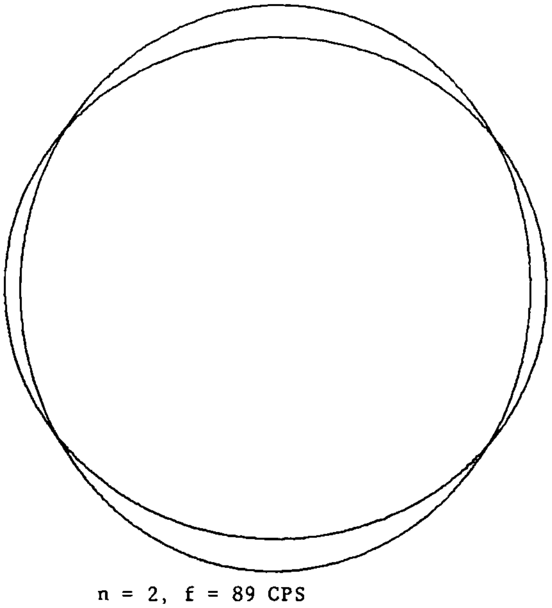

$n = 2,\ f = 89$ CPS
$v_2(\theta) = -\ 0.83\ A_2 \sin\theta \cos\theta$
$w_2(\theta) = 0.50\ A_2\ (3\cos^2\theta - 1)$
FIGURE 12.1 c

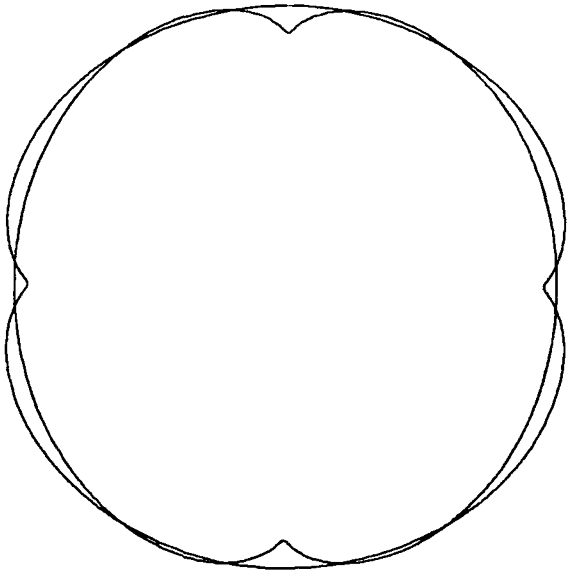

$n = 2,\ f = 899$ CPS
$v_2(\theta) = 16.76\ A_2 \sin\theta \cos\theta$
$w_2(\theta) = 0.50\ A_2\ (3\cos^2\theta - 1)$
FIGURE 12.1 d

FIGURE 12.1. MODE SHAPES

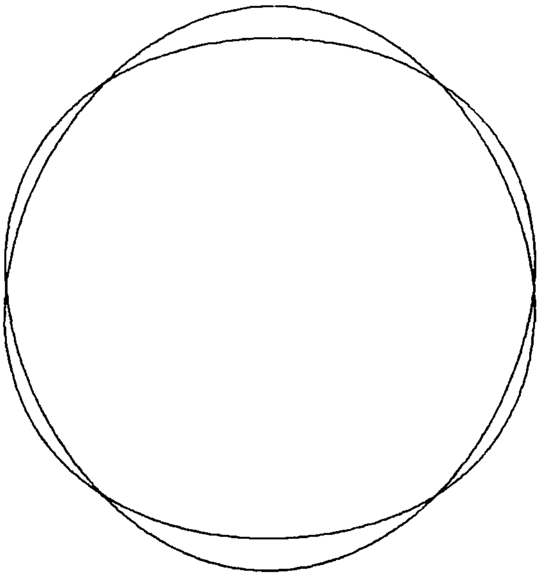

$n = 3$, $f = 118$ CPS

$v_3(\theta) = -0.22\ A_3\ \mathrm{SIN}\,\theta\,(5\ \mathrm{COS}^2\theta - 1)$

$w_3(\theta) = 0.50\ A_3\ \mathrm{COS}\,\theta\,(5\ \mathrm{COS}^2\theta - 3)$

FIGURE 12.1 e

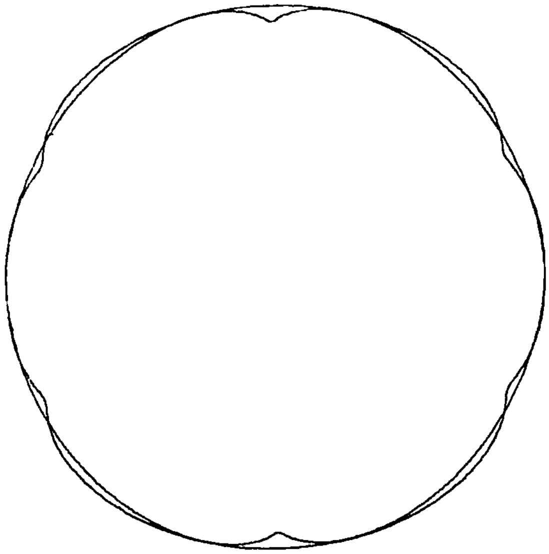

$n = 3$, $f = 1288$ CPS

$v_3(\theta) = 6.36\ A_3\ \mathrm{SIN}\theta(5\ \mathrm{COS}^2\theta - 1)$

$w_3(\theta) = 0.50\ A_3\ \mathrm{COS}\theta(5\ \mathrm{COS}^2\theta - 3)$

FIGURE 12.1 f

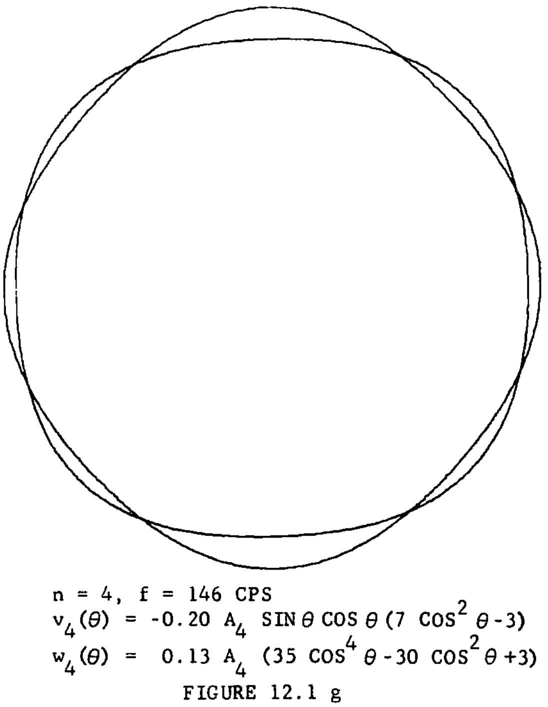

$n = 4$, $f = 146$ CPS

$v_4(\theta) = -0.20\ A_4\ \mathrm{SIN}\,\theta\,\mathrm{COS}\,\theta\,(7\ \mathrm{COS}^2\theta - 3)$

$w_4(\theta) = 0.13\ A_4\ (35\ \mathrm{COS}^4\theta - 30\ \mathrm{COS}^2\theta + 3)$

FIGURE 12.1 g

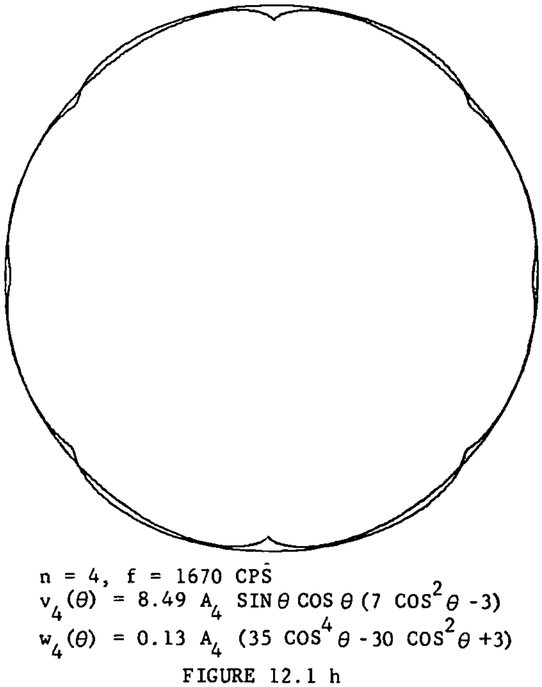

$n = 4$, $f = 1670$ CPS

$v_4(\theta) = 8.49\ A_4\ \mathrm{SIN}\,\theta\,\mathrm{COS}\,\theta\,(7\ \mathrm{COS}^2\theta - 3)$

$w_4(\theta) = 0.13\ A_4\ (35\ \mathrm{COS}^4\theta - 30\ \mathrm{COS}^2\theta + 3)$

FIGURE 12.1 h

FIGURE 12.1 (CONTINUED). MODE SHAPES

EYE NO. AND AGE	$d\sigma / dP \times 10^4$ RAD^2/SEC^2-MM Hg	R_{CALC} CM (n = 2)	$E_{CALC} \times 10^6$ $DYNES/CM^2$	R_{MEAS} CM	h_{MEAS} CM (SCLERAL)
1 5 DAYS	$0.434^{+0.025}_{-0.063}$	$1.05^{+0.09}_{-0.03}$	$0.9^{+0.4}_{-0.2}$	1.11 ± 0.05	0.048 ± 0.006
1 8 DAYS	$0.348^{+0.019}_{-0.047}$	$1.17^{+0.12}_{-0.02}$	$1.2^{+0.8}_{-0.1}$	1.11 ± 0.05	0.048 ± 0.006
2 5 DAYS	$0.400^{+0.010}_{-0.076}$	$1.11^{+0.11}_{-0.03}$	$1.2^{+0.7}_{-0.2}$	1.11 ± 0.05	0.046 ± 0.006
2 8 DAYS	$0.494^{+0.050}_{-0.059}$	$0.98^{+0.08}_{-0.04}$	$1.0^{+0.5}_{-0.2}$	1.11 ± 0.05	0.046 ± 0.006

TABLE 7.1. COMPARISON OF THEORY AND EXPERIMENT

Distribution List for Unclassified Reports Issued Under Contract Navy 0007 Task No. 064-495

Chief of Naval Research
Attn. Code 102 (Dr. F. J. Weyl)
423
439 (2)
468
Department of the Navy
Washington, D. C. 20360

Commanding Officer
ONR Branch Office
495 Summer Street
Boston, Massachusetts 02210

Commanding Officer
ONR Branch Office
219 S. Dearborn Street
Chicago, Illinois 60604

Commanding Officer
ONR Branch Office
Box 39, Navy 100
c/o Fleet Post Office
New York, New York 09510 (5)

Commanding Officer
ONR Branch Office
207 West 24th Street
New York, New York 10011

Commanding Officer
ONR Branch Office
1030 E. Green Street
Pasadena, California 91101

Commanding Officer
ONR Branch Office
U.S. Post Office & Courts Bldg.
1076 Mission Street
San Francisco, California 94103

U. S. Naval Research Laboratory
Attn: Technical Information Div.
Washington, D. C. 20390 (6)

Defense Documentation Center
Cameron Station
Alexandria, Virginia 22314 (20)

Commanding Officer
U. S. Army Research Off.-Durham
Attn: Mr. J. J. Murray
CRD-AA-IP
Box CM, Duke Station
Durham, North Carolina 27706

Commanding Officer
AMXMR-ATL
U. S. Army Materials Res. Agcy.
Watertown, Massachusetts 02172

Redstone Scientific Info. Center
Chief, Document Section
U. S. Army Missile Command
Redstone Arsenal, Alabama 35809

AMSMI-RKP
Attn: Mr. T. H. Duerr
Redstone Arsenal, Alabama 35809

Ballistic Research Laboratories
Attn Dr. A. S. Elder
Aberdeen Proving Ground
Aberdeen, Maryland 21005

Ballistic Research Laboratories
Attn: Mr. H. P. Gay
AMXBR-ID
Aberdeen Proving Ground
Aberdeen, Maryland 21005

Technical Library
Aberdeen Proving Ground
Aberdeen, Maryland 21005

Commanding Officer and Director
Attn: Code 042 (Cent. Lib. Br.)
050
700 (Struc. Mech. Lab.)
720
725
740 (Mr. W. J. Sette)
901 (Dr. M. Strassberg)
941 (Dr. R. Liebowitz)
945 (Mr. A. O. Sykes)
960 (Mr. E. F. Noonan)
962 (Dr. E. Buchmann)
David Taylor Model Basin
Washington, D. C. 20007

Undersea Explosion Research Div.
Attn: Mr. D. S. Cohen
Code 780
David Taylor Model Basin
Norfolk Naval Shipyard
Portsmouth, Virginia 23709

Commanding Officer & Director
Code 257, Library
U. S. Navy Marine Engr. Lab.
Annapolis, Maryland 21402

Commander
Technical Library
U. S. Naval Ordnance Test Station
Pasadena Annex
3202 E. Foothill Blvd.
Pasadena, California 91107

U. S. Naval Ordnance Test Station
Attn: Dr. Arnold Adicoff
Code 5056
China Lake, California 93557

Commander
U. S. Naval Ordnance Test Station
Mechanical Engineering Division
Code 556
China Lake, California 93557

Commanding Officer & Director
U. S. Naval Civil Engr. Lab.
Code L31
Port Hueneme, California 93041

Shipyard Technical Library
Code 242L
Portsmouth Naval Shipyard
Portsmouth, New Hampshire 03804

U. S. Naval Electronics Laboratory
Attn: Dr. R. J. Christensen
San Diego, California 92152

U. S. Naval Ordnance Laboratory
Mechanics Division
RFD 1, White Oak
Silver Spring, Maryland 20910

U. S. Naval Ordnance Laboratory
Attn: Mr. H. A. Perry, Jr.
Non-Metallic Materials Divison
Silver Spring, Maryland 20910

Supervisor of Shipbuilding
U. S. Navy
Newport News, Virginia 23607

Shipyard Technical Library
Building 746, Code 303TL
Mare Island Naval Shipyard
Vallejo, California 94592

Director
U.S. Navy Underwater Sound Ref. Lab.
Office of Naval Research
P. O. Box 8337
Orlando, Florida 32806

Technical Library
U. S. Naval Propellant Plant
Indian Head, Maryland 20640

U. S. Naval Propellant Plant
Attn: Dr. J. G. Tuono
Research & Development Division
Indian Head, Maryland 20640

Chief of Naval Operations
Attn: Code Op-03EG
Op-07T
Department of the Navy
Washington, D. C. 20350

Director, Special Projects
Attn: Sp-001
43
2731
Department of the Navy
Washington, D. C. 20360

Executive Secretary PLRRD
Special Projects Office (Sp-00110)
Department of the Navy
Washington, D. C. 20360

U. S. Naval Applied Science Lab.
Code 9832
Technical Library
Building 291, Naval Base
Brooklyn, New York 11251

Director
Aeronautical Materials Lab.
Naval Air Engineering Center
Naval Base
Philadelphia, Pennsylvania 19112

Director
Aeronautical Structures Lab.
Naval Air Engineering Center
Naval Base
Philadelphia, Pennsylvania 19112

Director
Attn: Code 5360
5500
6200
6210
6250
6260
Technical Library
Naval Research Laboratory
Washington, D. C. 20390

Chief, Bureau of Naval Weapons
Attn: Code DLI-3
R-12
RAAD-2
RAAD-24 (Mr. E.M. Ryan)
RM
RMMP-2
RMMP-11 (Mr. I. Silver)
RMMP-22 (Mr. J.C. Ardinger)
RR
RRRE
RRRE-61 (Mr. W.J. Marciniak)
RU
Department of the Navy
Washington, D. C. 20360

Chief, Bureau of Ships
Attn: Code 210-L
305
345
421
423
430
440
442
443
1500
Department of the Navy
Washington, D. C. 20360

Commander
U. S. Naval Weapons Laboratory
Dahlgren, Virginia 22448

Bureau of Yards & Docks Tech. Lib.
Yards & Docks Annex
Department of the Navy
Washington, D. C. 20390

Commander, WADD
Attn: Code WWRMDD
AFFDL (FDDS)
Structures Division
AFLC (MCEEA)
Code WWRMDS
AFFDL (FDT)
Code WWRC
AFML (MAAM)
Code WCLSY
SEG (SEFSD, Mr. Lakin)
Wright-Patterson Air Force Base
Dayton, Ohio 45433

Commander
Chief, Applied Mechanics Group
U. S. Air Force Inst. of Tech.
Wright-Patterson Air Force Base
Dayton, Ohio 45433

Chief, Civil Engineering Branch
WLRC, Research Division
Air Force Weapons Laboratory
Kirtland AFB, New Mexico 87117

Commander
AFRPL (RPMC/Dr. F.N. Kelley)
Edwards AFB, California 93523

Commander
Attn: Mr. A.L. Skinner, OOMQQC
Hill AFB, Utah 84401

Commander
Mechanics Division
Air Force Office of Scien. Res.
Washington, D. C. 20333

Structures Research Division
Attn: Mr. R. R. Heldenfels, Chief
National Aeronautics & Space Admin.
Langley Research Center
Langley Station
Hampton, Virginia 23365

National Aeronautics & Space Admin.
Code RV-2
Washington, D. C. 20546

National Aeronautics & Space Admin.
Associate Administrator for Advanced
Research & Technology
Washington, D. C. 20546

Scientific & Tech. Info. Facility
NASA Representative (S-AK/DL)
P. O. Box 5700
Bethesda, Maryland 20014

Commandant
Chief, Testing & Development Div.
U. S. Coast Guard
1300 E Street, N. W.
Washington, D. C. 20226

Director
Marine Corps Landing Force Devel. Cen.
Marine Corps Schools
Quantico, Virginia 22134

Director
Attn: Mr. B. L. Wilson
National Bureau of Standards
Washington, D. C. 20234

National Science Foundation
Engineering Division
1951 Constitution Avenue, N. W.
Washington, D. C. 20550

Science & Tech. Division
Library of Congress
Washington, D. C. 20540

Director
STBS
Defense Atomic Support Agency
Washington, D. C. 20301

Commander Field Command
Defense Atomic Support Agency
Sandia Base
Albuquerque, New Mexico 87115

Chief, Defense Atomic Support Agcy.
Blast & Shock Division
The Pentagon
Washington, D. C. 20301

Director Defense Research & Engr.
Technical Library
Room 3C-128
The Pentagon
Washington, D. C. 20301

Chief, Airframe & Equipment Branch
FS-120
Office of Flight Standards
Federal Aviation Agency
Washington, D. C. 20553

Chief, Division of Ship Design
Maritime Administration
Washington, D. C. 20235

Deputy Chief, Office of Ship Constr.
Attn: Mr. U. L. Russo
Maritime Administration
Washington, D. C. 20235

Executive Secretary
Committee on Undersea Warfare
National Academy of Sciences
2101 Constitution Avenue
Washington, D. C. 20418

Ship Hull Research Committee
Attn: Mr. A. R. Lytle
National Research Council
National Academy of Sciences
2101 Constitution Avenue
Washington, D. C. 20418

Dr. D. C. Drucker
Division of Engineering
Brown University
Providence, Rhode Island 02912

Prof. M. E. Gurtin
Brown University
Providence, Rhode Island 02912

Prof. R. S. Rivlin
Division of Applied Mathematics
Brown University
Providence, Rhode Island 02912

Prof. P. J. Blatz
Materials Science Department
California Institute of Technology
Pasadena, California 91109

Prof. Julius Miklowitz
Div. of Engr. & Applied Sciences
California Institute of Technology
Pasadena, California 91109

Prof. George Sih
Department of Mechanics
Lehigh University
Bethlehem, Pennsylvania 18015

Solid Propellant Library
Firestone Flight Science Lab.
California Institute of Technology
Pasadena, California 91109

Prof. Eli Sternberg
Div. of Engr. & Applied Sciences
California Institute of Technology
Pasadena, California 91109

Prof. Paul M. Naghdi
Div. of Applied Mechanics
Etcheverry Hall
University of California
Berkeley, California 94720

Prof. J. Baltrukonis
Mechanics Division
The Catholic Univ. of America
Washington, D. C. 20017

Prof. A. J. Durelli
Mechanics Division
The Catholic Univ. of America
Washington, D. C. 20017

Prof. H. H. Bleich
Department of Civil Engr.
Columbia University
Amsterdam & 120th Street
New York, New York 10027

Prof. R. D. Mindlin
Department of Civil Engr.
Columbia University
S. W. Mudd Building
New York, New York 10027

Prof. B. A. Boley
Department of Civil Engr.
Columbia University
Amsterdam & 120th Street
New York, New York 10027

Prof. F. L. DiMaggio
Department of Civil Engr.
Columbia University
616 Mudd Building
New York, New York 10027

Prof. A. M. Freudenthal
Dept. of Civil Engr. & Engr. Mech.
Columbia University
New York, New York 10027

Prof. William A. Nash
Dept. of Engr. Mechanics
University of Florida
Gainesville, Florida 32603

Prof. B. Budiansky
Div. of Engr. & Applied Physics
Pierce Hall
Harvard University
Cambridge, Massachusetts 02138

Prof. P. G. Hodge
Department of Mechanics
Illinois Institute of Technology
Chicago, Illinois 60616

Prof. H. T. Corten
University of Illinois
Urbana, Illinois 61803

Prof. W. J. Hall
Department of Civil Engr.
University of Illinois
Urbana, Illinois 61803

Prof. N. M. Newmark
Dept. of Civil Engineering
University of Illinois
Urbana, Illinois 61803

Dr. W. H. Avery
Applied Physics Laboratory
Johns Hopkins University
8621 Georgia Avenue
Silver Spring, Maryland 20910

Prof. J. B. Tiedemann
Dept. of Aero. Engr. & Arch.
University of Kansas
Lawrence, Kansas 66045

Prof. S. Taira
Department of Engineering
Kyoto University
Kyoto, Japan

Prof. E. Reissner
Dept. of Mathematics
Massachusetts Inst. of Tech.
Cambridge, Massachusetts 02139

Library (Code 0384)
U. S. Naval Postgraduate School
Monterey, California 93940

Dr. Joseph Marin
Prof. of Materials Science
Dept. of Materials Sc. & Chem.
U. S. Naval Postgraduate School
Monterey, California 93940

Prof. E. L. Reiss
Courant Inst. of Math. Sciences
New York University
4 Washington Place
New York, New York 10003

Dr. Francis Cozzarelli
Div. of Interdisciplinary
Studies and Research
School of Engineering
State Univ. of N.Y. at Buffalo
Buffalo, New York 14214

Dr. George Herrmann
The Technological Institute
Northwestern University
Evanston, Illinois 60201

Director, Ordnance Research Lab.
The Pennsylvania State University
P. O. Box 30
State College, Pennsylvania 16801

Prof. Eugen J. Skudrzyk
Department of Physics
Ordnance Research Lab.
The Pennsylvania State University
P. O. Box 30
State College, Pennsylvania 16801

Dean Oscar Baguio
Assoc. of Structural Engr.
of the Philippines
University of Philippines
Manila, Philippines

Prof. J. Kempner
Dept. of Aero. Engr. & Applied Mech.
Polytechnic Institute of Brooklyn
333 Jay Street
Brooklyn, New York 11201

Prof. J. Klosner
Polytechnic Institute of Brooklyn
333 Jay Street
Brooklyn, New York 11201

Prof. F. R. Eirich
Polytechnic Institute of Brooklyn
333 Jay Street
Brooklyn, New York 11201

Prof. A. C. Eringen
School of Aero., Astro. & Engr. Sc.
Purdue University
Lafayette, Indiana 47907

Dr. S. L. Koh
School of Aero., Astro. & Engr. Sc.
Purdue University
Lafayette, Indiana 47907

Prof. D. Schapery
Purdue University
Lafayette, Indiana 47907

Prof. E. H. Lee
Div. of Engr. Mechanics
Stanford University
Stanford, California 94305

Dr. Nicholas J. Hoff
Dept. of Aero. & Astro.
Stanford University
Stanford, California 94305

Dr. Thor Smith
Stanford Research Institute
Menlo Park, California 94025

Prof. J. N. Goodier
Div. of Engr. Mechanics
Stanford University
Stanford, California 94305

Prof. Markus Reiner
Technion R & D Foundation, Ltd.
Haifa, Israel

Prof. Tsuyoshi Hayashi
Department of Aeronautics
Faculty of Engineering
University of Tokyo
BUNKYO-KU
Tokyo, Japan

Prof. R. J. H. Bollard
Chairman, Aeronautical Engr. Dept.
207 Guggenheim Hall
University of Washington
Seattle, Washington 98105

Prof. Albert S. Kobayashi
Dept. of Mechanical Engr.
University of Washington
Seattle, Washington 98105

Officer-in-Charge
Post Graduate School for Naval Off.
Webb Institute of Naval Arch.
Crescent Beach Road, Glen Cove
Long Island, New York 11542

Mr. K. W. Bills, Jr.
Dept. 4722, Bldg. 0525
Aerojet-General Corporation
P. O. Box 1947
Sacramento, California 95809

Dr. James H. Wiegand
Senior Dept. 4720, Bldg. 0525
Ballistics & Mech. Properties Lab.
Aerojet-General Corporation
P. O. Box 1947
Sacramento, California 95809

Dr. John Zickel
Dept. 4650, Bldg. 0227
Aerojet-General Corporation
P. O. Box 1947
Sacramento, California 95809

Mr. J. S. Wise
Aerospace Corporation
P. O. Box 1308
San Bernardino, California 92402

Dr. Vito Salerno
Applied Technology Assoc., Inc.
29 Church Street
Ramsey, New Jersey 07446

Library Services Department
Report Section, Bldg. 14-14
Argonne National Laboratory
9700 S. Cass Avenue
Argonne, Illinois 60440

Dr. E. M. Kerwin
Bolt, Beranek, & Newman, Inc.
50 Moulton Street
Cambridge, Massachusetts 02138

Dr. M. C. Junger
Cambridge Acoustical Associates
129 Mount Auburn Street
Cambridge, Massachusetts 02138

Dr. F. R. Schwarzl
Central Laboratory T.N.O.
134 Julianalaan
Delft, Holland

Mr. Ronald D. Brown
Applied Physics Laboratory
Chemical Propulsion Agency
8621 Georgia Avenue
Silver Spring, Maryland 20910

Research and Development
Electric Boat Division
General Dynamics Corporation
Groton, Connecticut 06340

Dr. M. L. Baron
Paul Weidlinger, Consulting Engr.
777 Third Ave. - 22nd Floor
New York, New York 10017

Supervisor of Shipbuilding, USN,
and Naval Insp. of Ordnance
Electric Boat Division
General Dynamics Corporation
Groton, Connecticut 06340

Dr. L. H. Chen
Basic Engineering
Electric Boat Division
General Dynamics Corporation
Groton, Connecticut 06340

Mr. Ross H. Petty
Technical Librarian
Allegany Ballistics Lab.
Hercules Powder Company
P. O. Box 210
Cumberland, Maryland 21501

Dr. J. H. Thacher
Allegany Ballistic Laboratory
Hercules Powder Company
Cumberland, Maryland 21501

Dr. Joshua E. Greenspon
J. G. Engr. Research Associates
3831 Menlo Drive
Baltimore, Maryland 21215

Mr. R. F. Landel
Jet Propulsion Laboratory
4800 Oak Grove Drive
Pasadena, California 91103

Mr. G. Lewis
Jet Propulsion Laboratory
4800 Oak Grove Drive
Pasadena, California 91103

Mr. J. Edmund Fitzgerald
Director, Research & Engr.
Lockheed Propulsion Company
P. O. Box 111
Redlands, California 92374

Library
Newport News Shipbuilding &
Dry Dock Company
Newport News, Virginia 23607

Mr. E. A. Alexander
Rocketdyne Division
North American Aviation, Inc.
6633 Canoga Avenue
Canoga Park, California 91304

Mr. Cezar P. Nuguid
Deputy Commissioner
Philippine Atomic Energy Commission
Manila, Philippines

Mr. S. C. Britton
Solid Rocket Division
Rocketdyne
P. O. Box 548
McGregor, Texas 76657

Dr. A. J. Ignatowski
Redstone Arsenal Research Div.
Rohm & Haas Company
Huntsville, Alabama 35807

Dr. M. L. Merritt
Division 5412
Sandia Corporation
Sandia Base
Albuquerque, New Mexico 87115

Director
Ship Research Institute
Ministry of Transportation
700, SHINKAWA
Mitaka
Tokyo, JAPAN

Dr. H. N. Abramson
Southwest Research Institute
8500 Culebra Road
San Antonio, Texas 78206

Dr. R. C. DeHart
Southwest Research Institute
8500 Culebra Road
San Antonio, Texas 78206

UNCLASSIFIED
Security Classification

DOCUMENT CONTROL DATA - R & D

(Security classification of title, body of abstract and indexing annotation must be entered when the overall report is classified)

1 ORIGINATING ACTIVITY (Corporate author) Department of Aeronautics and Astronautics Stanford University Stanford, California 94305	2a. REPORT SECURITY CLASSIFICATION 2b. GROUP

3 REPORT TITLE

DYNAMIC BEHAVIOR OF EYE GLOBES

4 DESCRIPTIVE NOTES (Type of report and inclusive dates)

Technical Report

5. AUTHOR(S) (First name, middle initial, last name)

Tuffias, Robert H.

6 REPORT DATE	7a. TOTAL NO OF PAGES	7b NO OF REFS
February 1967	142	24

8a CONTRACT OR GRANT NO N00014-C000170007 b. PROJECT NO NR-064-495 c. d	9a. ORIGINATOR'S REPORT NUMBER(S) SUDAAR NO. 302 9b. OTHER REPORT NO(S) (Any other numbers that may be assigned this report) TR No. 1

10 DISTRIBUTION STATEMENT

Reproduction in whole or in part is permitted for any purpose of the United States Government.

11 SUPPLEMENTARY NOTES	12 SPONSORING MILITARY ACTIVITY Structural Mechanics Branch Department of the Navy Office of Naval Research Washington, D. C. 20360

13 ABSTRACT The eye globe has been treated as a spherical shell (combined cornea and sclera) filled with (vitreous and aqueous) and surrounded by (tissue and fat) incompressible, inviscid, irrotationally flowing fluids. Its dynamic behavior has been investigated by making use of the Flügge shell equations and the appropriate inertia terms. The axisymmetric case has been solved in closed form, and the asymmetric case has been solved numerically. Some qualitative results for physiologically meaningful parameter values are

$$\sigma_{mn} = \frac{d\sigma_{mn}}{dP} P + (\sigma_o)_{mn} \qquad (1) \qquad\qquad \frac{d\sigma_{mn}}{dP} = g_1(n)g_2(R) \qquad (2)$$

$$(\sigma_o)_{mn} = (\sigma)_{mn}\Big|_{P=0} = E\, G_1(h,R,m,n) \simeq Eh\, G_2(R,m,n) \qquad n \le 4 \qquad (3)$$

where σ_{mn} is the eigenfrequency squared, P is a dimensionless intraocular pressure, g_1, g_2, G_1, and G_2, are functions of the variables shown, E is the effective Young's modulus, h is the mean scleral thickness, R is the middle surface radius, n is the symmetric mode number, and m is the asymmetric mode number.

Static and dynamic experiments were performed on enucleated dog eyes. The static experiment measured the change in volume of the eyes as a function of time at various pressures. The results of this experiment indicated that the eyes were viscoelastic with an associated time constant of approximately 20 minutes.

(continued)

DOCUMENT CONTROL DATA - R & D

UNCLASSIFIED 13. Abstract (continued)

The dynamic experiments measured the fundamental frequency as a function of the intraocular pressure. The results of that experiment indicated that the $n = 2$ (axisymmetric ellipsoidal mode) was excited. At intraocular pressures below 40 cm H_2O, the data were in agreement with the theoretical analysis within experimental error. At higher pressures σ_{02} vs P curves became non-linear with decreasing slope. If Young's modulus exhibits a frequency and pressure dependence of the form

$$E = E_1 - \sigma E_0$$

where E_1 is a constant obtained from linear elastic theory and E_0 is a function of P, it is possible to explain the non-linear behavior of the vibration data. The dynamic results seem to imply that the inner elastic layer of the sclera governs the dynamic behavior of the eye up to a certain critical intraocular pressure. Above this critical pressure the outer layer conceivably contributes to a frequency-pressure dependent elastic behavior.

KEY WORDS	LINK A		LINK B		LINK C	
	ROLE	WT	ROLE	WT	ROLE	WT
Occular Pressure						
Intraocular Pressure						
Eye Pressure						
Occular Eigenvibration						
Vibratory Response of the Eye						
the Eye						
Dynamic Response of the Eye						
Viscoelastic Behavior of Sclera						